INFORMATION TO USERS

RICE UNIVERSITY

Longitudinal Recording on FePt and FePtX (X=B, Ni)

Intermetallic Compounds

by

Ning Li

A THESIS SUBMITTED

IN PARTIAL FULFILLMENT OF THE

REQUIREMENTS FOR THE DEGREE

Doctor of Philosophy

APPROVED, THESIS COMMITTEE:

Bruce M. Lairson, Chair
Associate Professor of Materials Science

Rex. B. McLellan
Professor of Materials Science

William Wilson
Professor of Electrical Engineering

Michael Smayling
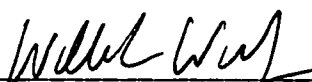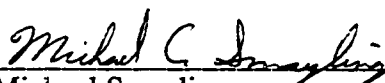Fellow, Texas Instruments Corp.

Houston, Texas

August 1998

Abstract

Longitudinal Recording on FePt and FePtX (X=B, Ni) \Intermetallic Compounds

by

Ning Li

Near field recording on high coercivity FePt intermetallic compound media using a high B_{sat} write element was investigated. Untextured FePt media were prepared by magnetron sputtering on ZrO_2 disks at a substrate temperature of $450°C$, with post annealing at $450°C$ for 8 hrs. Both multilayer and cosputtered precursors produced the ordered tetragonal $L1_0$ phase with high coercivity between 5kOe and 12kOe. To improve readback noise and decrease magnetic domain size, FePtB media were subsequently prepared by cosputtering. Over-write, roll-off, signal to noise ratio and non-linear transition shift (NLTS) were measured by both metal in gap (MIG) and merged MR heads. FePtB media showed similar NLTS to commercial CoCrPtTa longitudinal media, but 5dB lower signal to noise ratio. By operating recording transducers in near contact, reasonable values of overwrite (>30dB) could be obtained.

VSM Rotational Transverse Magnetization has been used for measuring the anisotropy field of magnetic thin films. Magnetization reversal during rotation of a 2D isotropic sample in an applied field is discussed. The relationship between the transverse magnetization M_y and the applied field H was numerically solved. An excellent approximation for the transverse magnetization is found to be: $M_y / M_s = A(1 - H / H_k)^{2.5}$, where A=1.1434, and H_k is the anisotropy field. For curve fitting to experimental data, both A and H_k were

used as fitting parameters. Comparison between a constructed torque hysteresis method and this VSM RTM method have been made theoretically and experimentally. Both results showed that VSM RTM will give better extrapolation of the anisotropy field. The torque measurement will slightly overestimate the anisotropy field.

The anisotropy fields of FePt and FePtX (X=B, Ni) films were characterized using this VSM RTM technique with comparison to a CoCrTaPt disk. Anisotropy energy was derived. H_c/H_k was used as an indicator for coherent rotation of a single domain. Interactions between magnetic domains were characterized by Kelly-Henkel plot and interactive field factor (IFF). Correlation between coercive force and magnetic anisotropy of grains and the degree of magnetic isolation among grains were discussed. B and Ni were used as diluting agents to the FePt system to decrease saturation magnetization, coercivity, anisotropy field and anisotropy energy. They also decrease the magnetic coupling between neighboring domains, and promote coherent rotation inside each domain.

Acknowledgments

My four years study at Rice is the culmination of my academic education. Without the support and love from all the people, I would not be at this point.

My advisor, Dr. Bruce Lairson, has been instrumental in my success in the Ph.D. process here at Rice. Throughout the four years, he has helped me immensely in understanding how to define a problem, ask the right questions, choose the appropriate approach and reach the solution and answers. He has always been challenging and encouraging, greatly shaped my professional personality, and made it a strong one. His sharp scientific insight, "no fear" attitude and hard working have led me and others in the group to overcome all kinds of limitation and to challenge the farthest frontier in each project.

I'd like to thank the faculty in the Materials Science program at Rice for offering good courses, and staff members for helpful administration. Especially my committee members Dr. McLellan, Dr. Wilson, and Dr. Smayling, for their teaching and advising.

It is also lucky to work with a group of intelligent and diligent graduate students in Bruce's group, Wenhong Liu, Kris Schouterden, Lin Mei, Kuoksan Ho, Julius Barnes, Brian Mayeaux and Scott Stokes. Friendship will last even though each of us is working for industry competitors. A lot of Rice Chinese students have share their friendship and made my life at Rice enjoyable.

I have always been blessed by a loving and caring family. Over the years my parents shaped me into the individual I am and instilled in me my courage, values, and beliefs. My husband, Kaiyu, the single most important person in my life has made spectacular achievements in his own career as well as given me countless, selfless support and love. Words alone can not express my love for and gratitude toward him and my parents.

Hopefully, this Ph.D. is the last academic degree I would like to have. By no means it would be the end of education and learning, I have always believed in the value of knowledge and how it would change human being and the world. For sure I will enjoy the philosophy and methodology of learning and self-educating which I learned in my Ph.D. process.

Table of Contents

List of Tables

List of Figures

Chapter 1:   Introduction and Motivation

1.1 Historical review of $L1_0$ compounds as recording media candidate

In the hard disk drive industry, Co alloys have been dominant as recording media for more than ten years. The recording areal density increases at a compounded 60% per year rate with a correspondingly smaller bit size [1.1], 11.6Gbit/in^2 was demonstrated in the research level in 1998[1.2]. The reduction of grain size is required for thin film recording media to achieve ultrahigh density recording. However, the size reduction increases magnetic viscosity owing to thermal agitation of the spins comprising the magnetic moment. Magnetic viscosity, the time dependence of the magnetization, originates from thermally activated magnetization transitions over anisotropy energy barriers. With the thermal agitation of the spins of the individual electrons in a particle, the magnetization of a uniaxial particle can surmount the energy barrier and switch from one stable direction to the other. This means there is a recording density limit when the grain of the recording media is too small to maintain a stable magnetization for a long time because the magnetic viscosity is too high.[1.3]

Such spontaneous demagnetization is inhibited by the anisotropy energy of the entire particle, which is proportional to particle volume and which forms a potential energy barrier to thermal demagnetization. Quantitatively, thermal stability is exponentially dependent on $K_u V/kT$, where K_u is the anisotropy energy per unit volume of the material; V is the particle volume, or more precisely, the magnetic switching volume; k is the Boltzmann's constant and T is the absolute temperature. When $K_u V/kT$ falls below a critical value, the particle becomes paramagnetic.

It has been reported that the paramagnetism limit is about K_uV/kT in the range of 40~60, beyond this value the information stored in the media will be thermally unstable. For Co media with K_uV/kT~60, the thermal decay increased the medium noise so that signal-to-noise ratio dropped by 6 dB over 6 months.[1.5] If based on the current Co alloy parameters, the superparamagnetic limit of storage density for Co media is about $50Gbit/in^2$. To achieve even higher recording density, progress could be made in several aspects of the recording system; including improving the recording channel, exploring near contact recording, and looking at other alternative recording materials.

The ideal recording medium should be composed of small single-domain Stoner-Wolhfarth-like particles. These particles are magnetically isolated, with uniform size to minimize the noise, with small grain size and maximized anisotropy energy.[1.6] The key to achieving both high coercivity and small isolated grains simultaneously is to use a material with very high magnetic anisotropy. One approach to achieve high anisotropy in Co alloys is to build grains of such crystalline perfection that the magnetocrystalline anisotropy is maximized. The alignment of the anisotropy axis along the record track direction will also help to maximize the coercivity. However, there is modeling evidence that this type of orientation may increase medium noise.[1.7] Materials systems other than Co alloy with natural higher anisotropy energy have been studied as alternative recording media, including Barium Ferrite, SmCo, and $L1_0$ intermetallic compounds such as FePt or CoPt. All these systems have anisotropy originating from compositional and structural short-range order, and have higher coercivity than the known Co alloys. Figure 1.1 shows that the IBM commercial hard drives have adopted disks with increasingly higher coercivity through the years, and this trend is expected to continue. This may lead to the need for new materials.

Barium ferrite(BaM) has been developed primarily for perpendicular recording for more than a decade. The discovery in 1993 of self-textured longitudinal BaM thin film, with good magnetic, chemical, mechanical and tribological properties, has generated interest in using it as a potential overcoat-free medium for future high density recording. It provides a possible approach to reduce the head to medium spacing, and eventually could lead to contact recording.[1.9], [1.10]
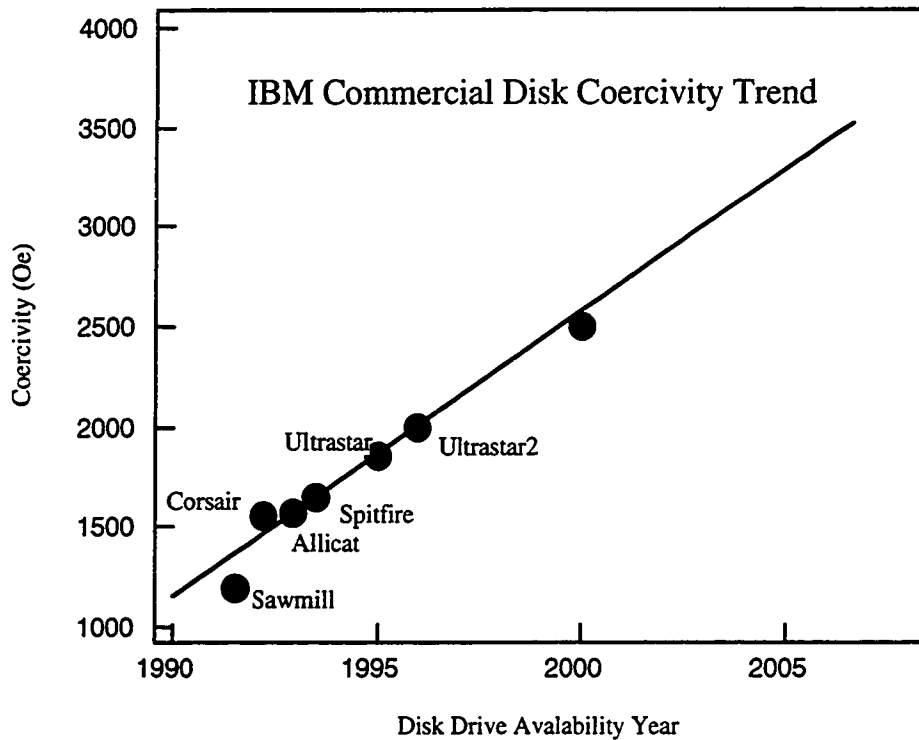
Fig. 1.1 IBM commercial disk coercivity trend[1.8]

SmCo thin films exhibit high magnetic anisotropy in both the amorphous and crystalline states. A Cr(110) underlayer is used to induce microcrystallinity and significantly reduce the exchange interaction and hence the noise level in SmCo media. SmCo/Cr hard disks have demonstrated low medium noise and high signal to noise ratio. [1.11][1.12]

Bulk $L1_0$ phase materials, typically equiatomic CoPt and FePt, are known for their high magnetocrystalline anisotropy and magnetic moment. Studies showed that their thin film forms have optimum hysteresis behavior as well.[1.13][1.14] Thin film intermetallic compounds such as CoPt and FePt with $L1_0$ phase structure have naturally higher crystalline anisotropy, and higher coercivity than the conventional Co alloys.[1.14] Approaching the limitation on recording density imposed by thermal stability (also known as the superparamagnetic limit), such recording media with anisotropy energy ten times higher than Co alloy and with higher coercivity, smaller switching volume could have superior recording performance over the conventional Co alloy media. [1. 15]
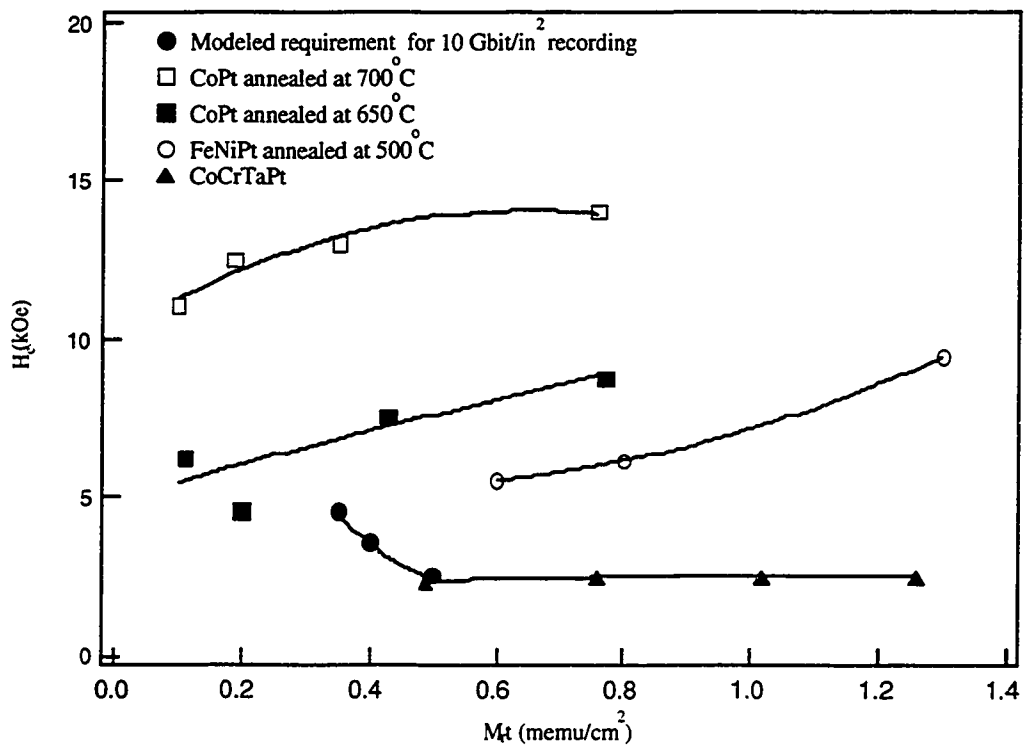
Fig. 1.2 Variation of H_c and M_t for CoPt $L1_0$, FeNiPt $L1_0$, CoCrPtTa media and modeled requirement for 10Gbit/in^2 recording

Figure 1.2 is the range of magnetic parameters of H_c and $M_r t$ for CoPt[1.14] and FeNiPt (from this dissertation) $L1_0$ intermetallic compounds, with comparison to commercial CoCrPtTa media and modeled requirement [1.15] for 10Gbit/in^2 recording. The recording properties of the CoPt intermetallic compound was studied by IBM scientists [1.14], but no recording results have ever been published on the FePt compound. In this dissertation, we will explain why we choose FePt system and how to prepare FePt and FePtX(X=Ni,B) media, and evaluate their magnetic recording performance.

1.2 Ordered FePt Intermetallic Compound with $L1_0$ Structure

The Fe-Pt system possesses many interesting physical properties. It has a continuous range of solid solutions, and both stoichiometric intermetallic compounds and nonstoichiometric alloys with various degrees of order can be prepared. The ordered phases of Fe_3Pt and $FePt_3$ with $AuCu_3$ type crystal structure, and the ordered phase of FePt with AuCu(I) type crystal structure can be grown. The near equiatomic ordered intermetallic compound of FePt with the $L1_0$ structure have been known as high magnetocrystalline anisotropy materials in their bulk form with a mean atomic magnetic moment of 0.77 uB, and FePt polycrystalline thin films have been previously reported. Another important factor to evaluate the media is the magnetic switching volume, which is derived by the magnetic viscosity behavior study and related to the media noise. It is reported that the FePt thin films could have small magnetic switching volume. It is also reported that in the FePt system, the higher coercivity, the smaller the switching volume.[1.16]

Magnetic properties of the FePt binary system are associated with the order-disorder transformation in the phase diagram. The equiatomic compound undergoes an

ordering transformation from a disordered face-centered cubic structure to an ordered face-centered tetragonal structure. The ordering reaction can occur for some atomic percent on either side of the equiatomic stoichiometric FePt composition. Study had shown that the preferred FCT structure could occur over a range of 37.5 at% to 67.5 at% iron as well as the exact equiatomic FePt.[1.17] The structures involved in the disorder-order transformation between FCC and the $L1_0$ phase are depicted in Figure 1.3.

(a) **Disordered FCC**

● **A or B atom**

(b) **Ordered FCT**

● **Atom A (Fe or C**

○ **Atom B (Pt)**
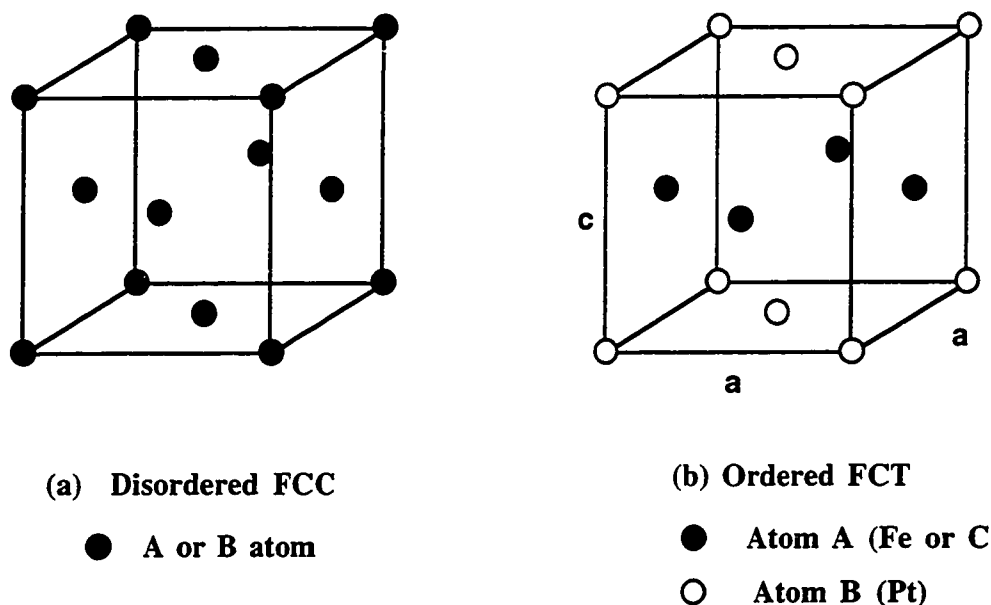
Fig. 1.3 Crystal structure of disordered FCC AB and ordered $L1_0$ AB

Generally, above the ordering temperature (825°C for CoPt and 1300°C for FePt)[1.18], the A atoms (Fe or Co) and B atoms (Pt) are distributed randomly in the FCC cell, as each particular site will have an equal possibility to accommodate either A or B atomic species. At equilibrium below the ordering temperature, the atoms occupy the specific site corresponding to the stacking of individual atomic layers of the constituent atoms along the [001] direction. This stacking destroys the three-fold

symmetry characteristic of cubic structures while retaining a single four-fold axis along the [001] direction. Strictly speaking, this $L1_0$ structure is in the P-tetragonal crystal class. But to simplify the comparison between the disordered and ordered structure, we choose to use the notation of the Face Centered Tetragonal (FCT) structure as in Fig 1.3(b).

Coffey, et al. reported on longitudinal recording on tetragonal $L1_0$ CoPt intermetallic compounds[1.14]. In comparison, FePt has a higher magnetocrystalline anisotropy energy of $7*10^7$erg/cc [1.19] compared to CoPt which is $2.8*10^7$ erg/cc.[1.20]. FePt also has a higher free energy driving force[1.18] for ordering, due to the higher transformation temperature to the FCC phase[1.21] and can be prepared at somewhat lower substrate temperatures than are possible with CoPt. This would ease the requirement for annealing during processing, increase the number of substrate candidates and reduce the homologous temperature for phase formation.

Intermetallic FePt thin films have previously been studied as possible high density magneto-optical recording media because of their high polar magneto-optical Kerr rotation θ_k in the short wavelength region and their high coercivity force. C-axis oriented epitaxial FePt with perpendicular magnetic anisotropy was formed by annealing [001] oriented multilayer precursors[1.22]. Evaporation and sputtering to directly form c-axis oriented FePt at equilibrium growth temperature from elemental sources were reported on MgO substrates with a Pt buffer layer[1.23][1.24]. The dynamics of such a process is governed by the adatom mobility at the growing film surface rather than by bulk diffusion as in post-annealing. Control of the axes of chemical ordering and magnetic anisotropy in epitaxial FePt films were discussed[1.25]. Near-complete chemical ordering of FePt(001) was achieved for film growth on Pt(001)/MgO for both a 15nm and a 0.7nm thick Pt seed layer at

500°C. Anisotropy energy K_u was found to be 10^8 erg/cc for these films[1.26]. Formation of (111) oriented FePt was also reported[1.27]

Magnetically hard equiatomic FePt is a compound resulting from chemical ordering, therefore its formation requires precise control of the stoichiometry of Fe and Pt and adequate annealing temperature-time products to overcome the energy barriers for diffusion and superlattice ordering[1.28]. Such annealing must also produce small switching volumes because of recording requirements. Excessive annealing is harmful for both magnetic hardness and recording properties. It will cause grain coarsening, increasing the noise and decreasing the coercivity.[1.29],[1.30] The optimum magnetic properties of the compound are associated with the formation of nuclei of the ordered phase in the disordered material. The coherent nuclei of the ordered phase within the disordered matrix could result in large localized lattice strain, which contributes to the high coercivity value. Further annealing could cause the region of ordered structure to break away as separate phases, relieve the coherency strain and weaken the hard magnetic properties.

Magnetic viscosity studies showed that an FePt film with high coercivity can have a small switching volume[1.31][1.32]. Theoretically, media with higher coercivity and low $M_r t$, if combined with small switching volumes, will display superior non-linear transition shift[1.33], thermal decay and signal to noise ratio. However, the high coercivity of FePt leads to poor writability using traditional writers. In this dissertation, we have experimentally explored the possibility of using near field recording on high coercivity FePt intermetallic compound media, using higher saturation magnetization write elements in near contact. Subsequently, boron and nickel was added to the ordered FePt compound to lower coercivity and to isolate

grains. Compared with FePt, FePtB showed an improved signal-to-noise ratio and nonlinear transition shift(NLTS).

1.3 Near Field Recording
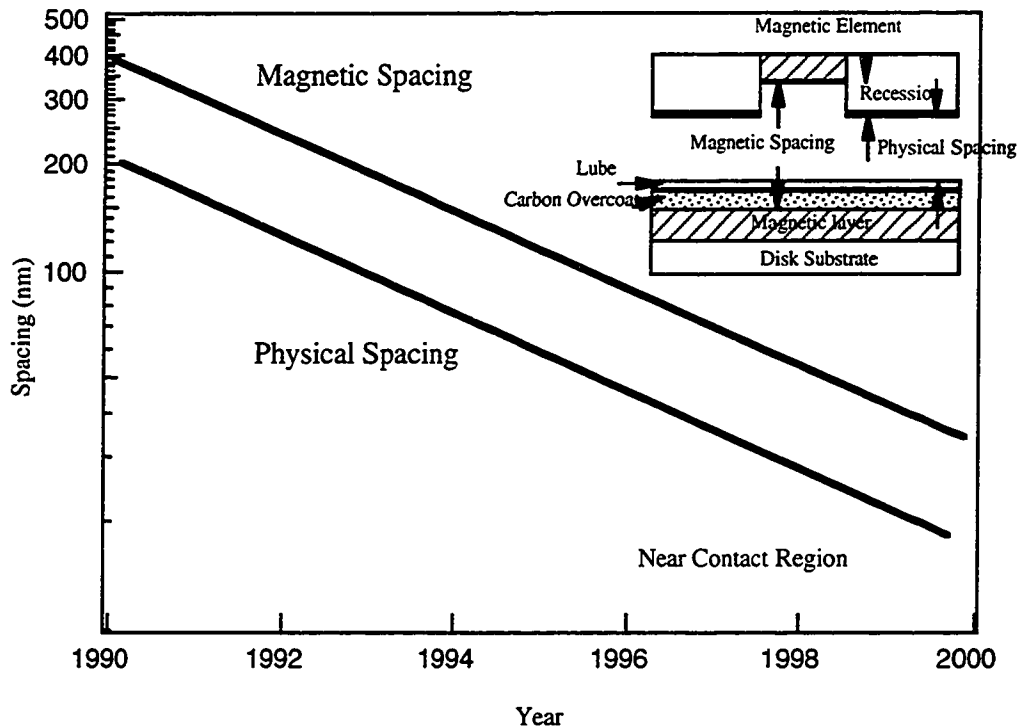
Fig 1.4 Magnetic/Physical spacing evolution for IBM

commercial disks[1.34]

Traditionally, coercivity in a storage medium is held to less than about 20% of the saturation magnetization of the write pole material, to achieve the maximum field gradient in the medium. In the future, in the absence of higher moment pole materials, it may be necessary to perform writing at much higher relative coercivities. Such an approach may be possible if the writer is operated in close proximity to the medium, such that high write fields are available with large gradients. On the other

hand, it has also been an industrial trend for the magnetic and physical spacing to continue to get smaller as shown in Figure 1.4.

Our work with FePt involves coercivities that are substantial compared with the saturation magnetization of possible write materials. It is thus illustrative to consider writing at very small magnetic spacing.

Fig 1.5 is an illustration of the head gap region. There are some generalized assumption in the head field approximation. It is assumed that the track width is large compared to the gap length g and the flying height d so that the fields are virtually constant over the width of the track, so that two dimensional analysis applies. It is also assumed that the head is infinitely long and wide with an infinitely deep gap.
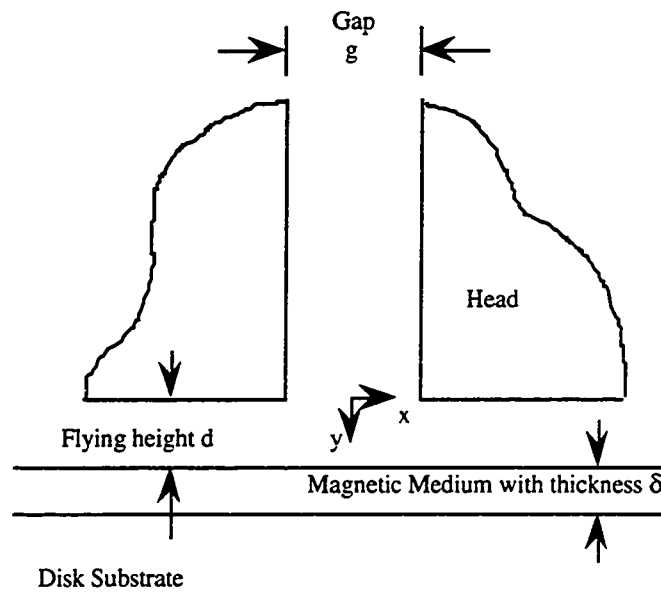
Fig. 1.5 Head Gap Region

According to classic electrodynamic theory, the surface potential of a magnetic head can be solved from the Green's function

$$H_x(x,y) = \frac{y}{\pi} \int_{-\infty}^{+\infty} \frac{dx' H_x^S(x')}{(x-x')^2 + y^2}$$

$$H_y(x,y) = \frac{1}{\pi} \int_{-\infty}^{+\infty} \frac{dx' H_x^S(x'-x)}{(x-x')^2 + y^2}$$

(1.1)

For the far field approximation, the gap is infinitesimally small, the field originates just from the center point of the head.

$$H_x^S(x) = \begin{array}{ll} H_0, & x = 0 \\ 0, & x > 0 \text{ or } x < 0 \end{array}$$

(1.2)

And the magnetic field is :

$$H_x(x,y) = \frac{NIEy}{\pi(x^2 + y^2)}$$

$$H_y(x,y) = \frac{NIEx}{\pi(x^2 + y^2)}$$

(1.3)

The medium field approximation (also known as Karlqvist Approximation), assumes that the potential varies linearly across the gap. A linear potential yields a constant head surface field across the gap:

$$H_x^S(x) = \begin{array}{ll} H_0, & -\frac{g}{2} \leq x \leq \frac{g}{2} \\ 0, & x > \frac{g}{2}, x < -\frac{g}{2} \end{array}$$

(1.4)

Integrating of Eq. (1.1) and (1.4) , the longitudinal and perpendicular components of the Karlqvist head field are obtained as:

$$H_x(x,y) = \frac{H_0}{\pi} (a\tan\frac{g/2+x}{y} + a\tan\frac{g/2-x}{y})$$

$$H_y(x,y) = \frac{H_0}{2\pi} \ln\frac{(g/2-x)^2 + y^2}{(g/2+x)^2 + y^2}$$

(1.5)
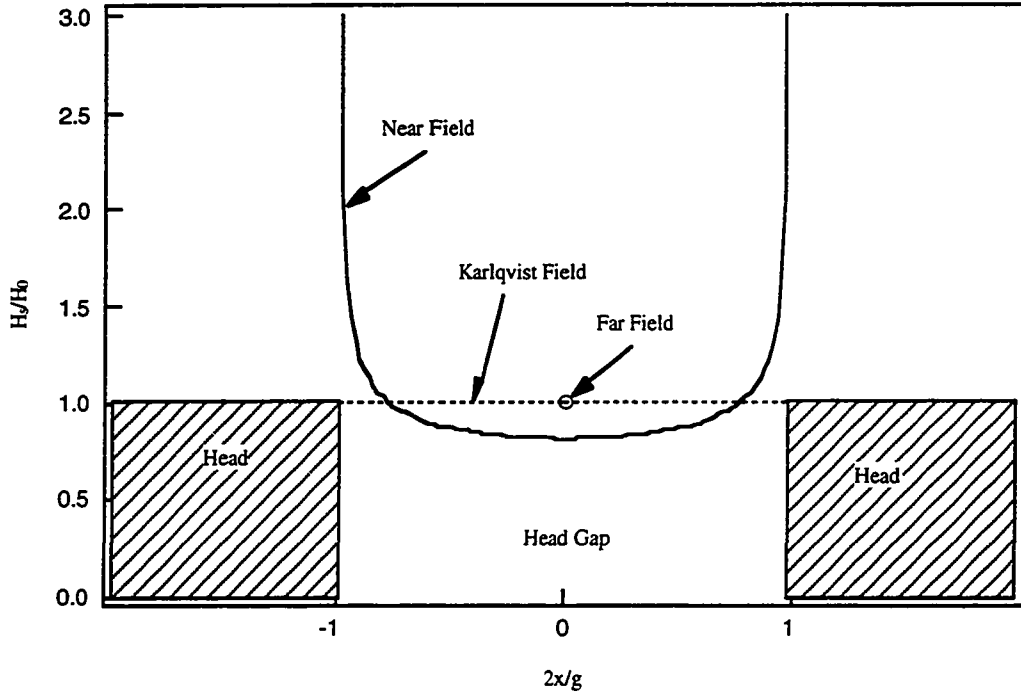
Fig 1.6 The head surface field corresponding to far-field, medium-field (Karlqvist field), and near-field approximation

The Near Field approximation takes consideration on the effect of the head poles. Therefore, it is a more realistic assumption. The head surface field is no longer constant. Instead, it is infinite when it approaches the two poles. Using conformal mapping, the 2-D boundaries are mapped into a simple infinite half-plane boundary. The solution for the half-plane boundary is well defined and can be easily obtained. Transforming the coordinates back to the normal (x,y) coordinates, the surface field across the gap is as shown in Eq. 1.6. The surface field of the head for all three different approximations are shown in Fig. 1.5.

$$H_x^s(x,) = \frac{H_0}{2}(1 + \frac{2}{\pi\sqrt{1-(2x/g)^2}}), \quad -\frac{g}{2} \le x \le \frac{g}{2}$$
$$0, \qquad\qquad x \ge \frac{g}{2} \text{ or } x \le -\frac{g}{2}$$

(1.6)

Integrating (1.1) and (1.6), the head field for near-field approximation can be described as [1.33]:

$$H_x(x,y) = \frac{H_o}{2\pi}(a\tan\frac{g/2+x}{y} + a\tan\frac{g/2-x}{y}) +$$

$$\frac{g}{2\sqrt{2\pi}}\left\{\frac{\{\sqrt{[x^2-y^2-(g/2)^2]^2+4x^2y^2}-x^2+y^2+(g/2)^2\}^{1/2}}{\sqrt{[x^2+y^2-(g/2)^2]^2+4y^2(g/2)^2}}\right\}$$

$$H_y(x,y) = \frac{H_o}{4\pi}\log\{\frac{(g/2+x)^2+y^2}{(g/2-x)^2+y^2}\}$$

$$-sgn(x)\frac{g}{2\sqrt{2\pi}}\left\{\frac{\{\sqrt{[x^2-y^2-(g/2)^2]^2+4x^2y^2}+x^2-y^2+(g/2)^2\}^{1/2}}{\sqrt{[x^2+y^2-(g/2)^2]^2+4y^2(g/2)^2}}\right\}$$

$$(1.7)$$

The longitudinal components of the head field of the three different approximations are shown in Fig. 1.6 respectively. The head fields from the Karlqvist and the near field approximation are close to each other, and but the head field gradient in the near field approximation is larger than the Karlqvist approximation. When the ratio of magnetic spacing to the field gap is less than 1/8, the near field approximation is more accurate for modeling the head field. Also it is clear that as the flying height decreases, the near field gets closer to the deep gap field H_0.
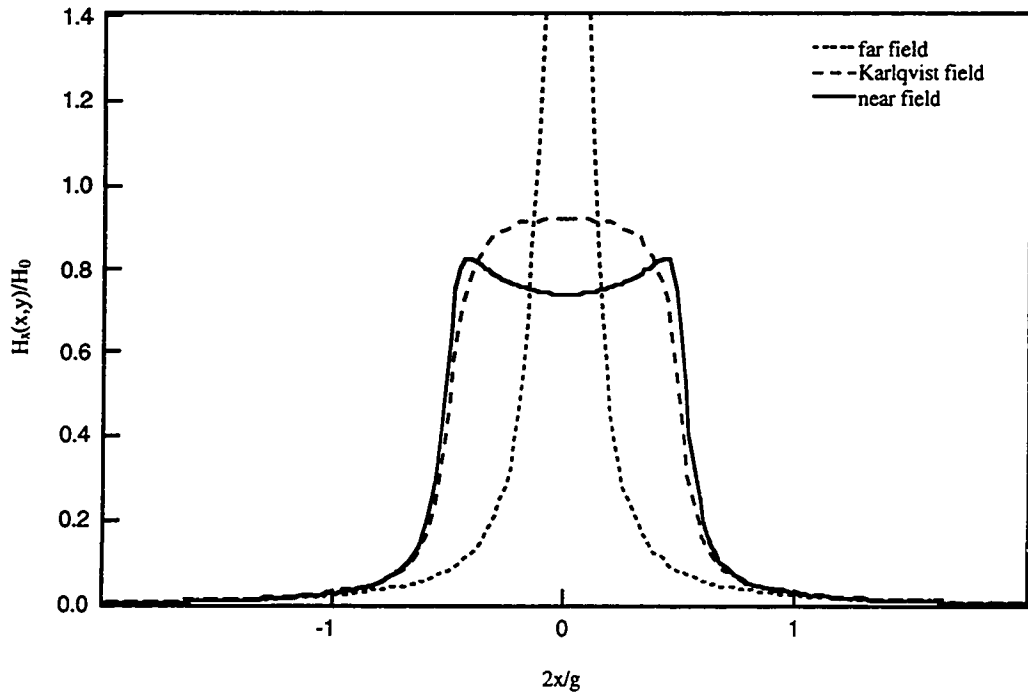
Fig. 1.7 Longitudinal field as a function of x/g for far-field, Karlqvist field and near-field approximation for y=g/16

Operating the head and disk as close as possible can maximize the performance with the available head, media and signal processing combination, but there exists constraints of media roughness, lubricant thickness and air-bearing formation at the interface. The rapid drop of the writing head field from the gap during writing greatly affects the read back signal[1.35]. Within the near contact region, a higher writing head field and steeper head field gradient can be achieved.

Both experimental observation and theoretical simulation showed that signal to media noise ratios increase with lowered head media separation, with the biggest contribution from the lowered noise level. [1.36] Medium noise is also dependent on the head field gradient. A significantly sharper head field gradient should decrease the transition noise for the media because the inherent transition noise is limited by the

head field gradient and not by the media microstructure[1.6]. The practical approach is to use a head with the smallest available gap and to fly it as low as possible.

Narrowed magnetic spacing could also benefit the read back process, improving the read efficiency at high resolution. The Wallace spacing loss factor (Eq. 1.8) can be much lower at near contact region.

$$SpaingLoss(dB) = -54.6(\frac{d}{\lambda})$$
(1.8)

λ: Written wavelength of the disk

d: the head-disk magnetic spacing

1.4 Recording Physics

1.4.1 Williams-Comstock Model

A model which predicts the shape of the magnetic transition was developed by M. Williams and R. Comstock and is referenced to as Williams-Comstock model. [1.33][1.38] It predicts that the derivative of magnetic transition M(x) at the transition location x_0 is given by:

$$\frac{dM}{dx}\bigg|_{x=x_O} = \frac{dM}{dH}(\frac{dH_{head}}{dx} + \frac{dH_d}{dx})\bigg|_{x=x_O}$$
(1.9)

The higher the value of dM/dx, the sharper the resulting transition. H_{head} is the head field, and H_d is the demagnetization field. dM/dH describes the "squareness" of the media's M-H loop. The closer the hysteresis loop is to the rectangular shape, the faster the magnetic medium switches its magnetization and the sharper the resulting transition. dH_{head}/dx is the gradient of the head magnetic field; in the other word, how fast this field decays with distance. If the gradient is large, the head field is

localized and therefore a sharp magnetic transition may be formed. Earlier in this section, we have illustrated how the head field gradient changes at different magnetic spacing, the Williams-Comstock model gives a quantitative view of how important the head field gradient will benefit the recording performance.

The Williams-Comstock model results in a length, called the transition parameter "a". It is defined as the length of the region where the transition happens. The smaller the "a" value the sharper the transition. This parameter is derived from Eq.(1.9) for longitudinal thin films.

$$a \approx \sqrt{\frac{M_r t(d + t/2)}{\pi y \left(-\frac{dH_x^h}{dx}\right)_{max}}} \approx \sqrt{\frac{M_r t(d + t/2)}{\pi H_c}} \qquad (1.10)$$

d: the non-magnetic head-media net spacing that includes medium overcoat of possible pole-tip recession.

t: thickness of the magnetic layer.

M_r: the remanent magnetization of the media

H_c: the coercivity of the media

The transition length is generally reduced by a reduction in head-medium spacing d, an increase in the loop coercivity squareness, head gradient dH_{head}/dx and a decrease in the medium flux content $M_r t$. The limitation of Eq.(1.10) is that it does not take into consideration micromagnetic effects, such as grain orientation, intergranular exchange interaction, and local magnetostatic effects.

1.4.2 Nonlinear Transition Shift (NLTS)

The demagnetization field H_d in the recording media is of great importance in determining the sharpness of the transition. And a number of important non-linear distortions in magnetic recording(hard/easy transition shift, overwrite, non-linear transition shift) are caused by demagnetization fields in the magnetic recording media.

At a distance x from the transition (where x is larger than the transition parameter a, x>a), the media demagnetized field H_d is:

$$H_d(x) = -\frac{M_r t}{\pi x} \qquad (1.11)$$

After considering the imaging effect from the magnetic head, the demagnetized field is given by Eq.(1.12). The smaller the magnetic spacing and media magnetic moment, the smaller the media demagnetization field.

$$H_d(x) = -\frac{4M_r t d^2}{\pi x^3} \qquad (1.12)$$

Generally, the non-linear transition shift (NLTS) could be calculated by Eq.(1.13):

$$\Delta = \frac{H_d}{(\frac{dH_h}{dx}\bigg|_{x=x_0})} = \frac{M_r t (d + \delta/2)}{\pi H_c B} F(d, \delta, B) \qquad (1.13)$$

M_r: the remanence magnetization

δ: medium thickness

d: the head-medium separation

H_c: the medium coercivity

B: the distance between transitions.

F(d,δ,B): a function depends on head imaging and can be unity to $(d+\delta/2)^2/B^2$.

The non-linear distortions are determined by the demagnetization field and its interaction with the head field. In order to minimize non-linear distortion, it is necessary for the head field gradient to be high and for the demagnetizing field to be small and decay fast so as to minimize the impact of the demagnetization field on the writing process. It is desirable to have low magnetic moment (M_rt), high coercivity, high squareness media and narrow magnetic spacing. When the amplitude of the demagnetized field $H_d(x)$ decreases as an inverse cube of distance, the NLTS caused by the previous transition is smaller; for a series of transitions, NLTS has fewer oscillations and settles faster if the medium is AC-erased.

1.5 Motivation and overview for the study of near field recording on FePt and FePtX intermetallic compound media

The FePt intermetallic compound has a magnetocrystalline anisotropy energy of more than 10^7erg/cc depending on annealing conditions and the degree of ordering. This large anisotropy energy yields K_uV/kT values of more than 40, with very fine grain size of 8-9 nm($V<10^{-18}$cm^3), which allows 10 years of data stability.[1.37]

The high coercivity, high anisotropy energy, and high thermal stability make FePt an attractive alternative for Co alloys as a recording media. Because the coercivity of FePt is naturally in the range of 8000-12000 Oe, it is almost impossible to write data on it with any currently available writing transducer. In this research project, we

approach this problem in two ways; using near field recording and diluting the FePt system with third elements.

Overall, the motivation and advantage for investigating FePt and near contact recording can be summarized in Fig. 1.7. The bottom line is to achieve good recording performance, such as higher signal noise ratio, better non-linear transition shift and etc. In the scope of this research, near field recording were performed using a high B_{sat} writing transducer at low flying height in near contact mode over the media. Third elements boron and nickel were added to the FePt system as a diluting agent, to decrease coercivity, saturation magnetization and anisotropy energy.
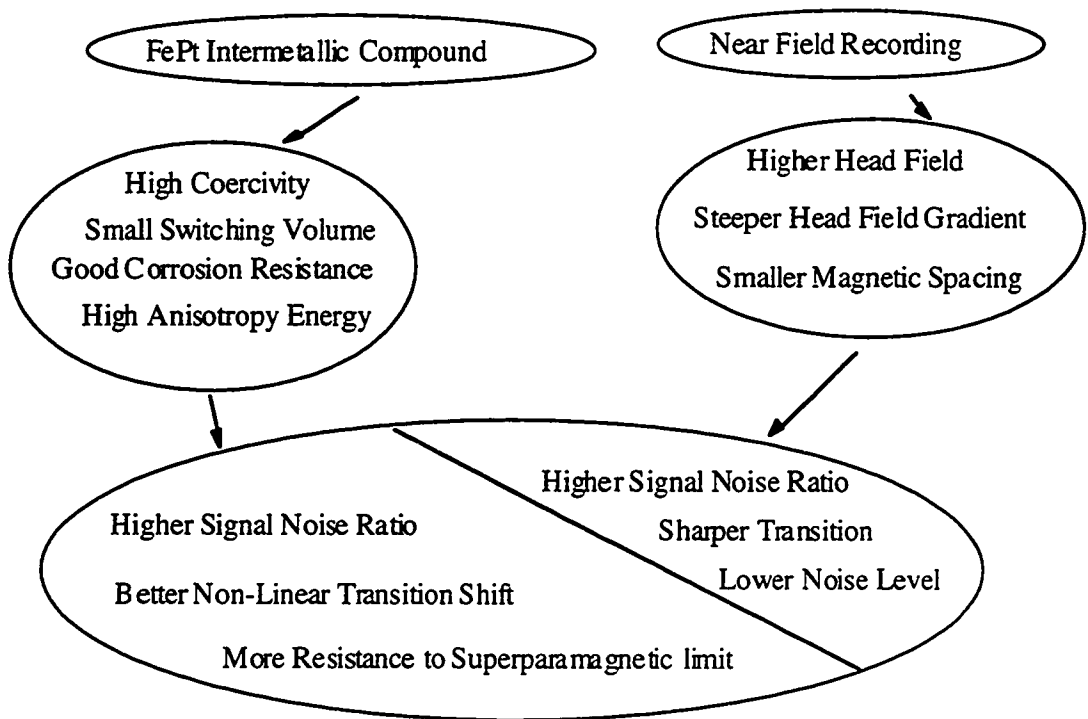
Fig. 1.8 Advantages of near field recording on FePt media

In chapter 2, different magnetometry techniques are discussed to characterize the magnetic properties of magnetic thin films. An expression for VSM Transverse

Magnetometry technique is theoretically derived. It provides a vital approach to investigate the magnetic anisotropy energy using a vibrating sample magnetometer. Chapter 3 discusses the development of high coercivity, high anisotropy energy media, and the investigation of the ordering of FePt compounds from different precursor on different substrates. Microstructure and magnetic characterization of the FePt and FePtB, FeNiPt thin films are also detailed. In chapter 4, performance of the near contact recording on FePt and FePtB media are evaluated, including the noise level, roll off curves, signal to noise ratio and non-linear transition shift. In chapter 5, suggestions for future work are proposed.

Chapter 2: VSM Magnetometry

The vibrating sample magnetometer (VSM) has become the most popular instrument to characterize magnetic thin films and recording media. Here we are going to review some basic VSM techniques, and discuss how to apply the obtained parameters in evaluating magnetic thin film as viable recording media. Also we will discuss theoretically a new technique: VSM Rotational Transverse Magnetometry(RTM), which is developed to characterize the anisotropy energy of the magnetic thin films.

2.1 Basic Magnetometry

The VSM mechanically oscillates a magnetic sample in a static magnetic field, measuring the component of M is the direction of H as H slowly varied in magnitude. Hysteresis loop and remanence magnetization curve can be routinely obtained.

2.1.1 Hysteresis Curve

Fig 2.1 shows the basic hysteresis loop for the FeNiPt thin film. The principle parameters which can be obtained from the loop are the coercivity H_c; the remanence magnetization M_r; the saturation magnetization M_s; the loop squareness S;

$$S = \frac{M_r}{M_s} \tag{2.1}$$

and the coercivity squareness S*.

$$\frac{dM}{dH}\bigg|_{H=H_c} = \frac{M_r}{H_c(1-S^*)} \tag{2.2}$$
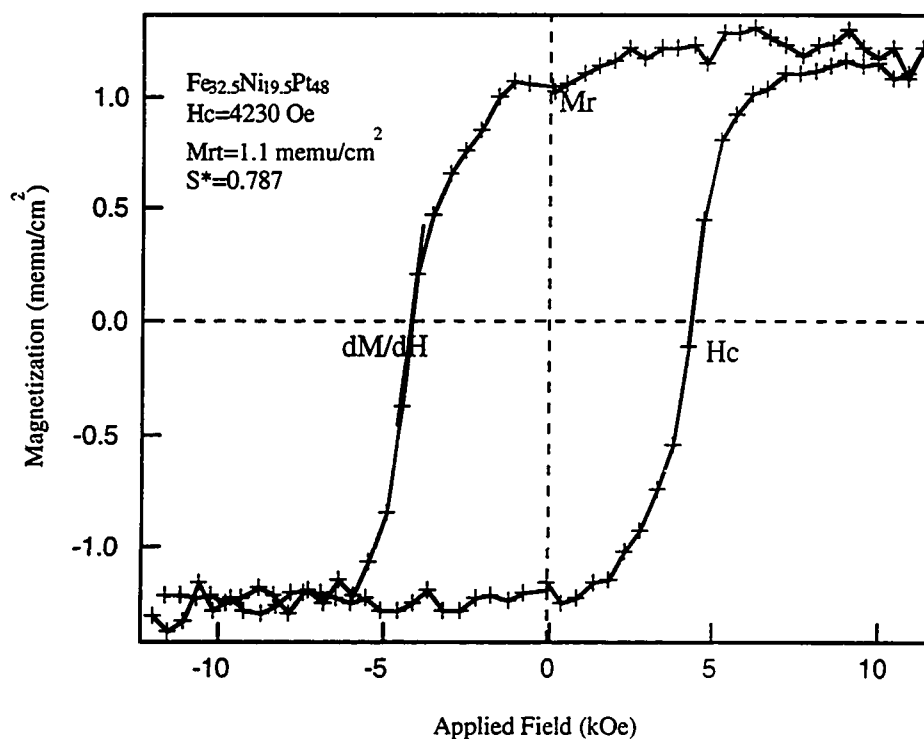
Fig. 2.1 Hysteresis loop of FePt thin film

2.1.2 Remanence Magnetization Curves

Since the hysteresis data contains components of magnetization derived from both reversible and irreversible changes, coercivity is not a field equal to the mean switching field, and only provides an ambiguous guide to the write field for a given material. It is important to study the remanence magnetization which depends only on irreversible magnetization change, since recording is only associated with irreversible changes in the media. When a single domain switches its magnetization from one anisotropy easy axis to another, the remanent state also changes. Remanence curves provide an appropriate measurement of the switching field distribution because only irreversible magnetization changes are measured.

There are two kinds of remanence curves: The isothermal remanent magnetization (IRM) and DC demagnetized (DCD). The IRM curve $M_r(H)$ is acquired starting from the ac-demagnetized state, by applying successively larger fields and measuring the remanence magnetization. The IRM remanence coercivity H_r' is defined as the field when normalized magnetization $M_r(H)=0.5$. The DCD curve $M_d(H)$ is acquired starting from the forward dc-demagnetized state $+M_{r\infty}$, applying successively larger reversal fields and measuring the remanence magnetization, until the reversed dc-demagnetization state $-M_{r\infty}$ are reached. The DCD remanence coercivity H_r is defined as the field when $M_d(H)=0$.[2.1],[2.2]

One useful extension of the IRM and DCD curves is the Kelly-Henkel plot (also called δM plot). δM is the difference between this two remanence states at a give applied field:

$$\delta M(H) = M_d(H) - (1 - 2M_r(H)) \tag{2.3}$$

where $M_d(H)$ is the DCD remanence curve as a function of the reversal field, and $M_r(H)$ is the IRM remanence curve as a function of the reversal field. Fig. 2.2 shows the ISM, DCD and δM plot for a conventional CoCrPtTa media.

δM measurement has been proposed as means of estimating the amount of intergranular exchange present in thin film recording media. In the limit of non-interacting particles[2.3], we can get:

$$M_d(H) = 1 - 2M_r(H) \tag{2.4}$$

That is $\delta M=0$. When interactions are present in the thin films, the δM value is no longer zero. The δM curve is most strongly influenced by two factors: (1)the particle interaction, either intergranular exchange coupling or magnetostatic coupling, (2)superparamagnetic, multidomain or incoherent rotation effects.[2.4] The physical meaning of the curves could

be explained by the following. Ac-demagnetization will break up the coupling between neighboring domains and minimize the domain size. The fraction of particles which switch at a particular field in IRM mode is the normalized $M_r(H)$ value, which is also the fraction of particles with no interaction and switch at a particular field. During the DCD measurement, the forward dc-demagnetized state $+M_{r\infty}$ will align particles with interactions to the field direction, the fraction of particle with interaction switching at the same particular field will be $0.5(1-M_d(H))$, the factor 0.5 is involved because the DCD curve goes from $+M_{r\infty}$ to $-M_{r\infty}$. δM is twice the difference between the fraction of particles switched at a particular field with interaction and without interaction.
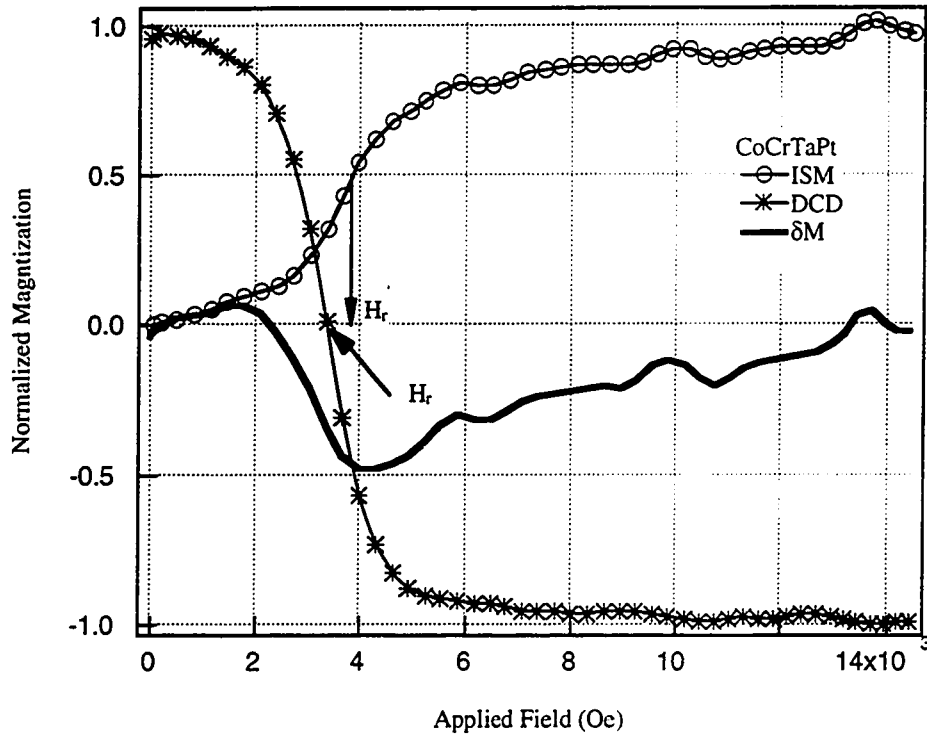
Fig. 2.2 IRM, DCD and δM curves of a commercial CoCrTaPt sample

Thus a positive δM value indicates strong positive interaction between particles, because there are fewer particles in the dc-demagnetized state that could be switched by the applied magnetic field. However, δM does not provide any information to distinguish between intergranular exchange coupling and magnetostatic coupling. On the other hand, a completely negative δM curve results from interactions that are negative. The interaction is actually promoting the magnetic switch at the same applied field, destabilizing the saturated state[2.4]. Non-zero δM implies many body effects arising from either exchange or magnetostatic interaction. Many body effects imply correlation, which can in principle be related to media noise [2.4]. Thus many papers relate δM curves to media noise.

Beardsley and Zhu [2.5] have theoretically evaluated the factors that affect δM, such as anisotropy, exchange coupling and magnetostatic coupling. They found that the domain shapes in the ac-erased state are critical in determining the shape of the δM curve. The effect of anisotropy is also dramatic. The shape of δM with essentially zero exchange depends on the anisotropy, and to a lesser extent, on the magnetostatic coupling and aspect ratio. The addition of intergranular exchange has a pronounced effect, no matter what the shape of the initial curve, shifting the ac-remanence curve to lower relative fields and promoting a positive difference. Magnetostatic coupling would cause a negative values to the δM curve but would not cause a major shape change.

The magnetic interactions within a thin film is complex. The intergranular exchange coupling depend on both the degree of segregation at grain boundaries and the exchange stiffness of the grains. Exchange coupling is a quantum effect forcing all the atomic

magnetic moments to point in nearly the same direction. The existence of exchange coupling is to lower the system's energy by aligning the uncompensated moments. Exchange coupling depends sensitively on the distance.

Interactions are believed to enhance the recording properties, by giving the media a square hysteresis loop. This is due to the alignment of the magnetic vectors when the sample is in a state of maximum remanence. As the coercivity field is reached, interaction causes particles to undergo cooperative switching, i.e. they switch in clusters rather than individually. The interaction increases media noise, because at the transition region, a contorted domain wall forms instead of a smooth ramp-like transition between bits. Randomly oriented grains form stable micromagnetic units such as circular domains, or vortices, which are energetically favored. Thus interaction is undesirable from the stand point of media SNR.

Sputtered thin metallic films typically consist of small crystallites with predominant uniaxial crystalline anisotropy and random planar distribution of their easy axes. This means they are magnetically isotropic in the plane. The major noise source in thin metallic film media is the transition noise, which originates from exchange-coupled crystallites which undergo cooperative magnetization reversals resulting in irregular zig-zag magnetization patterns in the transition region.

A strong correlation between signal to noise ratio and δM curves has been reported. Positive δM is always found in high noise media; low noise media have low positive or even negative δM values[2.6]. Generally, the higher the δM value, the higher the noise

level. Also the slope of the δM curve is reported related to the noise level, the higher the

$d(\delta M)/dH$, the higher the noise level. [2.7]

2.1.3 IFF factor

The interaction field factor [2.8] is given by

$$IFF = \frac{H_r - H_r^{'}}{H_c} \qquad (2.5)$$

Where H_r is the DCD remanence coercivity, and H_r' is the ISM remanence coercivity, as

shown in Fig.2.2. IFF is a measure of the interaction strength in the media in the region of

H_c and is therefore analogous to the δM curves. In the absence of interactions, the factor

equals zero. With strong intergranular or magnetostatic coupling, the IFF value is positive.

With weak and negative magnetostatic interaction, the IFF value is negative. Its absolute

value is proportional to the strength of the interaction.

2.1.4 H_c/H_k factor

Anisotropy field and anisotropy energy are important parameter in investigating magnetic

properties. Anisotropy is due to the spin-orbit coupling of the electron spins to the

electronic structure of the material. The greater the change in the spin-orbit coupling energy

with changes in magnetization direction, the greater the anisotropy. The uniaxial

anisotropy K_u (erg/cm^3) is simply the magnetic energy required, per unit volume to rotate

the magnetization from the easy axis to the hard directions orthogonal to the easy axis.

The anisotropy field H_k is the upper limit for the coercivity, and therefore is a prerequisite for coercivity to occur. The coercivity of the thin film is related to the distribution of the easy axis. When the easy axis of the domain aligns with the applied field, $H_c=H_k$, and the hysteresis loop is rectangular. When the easy axis does not coincide with the field direction, the magnetization reverses by a reversible rotation followed by an irreversible jump. The hysteresis loop is no longer rectangular and the coercivity depends on the orientation angle of the easy axis.[2.9],[2.10] These cases has been calculated by Stoner and Wohlfarth[2.11]. For an array of non-interacting identical particles with uniaxial anisotropy oriented at random, if only coherent rotation is assumed, the coercivity of this array is:

$$H_c = 0.48H_k \tag{2.6}$$

(A)   (B)   (C)
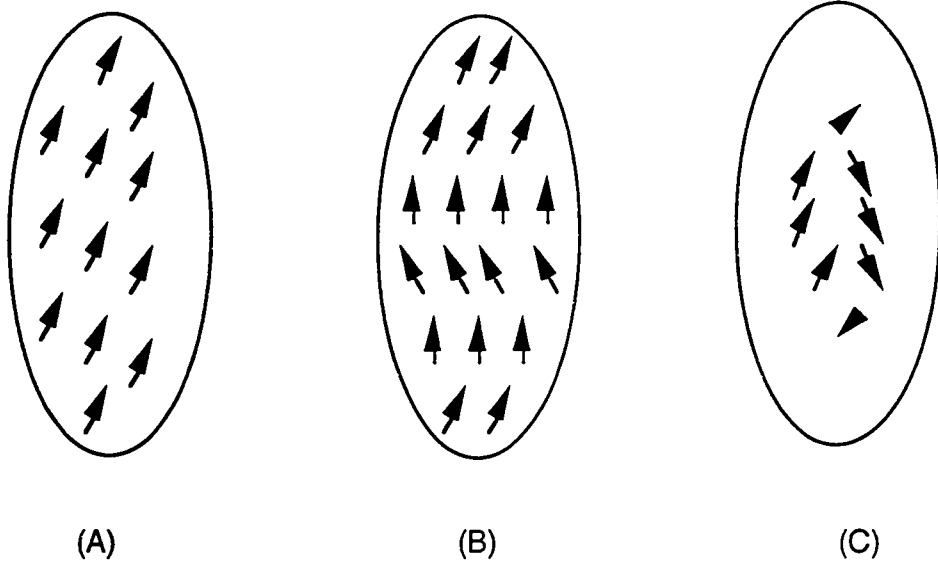
Fig. 2.3 Magnetization Reversal Modes (A) SW model with coherent rotation;

(B) Buckling or Fanning; (C) Curling

In reality, the irreversible magnetization change can take place incoherently and at a lower field than the corresponding coherent changes, leading to a decrease of the coercive force

compared to Eq.(2.5). For a metallic thin film with Stoner-Wohlfarth particulate microstructure, the magnetization reversal could be described as in Fig. 2.3[2.12], [2.13]:

(A) SW model: coherent rotation in Stoner-Wohlfarth ellipsoids or any other uniaxial single domain particle with simultaneous parallel rotation of all the atomic moments

(B) Buckling: moments reverse by fanning out in a plane, alternating in the sense of their rotation from one to the next.

(C) Curling: moments curl inside each domain

Coercivity and anisotropy field themselves are microstructural dependent parameters associating with the magnetization reversal mechanism. We adopt H_c/H_k as an indicator of the degree of incoherent rotation inside each single domain. For isotropically distributed particles with Stoner-Wohlfarth type coherent rotation (the case in the SW model), Stoner and Wohlfarth computed that H_c/H_k=0.479. Jacobs and Bean had calculated the case for the "chain-of-sphere" coherent rotation, showing that the average procedure was identical as the SW model and reported the numerical results to be also H_c/H_k=0.479. With the introducing of incoherent rotation, the H_c/H_k ratio will decrease.

2.2 VSM Rotational Transverse Magnetometry (VSM RTM) to measure anisotropy field

One way to characterize the anisotropy field is by studying magnetization change by rotation. Anisotropy field can be viewed as a barometer of the rigidity of the magnetization against rotating from a certain easy-magnetization axis. It is an intrinsic property of the material unaffected by thermal effects and reversal process. The anisotropy field is parallel to the easy axis. For a simple 2nd order anisotropy:

$$H_k = \frac{2K_u}{M_s}$$ (2.7)

where K_u is the anisotropy energy and M_s is the saturation magnetization.

2.2.1 Methods of Measuring Anisotropy Field

Measurement of the anisotropy field is usually carried out in a torque system by the rotational hysteresis loss method.[2.14]-[2.16] Theoretical curves of rotational hysteresis loss, and hysteresis integral W_r have been reported.[2.17]-[2.19] Torque measurements were made on CoCrTa, CoNiPt and CoCrPt media to evaluate the influence of the thin film microstructure on coercive force.[2.20]-[2.21] The rotational hysteresis loss, W_r, along the easy magnetization direction is plotted as a function of inverse of applied magnetic field, 1/H. Usually, W_r increases drastically with decreasing 1/H, reaches a maximum, and then gradually decreases. The magnetic field obtained by extrapolating the W_r curve in the high field region to $W_r=0$, is defined as H_k, the anisotropy field. When there are intergranular exchange and/or magnetostatic interactions, the measured value will be smaller than the intrinsic anisotropy field.[2.22] Other methods, including the experimental determination of the anisotropy distribution in ferromagnetic powders were also very intriguing.[2.23]

In this chapter, we propose a new technique, VSM Rotational Transverse Magnetization, to characterize the anisotropy field, and derive the numerical expression of the m_y-h relation.

2.2.2 Theoretical Fundamental of VSM RTM method

The thin film longitudinal media discussed here are assumed to be composed of domains with their easy magnetic axis 2-D-isotropically distributed in the media plane. Each domain with uniaxial easy axis is a cluster of Stoner-Wohlfarth type particles. Each particle is capable of coherent switching only. Each domain is capable of either coherent or other incoherent rotation as in Fig. 2.2. There exists magnetic interaction between particles inside one single domain, which means magnetization of one particle changes direction interacting with neighbor particles. The strength of this intragranular exchange is decisive on determining whether the domain will rotate coherently or incoherently. The intergranular magnetic exchange coupling was investigated by the δM curves.[2.1]-[2.5]

Because the film is isotropic, the demagnetization factor is negligible in any direction in the plane of the film.

When the applied field is small, H cannot induce any irreversible magnetization, and the transverse magnetization is zero because of the isotropy. When the field is larger than the anisotropy field, the magnetization is always aligned with H and no transverse magnetization occurs either. At intermediate fields, the magnetization follows the rotation of H at a dragged angle, resulting in different transverse magnetization values at different field strength. By extrapolating the applied field to the point $M_y=0$, we can obtain the anisotropy field $H=H_k$.

The mathematical relation between m_y and h can be numerically derived based on energy minimization. Consider a single domain in a prolate spheroid shape as in Fig. 2.4. The easy axis of magnetization is along the semi-major axis, which is also the axis of revolution. θ is the angle between the easy magnetization axis and M_s, and α is the angle

between easy axis and the applied field. When the applied field H rotates the M_s vector of a single domain out of its easy direction, the rotation takes place against the restoring force of some anisotropy.
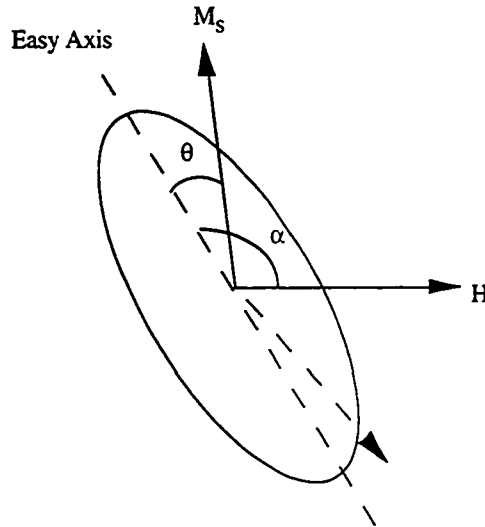
Fig. 2.4 Prolate spheroid shape domain

The anisotropy energy in this configuration is given by:

$$E_a = K_u \sin^2 \theta \tag{2.8}$$

and the potential energy due to the applied field is

$$E_p = -HM_s \cos\theta \tag{2.9}$$

so the total energy is:

$$E_{total} = K_u \sin 2\theta - HM_s \cos(\alpha-\theta) \tag{2.10}$$

Denoting $m_y = M_y/M_s$, $h = HM_s/2K_u$,

$$\frac{E_{total}}{K_u} = \sin 2\theta - 2h\cos(\alpha - \theta) \tag{2.11}$$

And the equilibrium position of M_s is determined by $dE_{total}/d\theta = 0$,

$$\frac{dE_{total}}{d\theta} = 2K_u \sin\theta\cos\theta - HM_s \sin(\alpha - \theta) \qquad (2.12)$$

The relationship between θ and α is:

$$\alpha = \theta + \sin^{-1}\frac{\sin 2\theta}{2h} \qquad (2.13)$$

which gives θ multiple values corresponding to a certain α value as in Fig. 2.5.
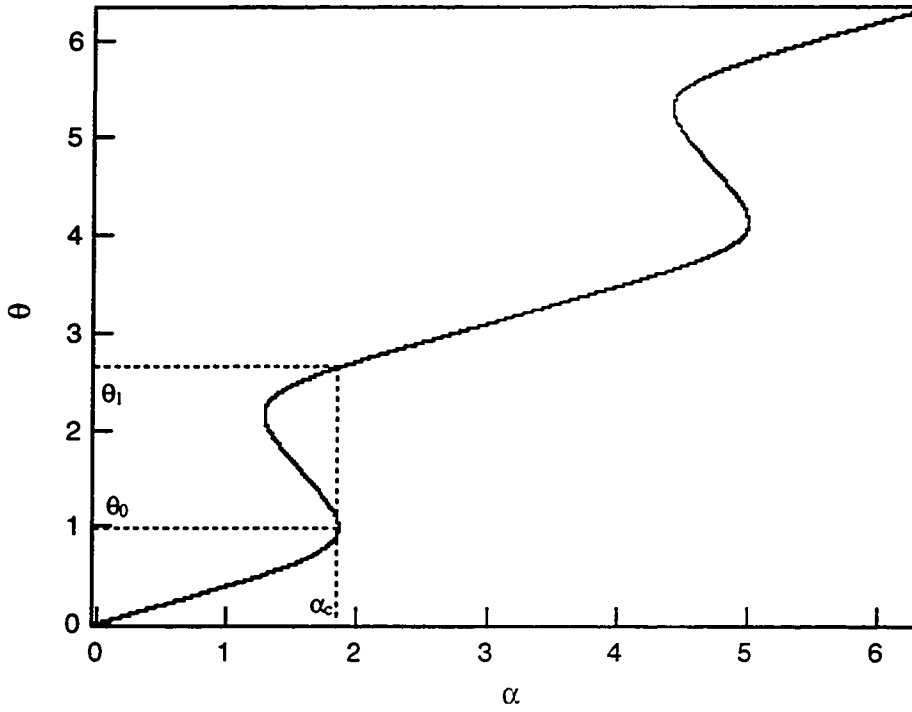
Fig. 2.5 The relationship between α and θ

The transverse magnetization is :

$$m_y = \frac{M_y}{M_s} = \sin(\alpha - \theta) \qquad (2.14)$$
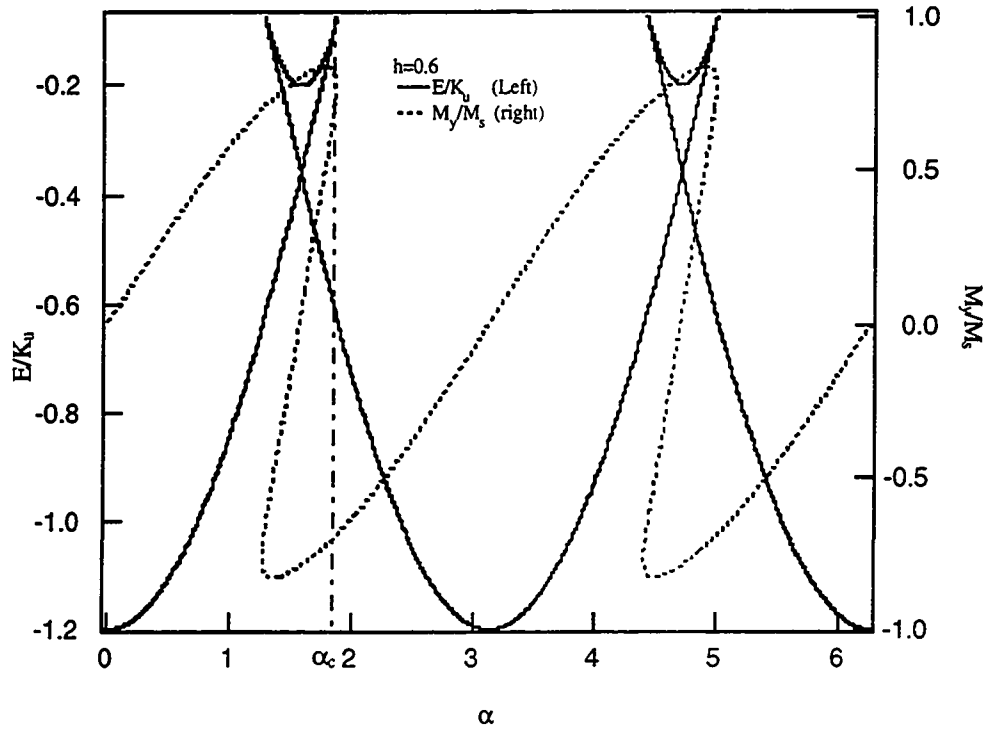
Fig. 2.6 E/K_u and M_y/M_S vs. α
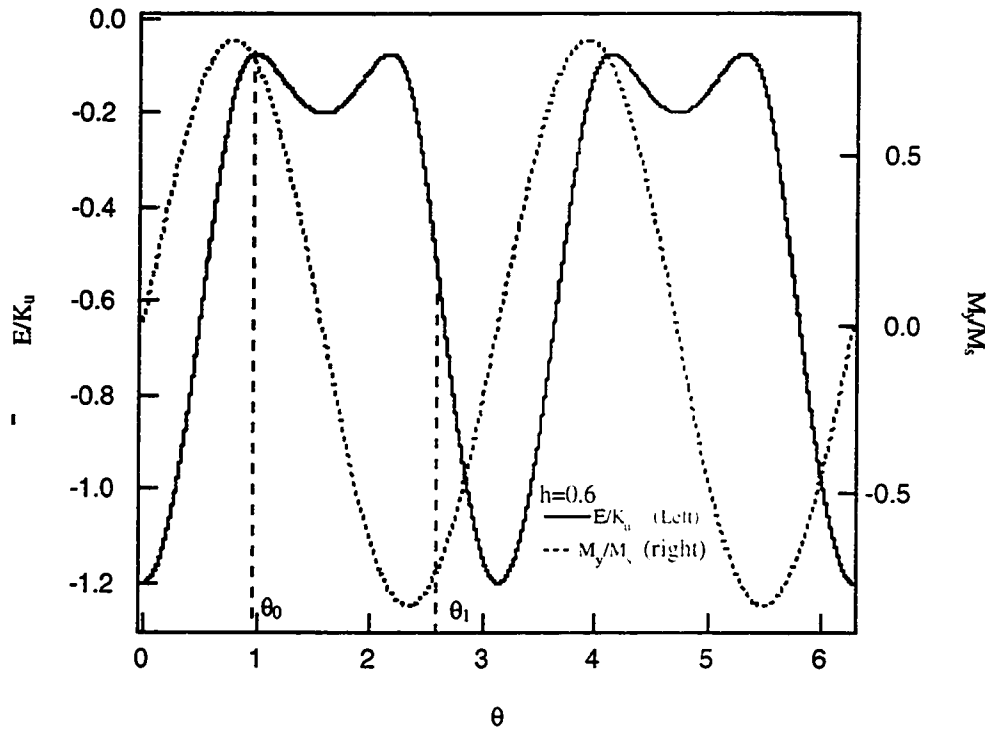
Fig. 2.7 E/K_u and M_y/M_S vs. θ

For each h value, the total energy and the transverse magnetization can be calculated. Fig. 2.6 and Fig. 2.7 show how at h=0.6 the total energy and transverse magnetization evolves with α and θ according to Eq.(2.9) and Eq.(2.12).

It would be more vivid to perform a transition in thinking, and to transfer the analysis of the 2-D isotropic distribution of easy axis into considering the behavior of the magnetization vector M_s when the domain is rotating about the applied field, as in Fig. 2.4. Starting from where M_s and the easy axis are parallel to H, with an anti-clock-wise rotation, M_S will lag behind the easy axis with an angle θ when α is smaller than $\pi/2$. When α exceeds $\pi/2$ and reaches a certain critical angle, α_c(as in Fig. 2.6), M_S will spontaneously flip to the fourth quadrant, as shown in Fig. 2.4 by the dashed arrow. This critical angle α_c depends on the strength of h, and corresponds with a θ_0 and θ_1 ($\theta_0<\theta<\theta_1$) values according to Eq (2.11) and Fig.(2.5), which are labeled in Fig.2.5.

$$\alpha(\theta_0) = \alpha(\theta_1) \tag{2.15}$$

It is obvious from Fig. 2.6 that α_c would correspond with two possible energy states decided by Eq.(2.6). At the critical angle α_c, M_S will flip to the lowest energy state. And it is clear now that those states in between $\theta_0 < \theta < \theta_1$ will be skipped over during the spontaneous flipping, since they are unstable.

The contribution to the hysteresis loss come from the irreversible magnetization changes, which only occur over the range 0.5<h<1. Based on the minimum energy principle, for

each reduced field h(h=0.5~1), we integrated m_y (h,θ) for each domain in the 2-D

distribution in range θ=0~2π, the actual m_y(h) is as following:

$$m_y(h) = \int_0^{\theta_0} m_y(h,\theta)d\theta + \int_{\theta_1}^{\pi} m_y(h,\theta)d\theta \qquad (2.16)$$

The calculated m_y (h) raw data are plotted in Fig. 2.8. It is very much similar to the

classical calculation of the hysteresis loss in torque technique in reference [2.15].
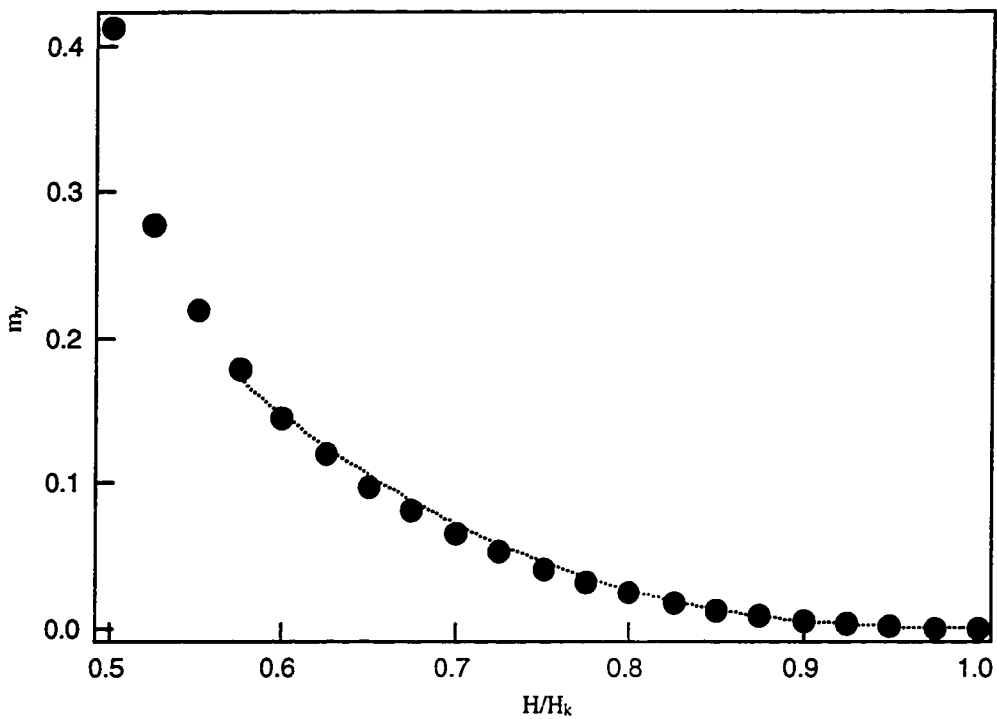
Fig. 2.8 m_y vs. h

Various kinds of polynomial functions were used to fit the m_y-h curve. Several functions

look fine on the theoretical value, but some exaggerate the error range or extrapolate

measured m_ys into negative H_k values. Others will give more stable results. We find that

Eq.(2.15) will give a precise extrapolation for H_k, the fitting function is the dashed curve

in Fig 2.8, where A=1.1434, and H_k is the anisotropy field. In curve fitting to experimental data, both A and H_k are fitting coefficients.

$$\frac{M_y}{M_s} = A(1 - \frac{H}{H_k})^{2.5}$$ (2.17)

There are certain limitations in this model. We did not go into the detail of the magnetization reversal mechanism inside each domain. We assumed they are all coherent rotation. We also omitted the interaction between neighboring domain. In reality, an interaction-dependence of the effective shape anisotropy coefficient should be taken into consideration, as well as a mutual magnetization change due to an interaction dependent rotation of the magnetization vector. [2.24]

2.2.3 Experimental Procedure for Transverse Magnetometry

In transverse magnetometry, the sample is mounted parallel to the direction of the applied field as in Fig 2.9. The detection coils need to be properly connected so that the M_y vector is measured, unlike the usual hysteresis loop measuring M_x and H using VSM.

At a fixed field, the sample is rotated both clockwise and anti-clockwise along the surface normal n as in Fig. 2.9. The transverse magnetization M_y is measured in each case. The resulting magnetization after rotation is depicted in Fig 2.10. The difference of the two measurements is twice the absolute value of the transverse magnetization, which arises from the delay the magnetization experiences with respect to the rotating applied field. By ramping the applied field, the relationship between M_y vs. H is obtained, and the M_s value could be derived from the hysteresis loop. The m_y–h is fitted by Eq.(2.17), and H_k value could thus be deduced.
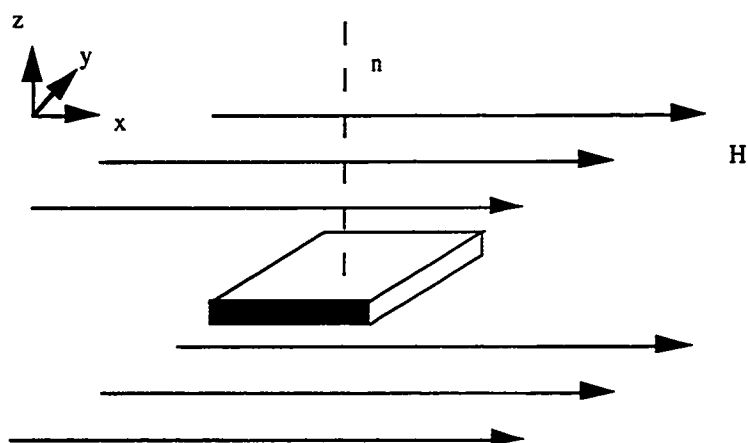
Fig. 2.9 Sample Mounting of Transverse Magnetometry
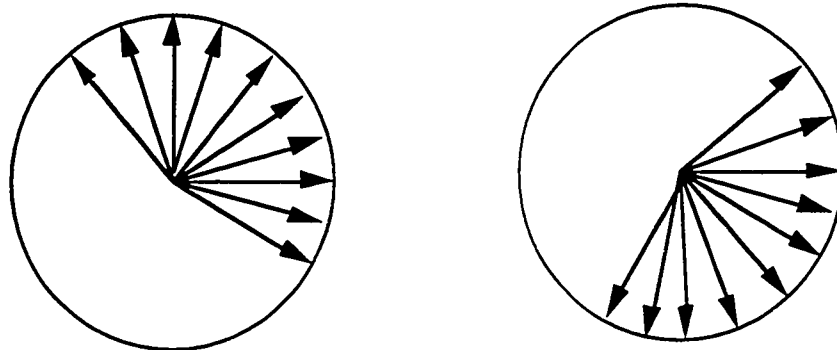
(a) Approch from clock-wise rotation   (b) Approach from anti-clock-wise rotation

Fig. 2.10 Transverse Magnetization from both clock-wise and anti-clock-wise rotation

2.2.4 Comparison of VSM Rotational Transverse Magnetometry and

Torque Rotational Hysteresis Loss Method

Bean and Meiklejohn had published a short bulletin about the calculation of the rotational hysteresis, i.e. the work required to slowly rotate a specimen 360° in a magnetic field[2.25]. The major part of their publication[2.25] is quoted as following:

"The computation is facilitated by the careful calculations on alternating hysteresis in single domain particles presented in the classic paper by Stoner and Wohlfarth. The principle results are that the rotational hysteresis is identically zero for fields less than half the anisotropy field H_k. $H_k=2K/M_s$, has a value for an aligned aggregate of 2.6K per cubic centimeter of ferromagnetic material at $H_k/2$, and falls rapidly with increasing fields. It becomes again identically zero for fields greater than the anisotropy field. Experimental measurements have been made on single domain particles of cobalt. Application of the calculation whose results are described above give an unambiguous measure of the distribution of anisotropy present which in principle permit a prediction of the magnetization curve. Due to the simplicity of analysis for anisotropy distribution, this technique is extremely useful in the study of single domain particles. "

Many papers has quoted this short bulletin, but unfortunately no detailed calculation was found, and a subsequent paper they claim would be published could not be located.

Since the torque value equals M_y*H, we plot the calculated results in the from of $(M_y*H)^{0.5}$ vs. $1/h$ in Fig. 2.11(b), to simulate the traditional torque rotational hysteresis loss curve. The torque rotational hysteresis loss curve doesn't exactly follow a straight line when H_k/H

approaches 1. Using a linear fit as many researcher have adopted will over estimate the H_k value, as shown in Fig. 2.11(b). While using our Eq.(2.17), the fit is very reasonable and more realistic, as shown in Fig. 2.11(a). More experimental data supporting this analysis is discussed in Chapter 3.
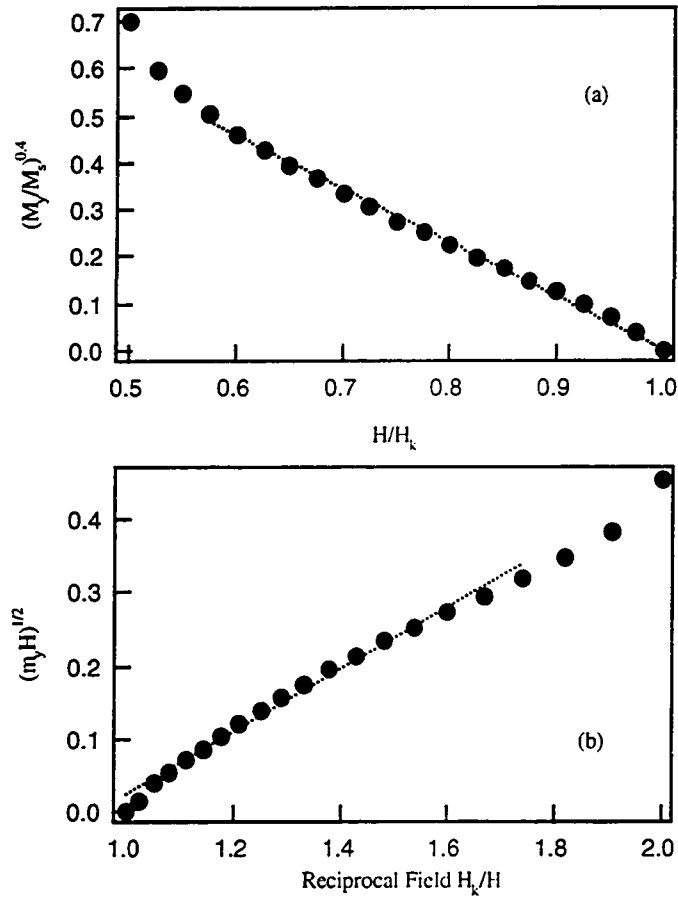
(a) Transverse Magnetization vs. H/H_k. dashed line is fitting curve
(b) Torque vs. H_k/H, dashed line is linear data fitting

Fig. 2.11 Numerical resolution of m-h relations

Chapter 3: Deposition and Characterization of FePt and FePtX (X=B, Ni) Intermetallic Compounds

Advanced magnetic disks are engineered both to support high density recording and to provide a very durable surface necessary for low flying heads across the disk surface. The disk is formed by sputtering thin magnetic and protective overcoat layers on very flat, low defect substrates. The switching volume is an important consideration in that it influences the media noise and thermal stability in high density magnetic recording. It is affected by the deposition conditions, such as magnetic layer thickness and sputtering pressure.

3.1 FePt, FePtB and FeNiPt Media Deposition

3.1.1 Experimental Details

FePt and FePtX(X=B, Ni) thin films were deposited in a high vacuum magnetron sputtering system from elemental sources onto heated substrates. The chamber was equipped with a 14" APD cryopump and multiple 1.3" sputtering sources. The samples were mounted 6" from the sputtering sources. The base pressure of the system was 8×10^{-9} Torr at room temperature, and 5×10^{-8} Torr at 450°C. The composition was adjusted by changing the sputtering power of each source. During cosputtering, the Fe, Pt and B or Ni elemental sources were confocally aimed at the substrate. For multilayering, the Pt/Fe structure was produced by sequential deposition of 15 monolayers of Pt (2.86nm) alternated with 15-monolayers of Fe (2.1nm). Subsequent annealing was carried out for all samples in a separate high vacuum furnace. The ordered $L1_0$ phase emerged from both of the cosputtered and the multilayered precursors. The furnace was equipped for precise temperature

control and was maintained at vacuum of 2×10^{-7} Torr at high temperature. X-Ray diffraction was used to characterize microstructures of the samples, and vibrating sample magnetometry was used to determine magnetic properties.

For ZrO_2 substrates, the optimized furnace annealing condition was found to be at 450°C for 8 hours. Based on the results of the small pilot samples, corresponding disks were sputtered on ZrO_2 substrates. The disks were annealed inside the sputtering chamber immediately following deposition. Heating was performed using tungsten wires behind the sample holder. Temperature measurements were obtained from a thermocouple attached to the back of the sample holder. This method allowed an entire 65mm disk to be annealed, but with considerably less control over the annealing conditions. Subsequent to annealing, 15nm of hydrogenated carbon was deposited onto the sample surface as a wear protection layer.

3.1.2 Substrate Selection

In order to syntheses ordered intermetallic alloy thin films such as FePt and FePtX (X=Ni, B), a high temperature substrate must be used. The requirements for a successful high temperature (e.g., up to 550°C) substrate are:(1) no harmful reaction with magnetic thin films during sputtering or high temperature, (2) no distortion by the heat treatment, and (3) no surface relaxation, such as relieving of residual stress, resulting in a surface undulation. We found that chemically strengthened glass and Si_3N_4 with a glass boundary phase were not thermally stable enough. Single crystal sapphire is extremely inert at high temperature, but too costly as a substrate material due to difficulties in processing. In addition, its crystallographic orientation may contribute to directionality of magnetic film properties.

Table 3.1 Properties of selected substrates

	ZrO$_2$*	Sapphire**	Si***	Glass***	NiP/Al***
Density (g/cm^3)	6.0	4.0	2.3	2.5	2.7
Young's Modules (GPa)	225	470	117	83	71
Hardness (GPa)	12.3	17.6	9.3	5.8	4.9
Thermal Conductivity (cal/cm sec K)	0.1	0.014	0.3	0.003	0.3
Thermal Expansion Coefficient (10^{-6}/K)	10.5	7.7	3	9	23
Heat Resistance (°C)	2677	2053	>1000	500	280

Data provided by:

*Saint-Gobain Industrial Ceramics Inc.

**Kyocera Corp.

***Shin-Estu Chemical CO., Ltd

Norton ZrO$_2$ substrates having polycrystalline grains of about 1μm were used in this study. The ZrO$_2$ was sintered from a powder compact of near net shape to about 98% of theoretical density prior to a hot isostatic pressing in an inert atmosphere to eliminate any pits and pores. This substrate does not exhibit any crystallographic orientation according to X-Ray diffraction, indicating a substantially random orientation. ZrO$_2$ has a relatively high Young's modulus of 225 GPa, which is about 3 times higher than those of aluminum alloy and glass substrates.

The present results indicate that the ZrO$_2$ substrates satisfy most requirements for high temperature substrates, enabling the development of new magnetic media. It is plausible that other polycrystalline substrates may be developed in the future to

facilitate a more broad approaches to develop the next generation media for a very high areal storage density beyond 10 Gbits/in^2.
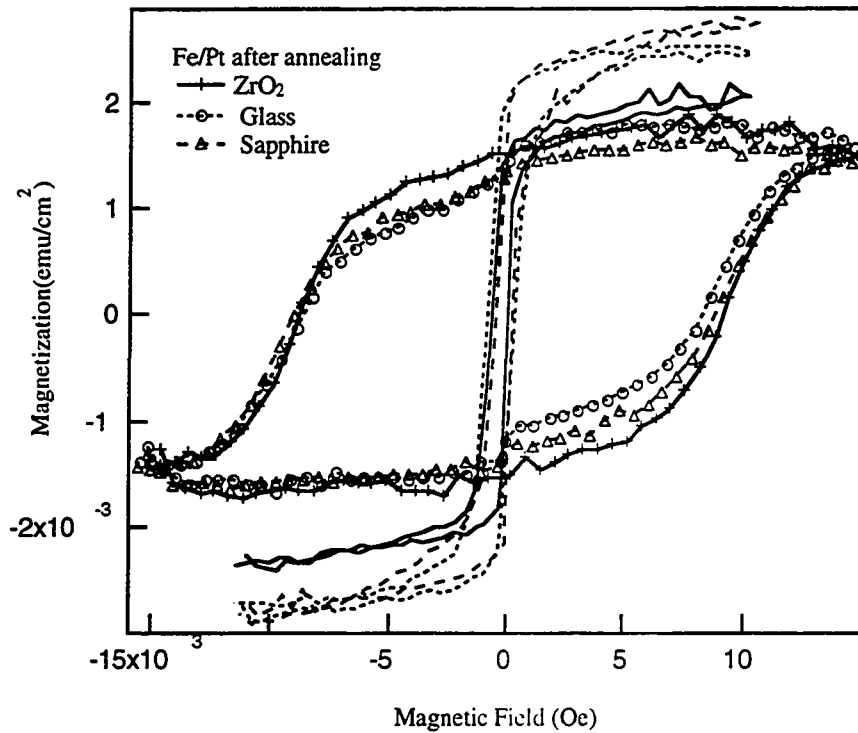
Fig. 3.1 Fe/Pt ordering on different substrate after same annealing

Disordered FePt and layered Fe/Pt were deposited onto untextured glass, Si_3Ni_4, ZrO_2 and R-plane-sapphire substrates. Generally, the sapphire and ZrO_2 substrates produced higher coercivity than glass or Si_3Ni_4 after annealing. To achieve comparable magnetic properties on glass substrates required much higher annealing temperature (550℃), sometimes resulting in deformation of the glass substrate.

3.1.3 Seed Layer Effect

The importance of crystalline orientation to thin film recording media is well known. For longitudinal recording with conventional hexagonal cobalt alloy media, seedlayers

have been required such as Cr or CrV, in order to achieve longitudinal magnetization. FCC metallic thin films tend to orient with a [1 1 1] fiber texture, and sometimes seed layers are used to promote epitaxial growth.
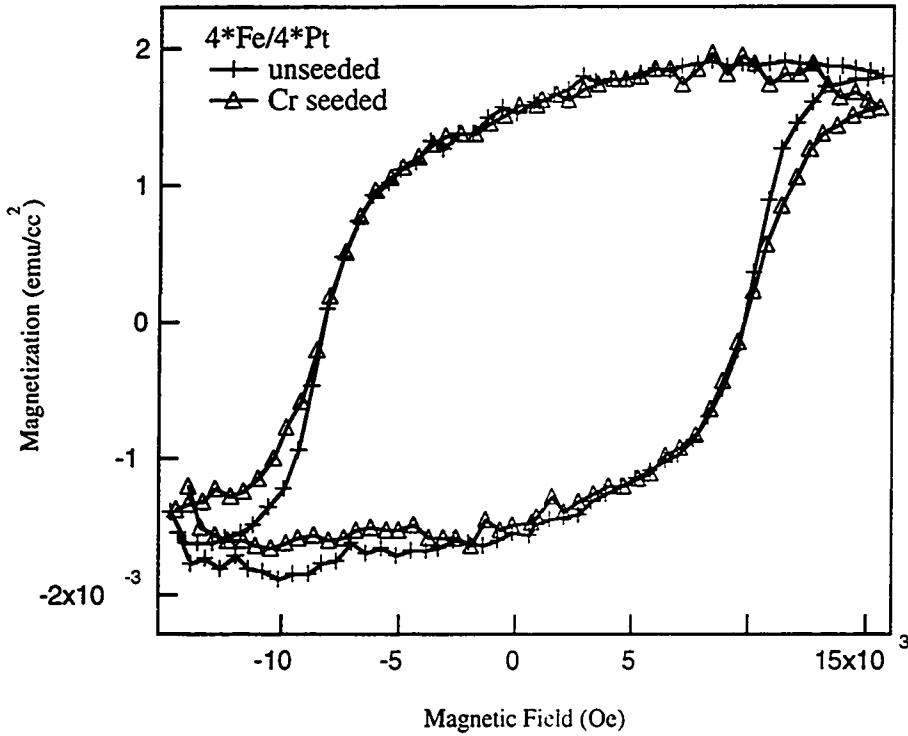
Fig. 3.2 Cr seed layer effects on ordered Fe/Pt

In our FePt system, a Cr seed layer yielded no distinguishable difference in coercivity and squareness of the M-H loops between samples with and without seed layer(Fig. 3.2). While a Cr seed layer might induce lower remanent magnetization, the possible reaction between Cr and Fe or Pt during annealing was judged to be unpredictable. So the samples developed and reported here used no seed layer.

3.1.4 Third Element Additive Approach

The binary FePt has coercivity too high for currently available write transducers, as the read/write results in chapter 4 will illustrate. To bring down the coercivity to a feasible value, parameters such as film thickness and sputtering pressure could be engineered, but third element additive is an attractive approach. During the processing, it was observed that lower thickness and higher sputtering pressure resulted in lower coercivity for the binary FePt intermetallic compound, consistent with other publications [3.1][3.2]. The changing in the sputtering gas pressure is expected to vary the strain-induced preferred phase transformation. Since a lattice axial ratio c/a is below unity, it has been suggested that compression stress along the c-axis is preferred to transform the FCC into FCT. These approaches were not explored in this dissertation.

Element additives in magnetic thin films have been known as an useful approach to reduce grain size, improve grain isolation and reduce coercivity. CoTi doping is well known for reducing the magnetocrystalline anisotropy while maintaining the saturation magnetization of barium hexaferrite. [3.3] Zirconia ZrO_x doping has been used to decrease the coercivity in the CoPt $L1_0$ system. [3.4]

Two kinds of additive, boron and nickel, have been cosputtered into the FePt system. Boron is expected to be immiscible with Fe and Pt; and upon annealing, it will precipitate to grain boundaries and provide phase segregation and inhibit grain growth. An FePtB disk was prepared and tested, although this sample was substantially less homogeneous than the others, as illustrated by the low value of coercivity squareness S* in Table 3.2. The boron concentration was measured to be

about 2% using wavelength-dispersive spectrometry(WDS), which was in agreement with the measured sputtering rate.

The mechanism for nickel doping is different, it is a case of ionic substitution employed to decrease the anisotropy and coercivity. When the nickel is substituted on some Fe sites, the crystal structure and magnetic order are changed. Sometimes, the tenary system is mentioned as quasibinary because the phase equilibrium in the FePt-NiPt system obey the Gibbs phase rule for binary systems.[3.5]. The 50at% Pt is retained and the iron is partially replaced by nickel. The nominal composition was chosen to cover the range from FePt to $Fe_{0.25}Ni_{0.25}Pt$. Usually the disorder-order transition reaction rate is lowered with increasing nickel composition. [3.6] [3.7]

3.1.5 Microstructure Characterization

Intermetallic compounds distinguish themselves from conventional alloy systems by having a particular stoichiometry, a certain type of chemical bonding and crystal structure. They also have specific physical and chemical properties, and a unique mode of formation. Their crystal structure is different from the crystal structure of their constituent chemical elements. So the analysis of the crystal structure is of importance in characterizing the intermetallic compounds.

The crystal structure of FePt was investigated in both the as-deposited and annealed samples so as to understand the resulting magnetic properties. Low-angle X-ray Reflectometry can provide detailed information about the thin film thickness. The low angle pattern features a steadily decreasing intensity of reflection due to the roughness, and oscillation peaks due to the finite layer thickness. In the kinematical

approximation, the angular distance between successive maxima relates to the thickness of the layer via a law similar to Bragg's law.

$$2t(\sin \theta_{i+1} - \sin \theta_i) = \lambda \qquad (3.1)$$

where i is the order of the reflection, and t is the thickness of the film. Low angle X-Ray Reflectometry scans were carried out on a Siemens powder diffractometer for thickness measurement. Fig. 3.3 is an example of the Disk FePtB, with a calculated thickness 28.6nm.
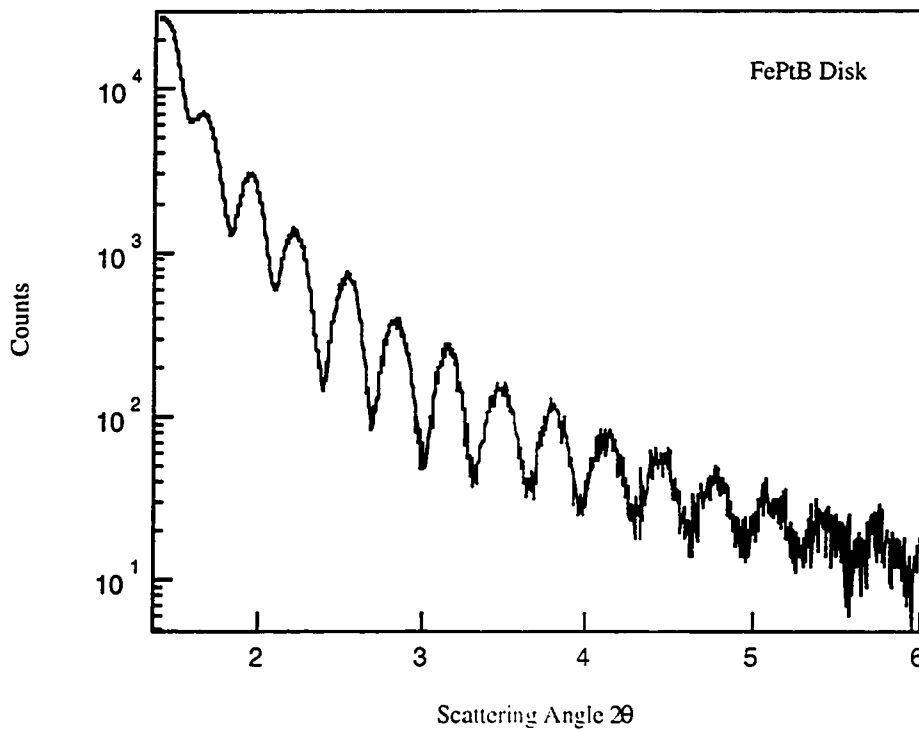
Fig. 3.3 Low Angle Reflectometry to calibrate thin film thickness

X-Ray diffractometry scans were performed on a Siemens D-5000 four-circle diffractometer for phase identification. The face-centered-tetragonal cell was used in peak identification because of the relationship between the ordered superlattice phase to the disordered FCC FePt phase. Figure 3.4 shows the X-Ray patterns of the as-

deposit and annealed FePt films. The as-deposited pattern exhibits a disordered FCC structure with a=3.8Å. The [111] axis is the preferred orientation in the direction perpendicular to the film plane, with some Pt(111) at the neighboring lower angle. The annealed pattern shows the (001), (110) and (112) superlattice lines of the annealed film. These peaks are not allowed by FCC symmetry but confirm the existence of an ordered FCT structure with and c=3.76Å (c/a~0.97). Rocking curve measurements showed no texture in the annealed samples. For the FePtB sample(Figure 3.5), the general observation of the FCC forbidden (001) peak at 23° after anneal indicated the ordering from FCC to FCT structure.
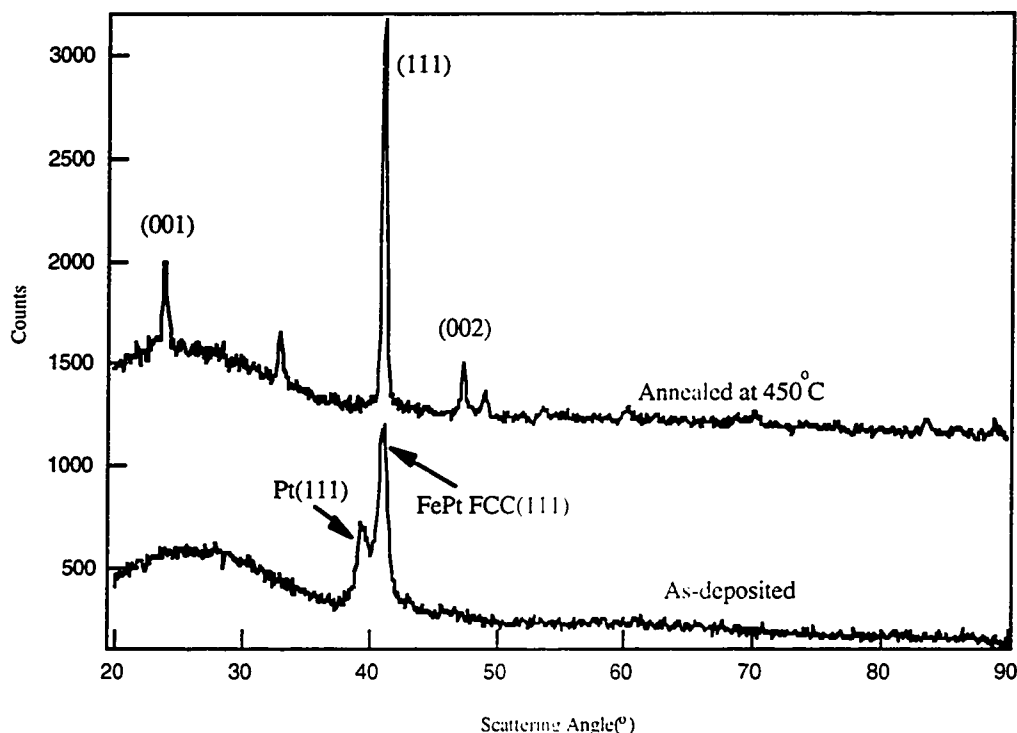
Fig. 3.4 Siemens D-5000 symmetric scan of FePt pilot sample

as-deposited and after annealing at 450°C for 8 hours
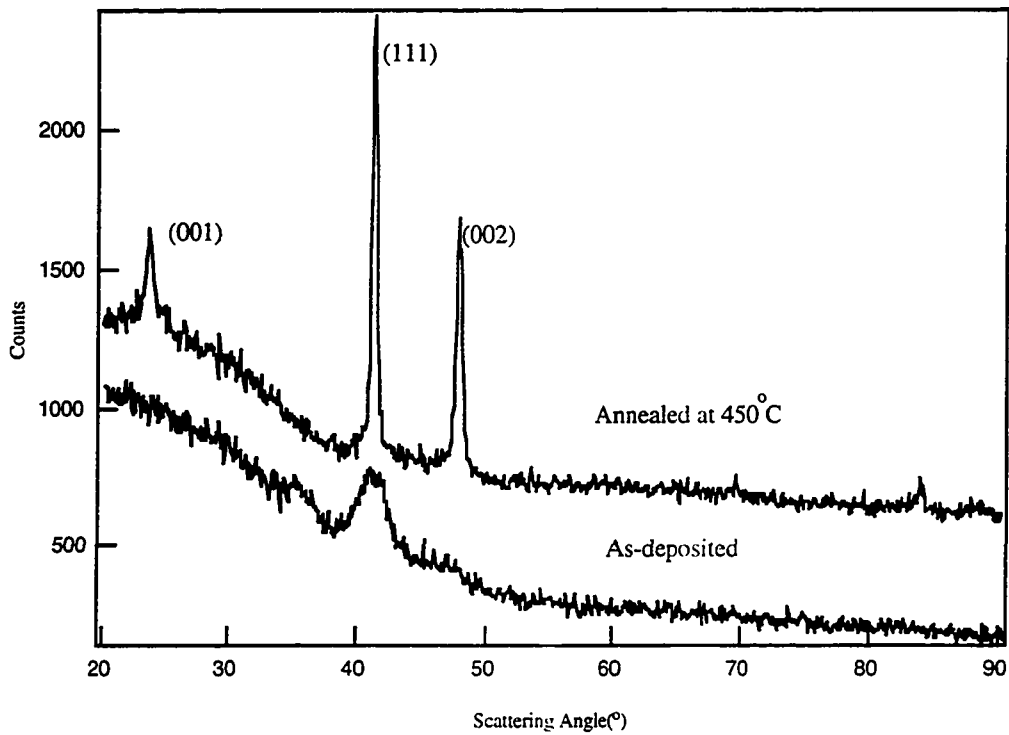
Fig. 3.5 Siemens D-5000 symmetric scan of FePtB pilot sample

as-deposited and after annealing at 450°C for 8 hours

Asymmetric scans were carried out on a Siemens Area Detector Diffractometer to determine grain size and the degree of chemical ordering[3.8]. The breadth of the diffraction peaks $\Delta 2\theta$ depends inversely on the grain diameter D and is also related to the inhomogenous strain distortion, Δd, as:

$$\Delta 2\theta \cos\theta = \frac{\lambda}{D} + 2(\frac{\Delta d}{d})^2 \sin\theta \qquad (3.2)$$

From the linear plot of $\Delta 2\theta \cos\theta$ vs. $\sin\theta$ in the inset to Fig. 3.6, the grain size, calculated from the intercept, was 24.2 nm for an FePt pilot sample annealed at 450°C for 8 hours. No significant difference was observed between the sizes of FCC

allowed and FCC forbidden peaks, suggesting that each crystal grain in the film consists of one tetragonal domain. This was generally observed in the annealed samples.
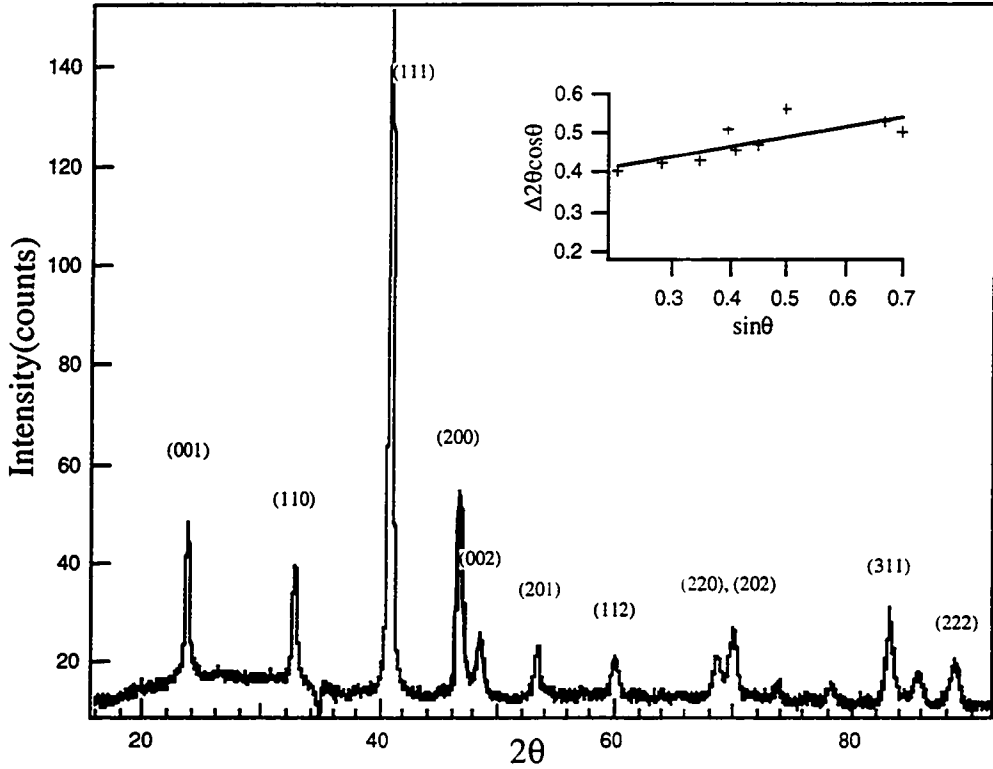
Fig. 3.6 Siemens GADDS scan of FePt pilot sample after annealing at 450°C for

8 hours. The inset is the extrapolation of grain size from peak width

The chemical ordering parameter S is defined as in Eq.(3.3). S reaches unity for perfectly ordered films of the stoichiometric composition of $Fe_{50}Pt_{50}$, and is zero for a chemically disordered film.

$$S = \frac{r_{Fe} - x_{Fe}}{y_{Pt}} = \frac{r_{Pt} - x_{Pt}}{y_{Fe}}$$ (3.3)

$x_{Fe(Pt)}$: the atomic fraction of Fe(Pt) in the sample

$y_{Fe(Pt)}$: the fraction of the Fe(Pt) sites

$r_{Fe(Pt))}$: the fraction of Fe(Pt) sites occupied by the right atomic species

The long range degree of ordering can be calculated using the ratios of integrated intensity from superlattice and fundamental peaks with an approximate Debye-Waller temperature correction [3.9]. The long range order parameter was determined from the ratio of the integrated area of the fundamental peak(002) and the superlattice peak (001).

$$A_{001}/A_{002}=(A_{001}/A_{002})_{S=1}*S^2 \qquad (3.4)$$

For the FePt sample in Fig 3.5, (002) peak was carefully separated from the (200) peak by double-Lorentzian curve fitting. The area of either a fundamental or a superstructure peak can be expressed as:

$$A \propto (LP)FF^* \qquad (3.5)$$

where LP is the Lorentz polarization factor for a single crystal and F and F* are the structure factor and its complex conjugate. For the $L1_0$ structure, we have

$$
\begin{aligned}
(FF^*)_{fund} &= 16(x_{Fe}f_{Fe}e^{-MFe} + x_{Pt}f_{Pt}e^{-MPt})^2 \\
(FF^*)_{super} &= 4S^2(f_{Pt}e^{-MPt} - f_{Fe}e^{-MFe})^2
\end{aligned}
\qquad (3.6)
$$

for fundamental and superlattice peaks respectively. e^{-M} is the Debye-Waller correction and f is the atomic scattering factor.

Table 3.2 Parameters used to estimate the chemical ordering for FePt

Peak	$T_{debye}(K)$	LP	M_{Fe}	f_{Fe}	M_{Pt}	f_{Pt}
(001)	430	44.57	0.0063	21.7	0.00603	69.73
(002)	230	9.31	0.025	16.72	0.024	58.58

Using the data is Table 3.2, the area ratio of (001) and (002) peaks were calculated to be calculated to be 2.01, which is very close with using the value from standard PC-PDF data. The calculated order parameter for $FePt/ZrO_2$ after 8 hours annealing was S=0.83.

The magnetic ordering provides the FePt system with high magnetocryatalline anisotropy, the orientational preference of atomic moments in a crystal for certain crystallographically equivalent directions. It is broadly understood that the anisotropy associated with any magnetic atom derives from the coupling between the spin and orbital moments of its d or f electrons. The orbital electronic motion interacts, in return, with the electrostatic fields produced by the local crystalline environment. The magnetocrystalline anisotropy depends on the crystalline symmetry and is weakest when the symmetry is highest. So when the chemical ordering brings the symmetry from 4-fold cubic to hexagonal, the crystalline anisotropy becomes large[3.5].

3.2 Magnetic Characterization of FePt, FePtB and FeNiPt compounds

The criteria for a good recording medium exist in intrinsic materials physical parameters other than the illustrative read-write results. In this chapter, we are discussing the magnetic characterization of FePt, FePtB, FeNiPt thin films with comparison to commercial CoCrTaPt medium. Correlation between coercive force and magnetic anisotropy of grains, the degree of magnetic isolation among grains, and grain size are discussed.

The chemically ordered FePt intermetallic compound is magnetically hard with coercivity over 10 kOe and with anisotropy energy over 70×10^6 erg/cc. Boron and Nickel doping adjusted the magnetic hardness and made the intermetallic compound suitable for magnetic recording. Boron is immiscible in either Pt and Fe, so it is likely the boron will concentrate at grain boundaries, especially after annealing. Studies of boron in other metallic compound system such as NiAl or Ni_3Al, showed that the boron will diffuse into the grain boundaries. Thus the FePtB intermetallic compound media have been developed and studied for high density longitudinal magnetic recording in this dissertation, and showed compatible SNR and non-linear transition shift with conventional CoCrTaPt media.

3.2.1 Hysteresis Loops

Table 3.3 Detailed Description of High $M_r t$ Samples

	$Fe_{45}Pt_{55}$	$Fe_{44}Pt_{54}B_2$	$Fe_{43}Ni_{10}Pt_{47}$
$M_r t (memu/cm^2)$	2.0	2.9	1.5
$M_s (emu/cm^3)$	650	604	478
$S=M_r/M_s$	0.965	0.917	0.928
S^*	0.688	0.699	0.798
H_c (Oe)	9833	4718	4388
H_k (Oe)	79402	34176	21630
H_c/H_k	0.123	0.138	0.202
$K_u (10^6 erg/cc)$	17.7	10.32	5.18
$H_r'(ISM)$	10182	4782	5262
$H_r(DCD)$	9368	4967	4592
IFF	-0.08	-0.17	-0.15

A vibrating sample magnetometer (VSM) was used to measure magnetic hysteresis loops. The properties of the FePt, FePtB and FeNiPt thin films with relatively high M_st value are listed in Table 3.3. Fig. 3.7 shows the VSM loops of the samples from which coercivity H_c, squareness and coercivity squareness were derived. The addition of B and Ni decreased the anisotropy energy, along with the saturation magnetization and coercivity. Meanwhile, H_c/H_k values increased with the addition of B and Ni, indicating more coherent rotation inside each domain than that in FePt film.
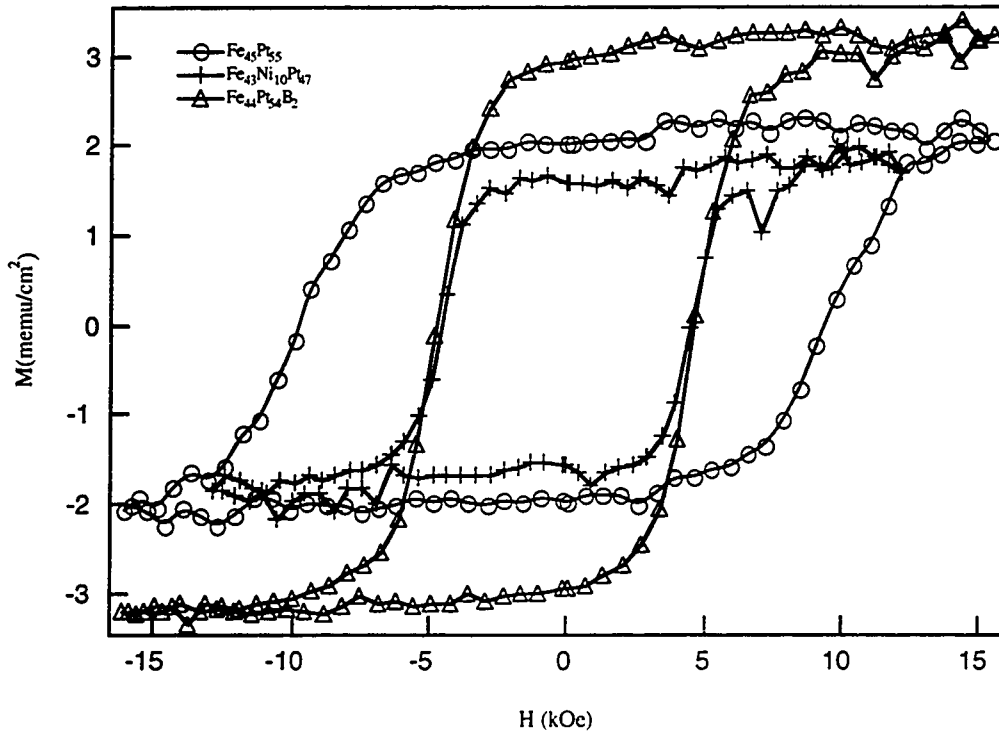
Figure 3.7. Hysteresis Loops of $Fe_{45}Pt_{55}$, $Fe_{44}Pt_{54}B_2$ and $Fe_{43}Ni_{10}Pt_{46}$

The coercivity is observed to closely follow the increase in the ordered fraction. In the bulk materials system, studies of the CuAu(I) type ordered alloy suggested that H_c might be controlled by antiphase boundary pinning of the domain wall within the microtwin structure.[3.10][3.11] The FePt thin films have a finer microstructure than

that of the bulk alloy, it is expected that the domain structure and magnetization process of the Fe-Pt films might differ from that of the bulk FePt magnets. It is reported the coercivity increases with the film thickness up to a certain value and then remains fixed beyond that thickness.[3.12] In our samples, the coercivity has been observed to decrease with thinner samples, which is consistent with results in CoPt.[3.1] Since making thin films with low $M_s t$ and high H_c is the goal for high density magnetic recording, this effect complicates our efforts to make low $M_s t$ disks.

We also found that even though the thin films are not 100% ordered, and are two phased, in most cases the M-H loops appear to be a single loop and not the superposition of two separate loops for a soft and hard phase. This indicates that the ordered (hard) and disordered (soft) regions are magnetically coupled.

To further investigate the influence of Ni doping in the FePt superlattice, we sputtered samples with different concentrations of Ni. These samples also have lower $M_s t$ values. They were adjusted to match a commercial CoCrTaPt disk to make the comparisons convenient. The magnetic properties of the FeNiPt samples and the reference CoCrTaPt disk are listed in Table 3.4 and VSM loops are plotted in Fig. 3.8.

With increasing concentration of Ni, the coercivity decreases, while the saturation magnetization decreases.

Table 3.4 Detailed Description of FeNiPt and CoCrTaPt Samples

	$Fe_{46}Ni_{9.6}Pt_{44}$	$Fe_{41}Ni_{17}Pt_{42}$	$Fe_{37}Ni_{22}Pt_{41}$	CoCrTaPt
$M_t t(memu/cm^2)$	0.57	0.55	0.45	0.74
$M_s(emu/cc)$	488	427	386	457
S	0.91	0.95	0.83	0.90
S*	0.629	0.701	0.609	0.737
H_c (Oe)	4778	3713	2317	2650
H_k (Oe)	30598	11952	6082	5657
H_c/H_k	0.150	0.281	0.358	0.471
$K_u(*10^6 erg/cc)$	7.47	2.55	1.17	1.29
$H_r'(ISM)$	5995	5922	3561	4000
Hr (DCD)	5310	4073	2469	2727
IFF	-0.14	-0.50	-0.47	-0.48
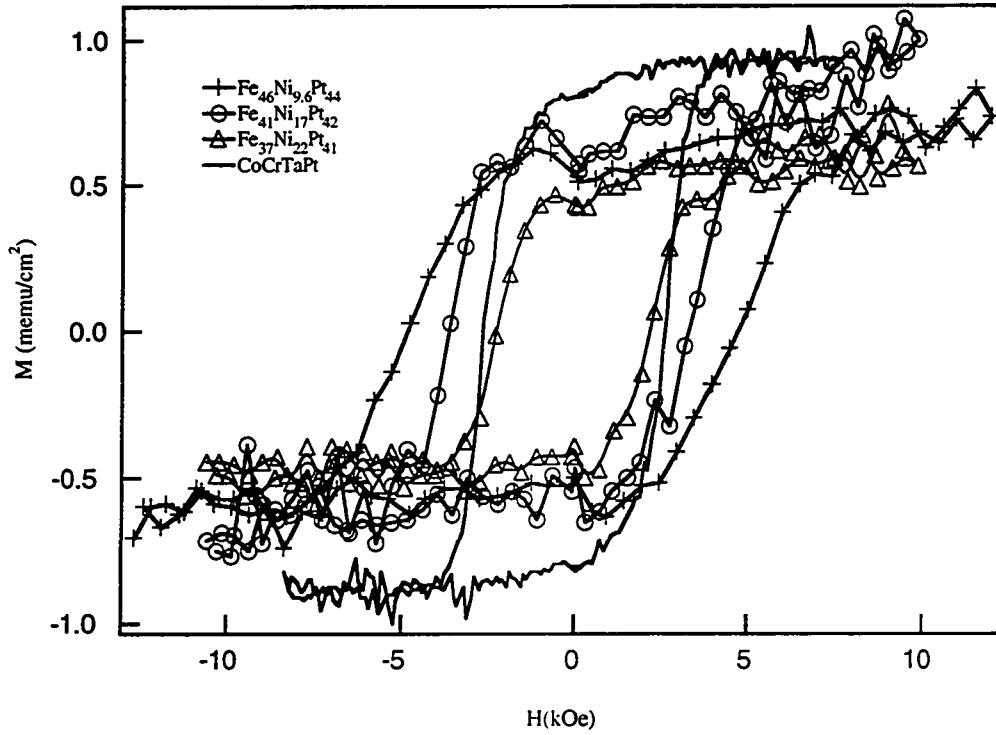
Fig. 3.8 Hysteresis loops of FeNiPt samples

3.2.2 Magnetic Anisotropy Field and Anisotropy Energy

The anisotropy field of each sample is deduced from the VSM rotational transverse magnetization curves in Fig. 3.9 and Fig 3.10 and listed in Table 3.4. The dashed curves are fitted function using Eq.(2.17) to extrapolate H_k. The anisotropy energy was calculated by $K_u = H_k M_s/2$. The characteristics of these rotational transverse magnetization curves are similar to the Torque Rotational Hysteresis Energy Loss curve. [2.18],[2.19]
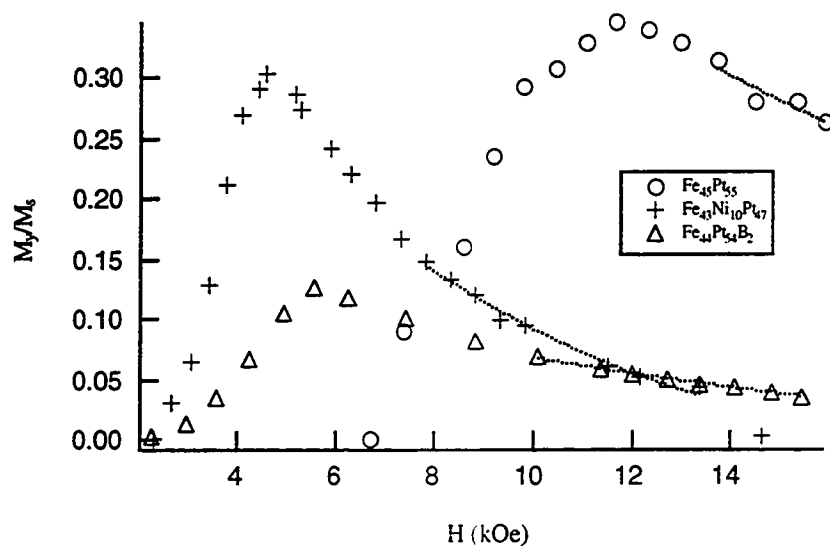
Fig. 3.9 VSM Rotational Transverse Magnetometry

Curves of $Fe_{45}Pt_{55}$, $Fe_{44}Pt_{54}B_2$ and $Fe_{43}Ni_{10}Pt_{46}$
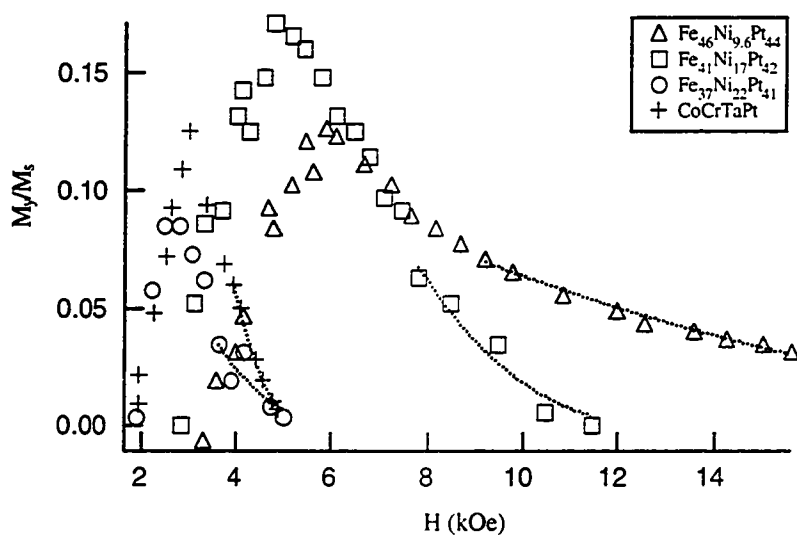
Fig. 3.10 VSM rotational Transverse Magnetometry curves

for FeNiPt and CoCrTaPt samples

Doping with boron and nickel into the FePt binary system helps the magnetic reversal mechanism evolve from incoherent rotation such as fanning or curling to coherent rotation, and results in a decrease in the initial field and the field where the M_y/M_s has its peak, as seen in Fig 3.9. Different nickel concentration could fine tune the decoupling effects. As seen in Fig 3.10, the more nickel incorporated in the thin film, the lower the initial field and the peak field of the M_y/M_s happens.

We have used this VSM RTM technique to characterize FePt, FePtB, FeNiPt and CoCrPtTa thin films. We also simulated the Torque analysis. Table 3.5 lists the values of H_k from both VSM RTM and Torque techniques. In cases where the anisotropy field was much greater than the field which could be applied by our magnet (16kOe), the extrapolated values using Eq.(2.17) were found to be more stable than those obtained from the conventional torque vs. 1/H extrapolation. When the anisotropy field is smaller than 16kOe, VSM RTM always gives H_k values a little lower than the torque extrapolation(as in Fig. 3.12), which is consistent with the theoretical analysis.

Table 3.5 Experimental value for H_k (Oe) from VSM RTM and Torque analysis

Samples	H_k by VSM	A	H_k by Torque
$Fe_{45}Pt_{55}$	79402	0.861	n/a
$Fe_{44}Pt_{54}B_2$	34176	0.481	22315
$Fe_{43}Ni_{9.6}Pt_{47}$	21630	0.765	n/a
$Fe_{41}Ni_{17}Pt_{42}$	11952	0.833	14095
$Fe_{38}Ni_{22}Pt_{40}$	6082	0.589	6986
CoCrPtTa	5657	1.0948	5774

n/a: refers that the extrapolation gives a negative value

In the Ni concentration range we studied (0~25% Ni), the anisotropy energy decreases with increasing amount of Ni (Fig. 3.11). The saturation magnetization also decreases with the amount of Ni doping in a linear fashion, as seen in Fig 3.12. This shows that nickel could be used to as a tuning agent to move the FePt system into the region with suitable coercivity, saturation magnetization and anisotropy energy.
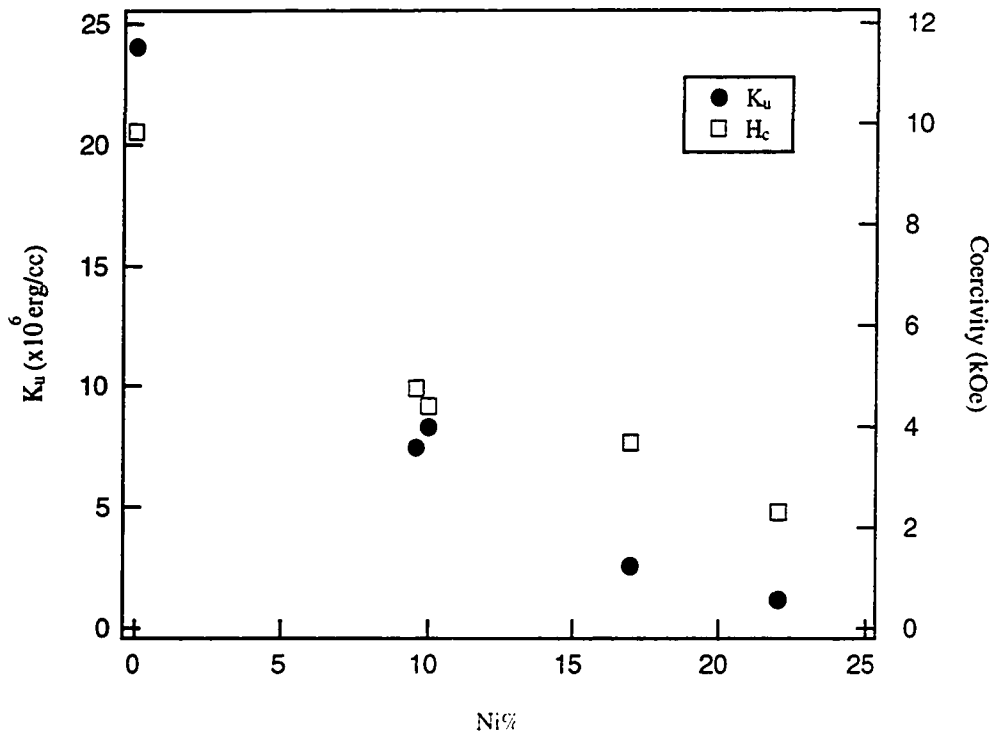
Fig. 3.11 Anisotropy Energy vs. Ni concentration
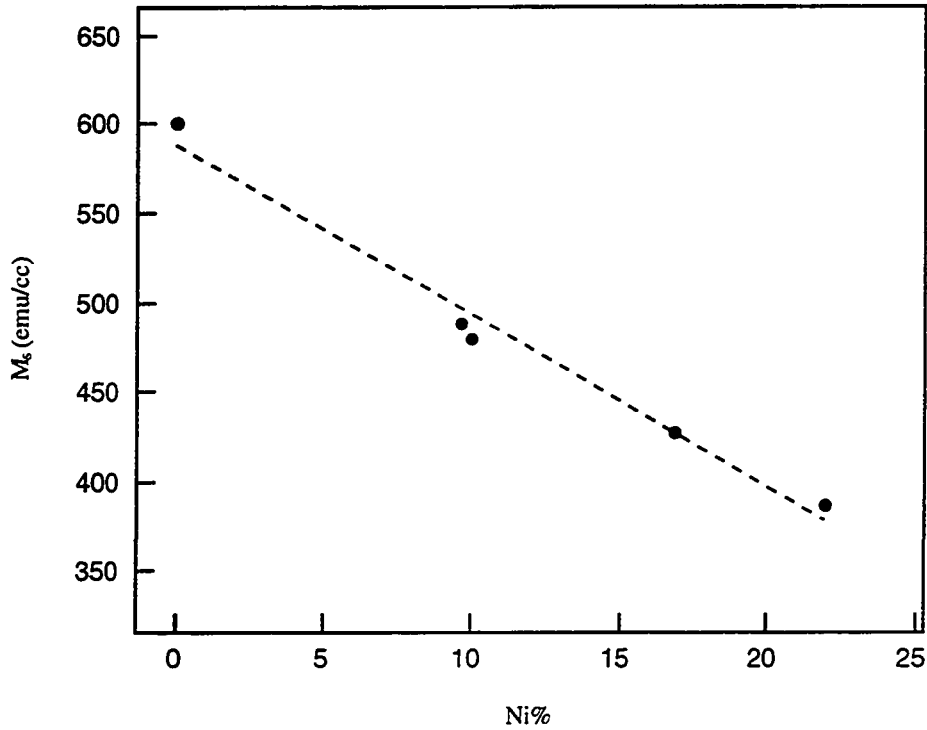
Fig. 3.12 Saturation Magnetization vs. Ni concentration

3.2.3 Remanence Magnetometry

δM curves of FePt, FePtB and FeNiPt thin films were shown in Fig. 3.13 and Fig

3.14, all with negative peaks indicating that the dominant interaction is the demagnetizing magnetostatic interaction, which favors demagnetizing the neighboring grains. Thus, cooperative switching is reduced and low media noise is expected. By doping with B and Ni, the peak is more negative, showing that the addition of B and Ni helped the decoupling between domains. The peak positions are in accordance with the coercivity values. Similar results have been reported on CoPt and CoPtP compounds. [3.17]
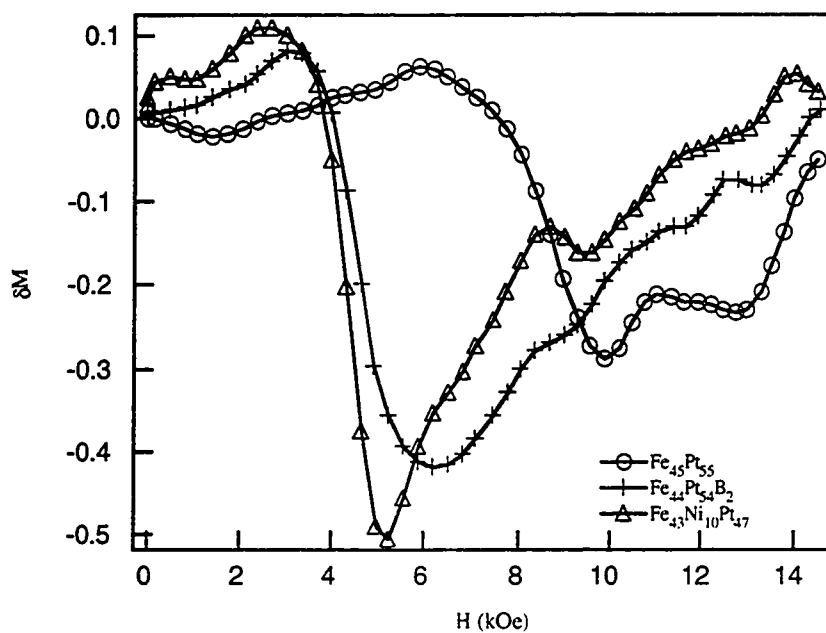
Fig. 3.13 δM Curves for $Fe_{45}Pt_{55}$, $Fe_{44}Pt_{54}B_2$ and $Fe_{43}Ni_{10}Pt_{46}$
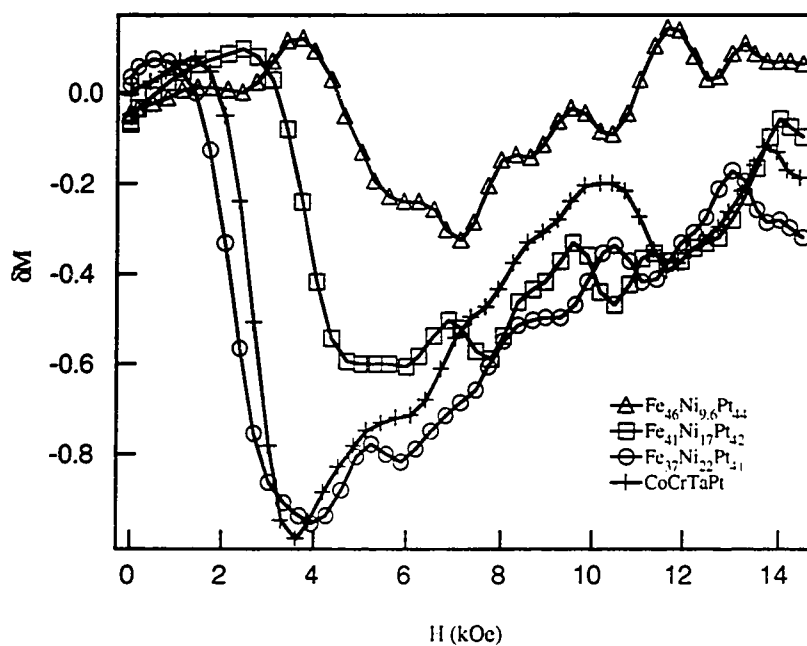
Fig. 3.14 δM curves for FeNiPt and CoCrTaPt samples

These negative features are really impressive as compared with other recording media. In Co alloy media, large positive δM is generally observed and believed to be caused by exchange coupling. The noise spectrum shows a linear and superlinear increase with the recording density, showing the noise source is transition related. With a thick and suitable underlayer, negative δM curves have been reported.

BaM media have been reported with both negative δM curves and positive δM overshoot depends on the underlayer situation. It is believed to be caused by magnetostatic coupling between acicular grains. The grains in Ba ferrite films are observed to be well isolated by clear grain boundaries, suggesting low exchange coupling between grains. In addition, the super-exchange interaction in BaM requires iron ions to be located at certain angles relative to oxygen ions, which makes exchange coupling more difficult among a group of polycrystallites. Since grains in BaM thin films have the elongated shape with c-axes perpendicular to their long axes, the average effect of magneto-static interactions factors constructive spin alignment among neighboring grains, which result in positive δM peaks. They also show an increases in their noise spectra with density.[3.15][3.16]

The Remanence coercivities H_r and H_r' has been defined from the ISM and DCD remanence curves. The Interactive Field Factor IFF is given by $IFF=(H_r-H_r')/H_c$, and it is a indication of the interaction strength in the in the region of H_c, more or less like a decoupling factor. The more isolated each domain, the lower the IFF value, for it represents the increasing dipolar interaction between two isolated particles. The calculated value for FePt, FePtB and FeNiPt are listed in Table 3.3 and Table 3.4.

3.2.4 Summary

The value of H_c/H_k corresponds to the degree of rotational coherency inside each magnetic domain. Since the coherency of the switching is largely decided by the interactions between neighboring domains, this value increases with decreasing the degree of the magnetic interaction. The ideal maximum value is about 0.48 for isotropic media with no intergranular magnetic coupling. Fig 3.15 illustrates that for all the media we studied in Table 3.3 and Table 3.4, the less interaction between these domains(that is, the more negative IFF and δM value), the more likely coherent rotation will occur in each domain(in other words, the higher H_c/H_k value).
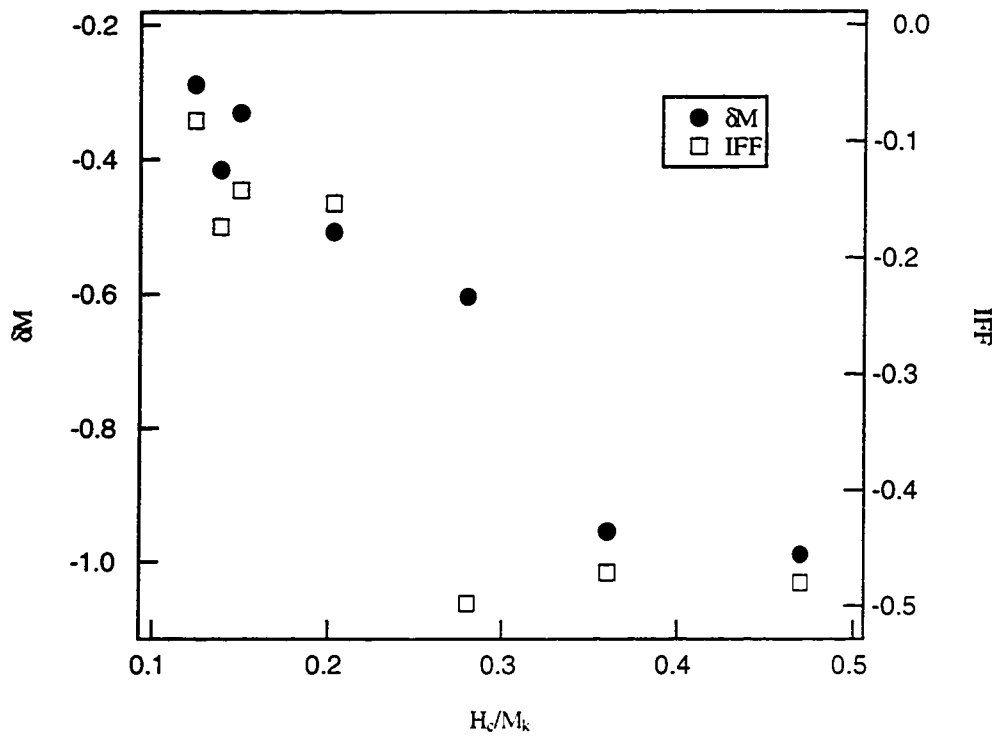
Fig. 3.15 Interactive Field Factor and δM vs. H_c/H_k

$K_u/2\pi M_s^2$ is a characteristic parameter depicting the degree of preferential alignment

of the uniaxial crystallites. Generally, three-dimensionally random or perpendicular

preferred alignment of the easy axes of the crystallites results in lower noise than in-

plane alignment, as would be expected from exchange energy consideration.[3.13]

The higher $K_u/2\pi M_s^2$, the higher the noise level. In CoCrTa media where the

intergranular magnetostatic coupling is predominant, the ratio $K_u/2\pi M_s^2$ indicates the

strength of the effect of the intergranular magnetostatic coupling on the coercive

force.[3.14],[3.19] Generally in the magnetic thin films FePt, FePtB, FeNiPt and

CoCrPtTa we have studied, the boron and nickel brings down the $K_u/2\pi M_s^2$ value and

can be compatible to the CoCrTaPt medium as in Fig 3.16.

Fig. 3.16 $K_u/2\pi M_s^2$ vs. H_c/H_k

Chapter 4: Read-Write Tests of FePt and FePtB Media

4.1 Disk Specification and Spin Stand Setup

FePt and FeNiPt disks were tested on an air bearing spin-stand to evaluate their read-write performance. After spin stand testing, the disks were broken up with the exact testing spot identified, and the small piece containing this spot was then characterized. Each disk was processed according to the same recipe of a small pilot sample with the desired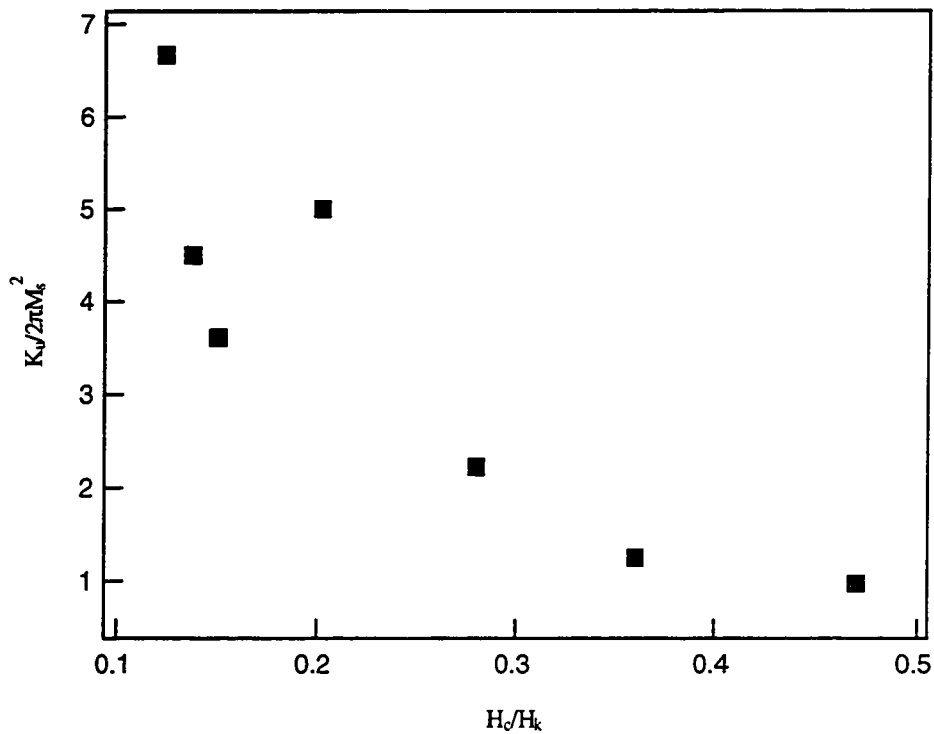 magnetic properties. Fig. 4.1(a) shows the hysteresis loops of the small pilot samples, and Fig. 4.1(b) shows those from the disks with the same sputtering conditions.

There are substantial differences between the small pilot samples and subsequently produced 65mm disks. Generally, while reproducibility was possible with the pilot samples, no clear relationship emerged between the pilot and disk samples prepared under similar conditions. As discussed in Chapter 3, the annealing control in the sputtering chamber for the disks is much less precise than the control of the vacuum furnace for small samples. Different degrees of superlattice ordering and significantly different M-H loop appearances resulted. However, it was not possible to more tightly control the disk processing given other constraints, such as the need for in situ processing and the need for a subsequent adhesion carbon layer on the medium.

The properties of the FePt, Fe/Pt and FePtB disks are listed in Table 4.1. Two commercially available CoCrPtTa media on textured NiP/Al disks were used for comparison in recording tests, their coercivity and $M_r t$ values were supplied by the vendor.
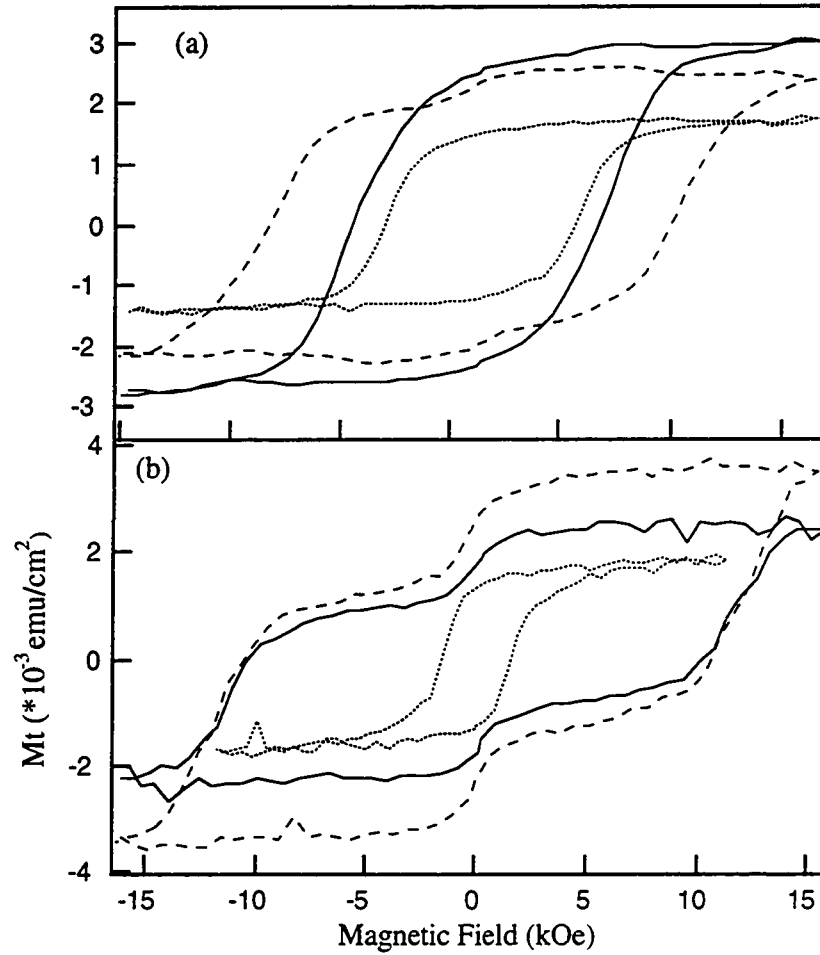
(a) Pilot samples on ZrO_2 ——FePt - - -Fe/Pt······ FePtB
(b) ZrO_2 Substrate Disks ——FePt - - -Fe/Pt······ FePtB

Fig. 4.1 Hysteresis loops for the pilot samples and disk media

Read-write tests were carried out on an air bearing Adelphi spin-stand. A HP 8091A Rate Generator (1GHz) was used to generate written signals, a Tektronix TDS 744A Digitizing Oscilloscope was used to display and analyze the written and read signals. Data were collected by a PC programmed GPIB board. Digital oscilloscope captures were used to compute roll-off curves, signal-noise ratio, and nonlinear transition shift (NLTS)[4.1].

TABLE 4.1 Disk Descriptions

Disks	Cosputtered FePt	Pt/Fe multilayer	FePtB	CoCrPtTa I	CoCrPtTa II
Substrate	ZrO_2	ZrO_2	ZrO_2	NiP/Al	
H_c (Oe)	10016	11212	1710	2480	2480
S^*	0.71	0.80	0.37		
S	0.77	0.69	0.75		
M_r (emu/cm^3)	590	600	520		
$M_r t$ (memu/cm^2)	2.22	2.98	1.43	1.26	0.8

Write elements with high saturation magnetization are necessary for the high coercivity media. Comparative read-write tests were carried out on the cosputtered FePt, the multilayered Fe/Pt and the conventional CoCrPtTa(I) media using a MIG head, at a linear head velocity of 218ips. The composition of the write element for the MIG head was not determined. The gap of the MIG head is observed under SEM to be 0.2 um and the turns to be 13 under optical microscope. The write current was 55mA for the MIG head, which was the maximum currents available from the preamplifier. Thus a deep gap field of 44 kOe (e.g., a saturated write pole) was calculated.

A MR head was used to compare the low moment FePtB and CoCrPtTa(II) media at 90.6ips (which is just above the head take off velocity), The write element of the MR head is equiatomic FeNi with a moment of 15kG. the write current was 45um which was the maximum currents available from the preamplifier. With 7 turns on the coil and a gap of 0.35um, the deep gap field is calculated to be 11.3 kOe. The selected head speeds coincided with the observation of occasional unburnishable hits of the

head on the disks, implying that the heads were nearly in contact with the carbon overcoat.

The relative comparison between the FePt and FePtB media later in this chapter is reasonable by bridging over the CoCrPtTa media. Since FePt and Fe/Pt media has higher $M_r t$ value than FePtB medium, we compare them with CoCrPtTa(I) which has a higher $M_r t$ value than CoCrTaPt (II). The relative strength of the magnetic moment $M_r t(FePt)/M_r t(CoCrPtTa\ I)$ is kept consistent with $M_r t(FePtB)/(M_r t(CoCrPtTa)$.

4.2 Overwrite

Overwrite specifies the effectiveness of writing one frequency (f_2) signal over a previously written pattern at a different and usually lower frequency (f_1). It is an important parameter in determining whether the disk coercivity is too high. The overwrite should exceed 30dB in magnitude to have high fidelity writing. To achieve good overwrite, it is generally required that the head produce a record field 2.5 times the coercivity at the back of the medium. In our testing, overwrite was measured as the ratio between a 3MHz signal before and after being overwritten by a 9MHz signal. Fig. 4.2 shows overwrite with the MIG head on the commercial CoCrPtTa(I) medium compared with the cosputtered FePt medium and multilayer Fe/Pt medium. The cosputtered FePt showed better overwrite than the multilayer Fe/Pt media, because of the slightly lower coercivity and lower $M_r t$ value.

Residual overwrite signal is caused predominately by three phenomena: residual recorded signal, timing shifts of f_2 at the f_1 rate, and residual edge track effect. If insufficient record current exists, the f_1 magnetization is not completely erased and the actual signals from residual recorded patterns occur. Even if the original signal is

erased, the magnetostatic fields from the incoming f_1 pattern extend across the gap and modulate the zero crossing of the newly recorded f_2 pattern, yielding a frequency component at the f_1 rate. Further incomplete erasure of edge-track magnetization can leave a residual f_1 pattern that is somewhat independent of current.
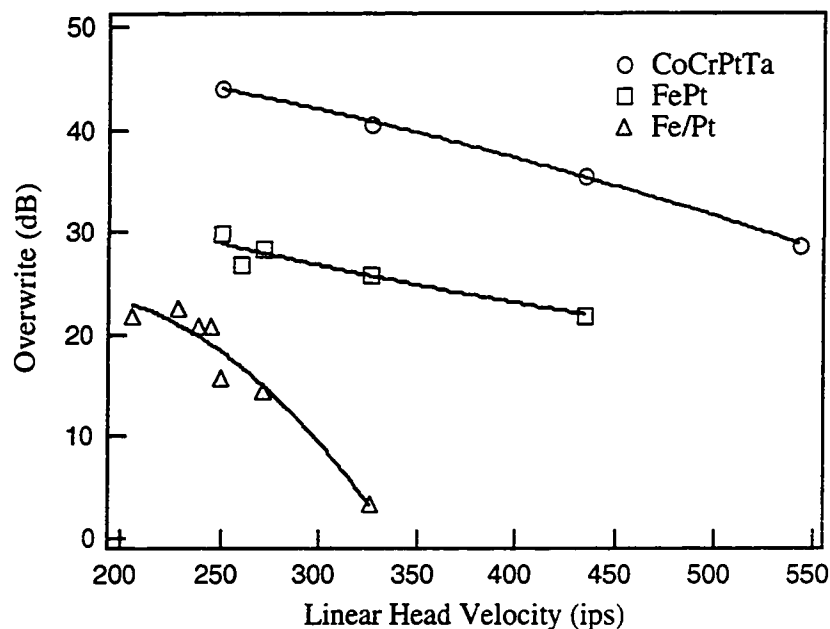
Fig. 4.2. Overwrite vs. linear head velocity using MIG head on the
FePt, Fe/Pt and CoCrPtTa (I) media

Generally, the overwrite for samples with coercivity above 5,000 Oe was observed to be poor, making the higher coercivity samples unsuitable for recording performance evaluations. However, overwrite did improve dramatically even for the samples with coercivities above 10kOe as the medium velocity was reduced and the magnetic spacing correspondingly narrowed.

Fig. 4.3 shows overwrite as a function of the magnetic spacing between the media and the MR head. At low flying height, acceptable values for overwrite were obtained on FePtB. Interestingly, while $M_r t / H_c$ for FePtB is higher than for

CoCrPtTa, lower overwrite was obtained[4.2]. The lower overwrite is probably representative of inhomogeneous grains in the FePtB medium which cannot be written by the available write field. Such grains are apparent, for instance, in the long "tail" of the hysteresis loop in Fig. 4.1(b).

Both the Karlqvist approximation and the near field of the recording head were calculated according to Equation (1.3) and (1.5) for flying height of 20 nm and 60 nm respectively (Fig. 4.4). There is a 20% increase in the head field when flying height decreased from 60nm to 20nm. For the flying height at 20nm, $y/g=17.5$, so that Karlqvist approximation is no longer valid. Realistically we should compare the head The Karlqvist field value for 60nm spacing with the near field value at 20nm magnetic spacing, we can see how significant improve the head gradient has gained. For the high coercivity media such as FePt and FePtB intermetallic compound, near contact recording is a feasible solution. Also according to Eq. (1.8), the decrease of flying height from 60nm to 20nm will lower spacing loss by 2.8 dB.

Beside the improvement of the overwrite, Signal to media noise ratio will also increase with lowered head media write separation. Part of the increase comes from the narrow transition yielding higher signal amplitude. In addition, the media noise decreases. Computer simulation agrees with the experimental observation of lowered media noise with lowered head-media separation, even for exchange coupled media.[4.3]

These results also indicate that FePt is not likely to be successful as a recording material for conventional recording transducers, unless ternary compound such as FePtB, are employed.
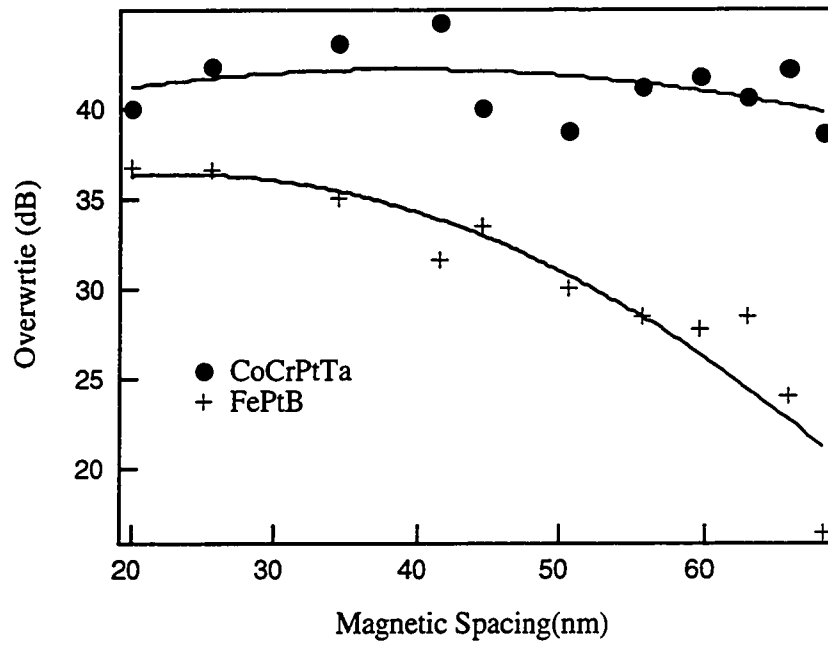
Fig. 4.3. Overwrite vs. magnetic spacing on FePtB and
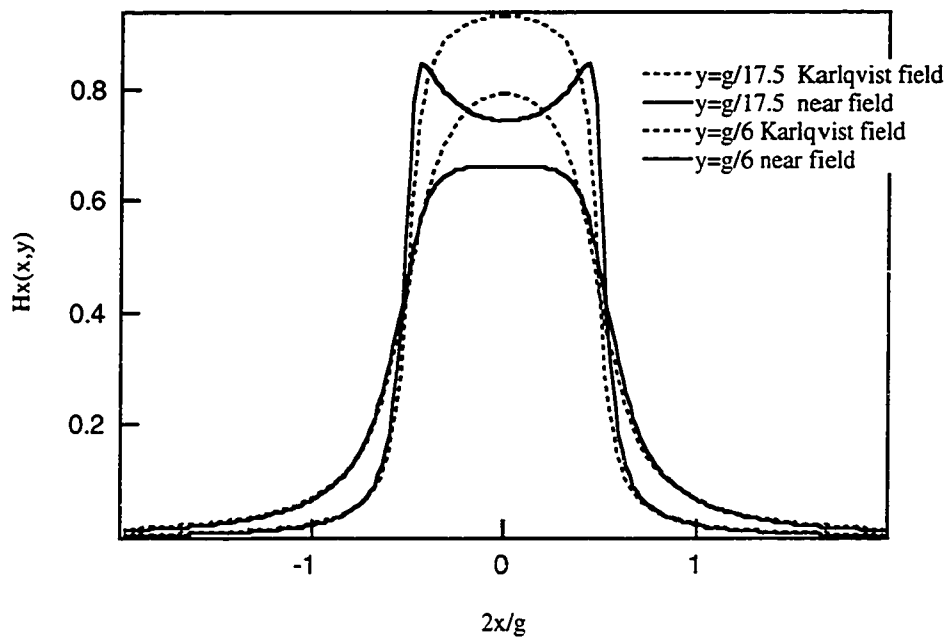CoCrPtTa (II) media with MR head

Fig. 4.4 Head field calculating for the MR head

4.3 Roll off curves and Signal to Noise Ratio

The variation of the Peak-to-Peak voltage (V_{p-p}) versus the flux change density of the all 111's pattern is called a roll-off curve. It is used to define the resolution of the system. At each frequency, 1000 digital oscilloscope captures were averaged to get an averaged isolated single average pulse as in Fig 4.5. The FePt and Fe/Pt media support pulses with higher amplitude due to higher Mrt value, but broader width.
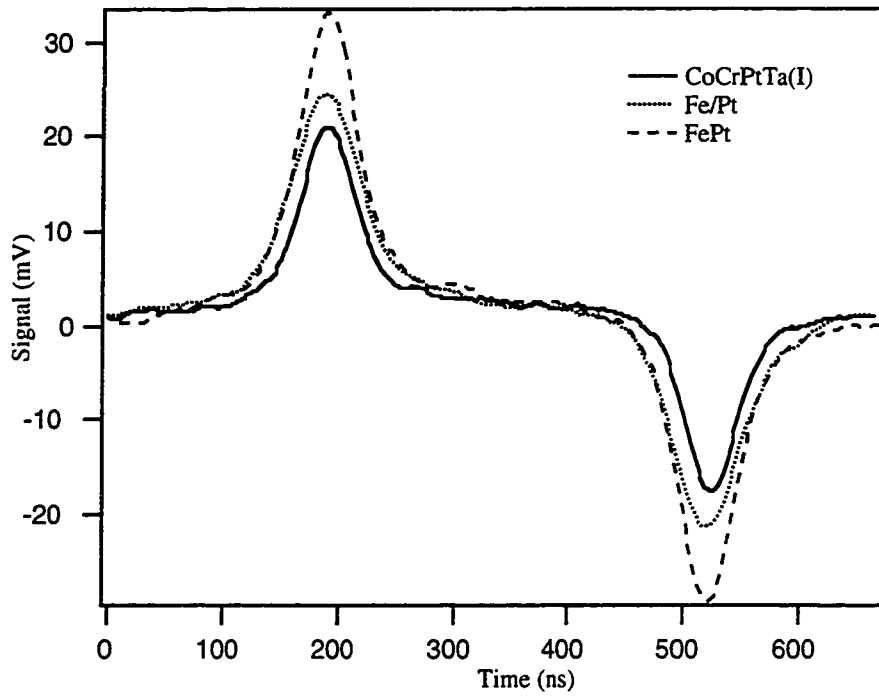
Fig. 4.5 Isolated pulse for FePt, Fe/Pt and CoCrTaPt(I)

Signal to Noise Ratio (SNR) S/N_m is defined as carrier power to integrated medium noise power, with the electronic background subtracted. A digital filter(Eq 4.1) were used to simulate the analog electronic circuit.

$$Filter = \frac{1.31703 - 0.8x^2}{x^2 + 1.68495 + 1.31703} \quad \frac{2.95139}{x^2 + 1.54203x + 2.95139} \quad \frac{5.37034}{x^2 + 1.14558x + 5.37034} \quad \frac{0.86133}{x + 0.86133}$$

(4.1)

Fig 4.6 is the power spectrum showing harmonic peaks on FePt, Fe/Pt and CoCrPtTa media. The FePt and Fe/Pt have higher signal power, much higher noise power, and the harmonic peaks decays faster than that of the CoCrPtTa medium.
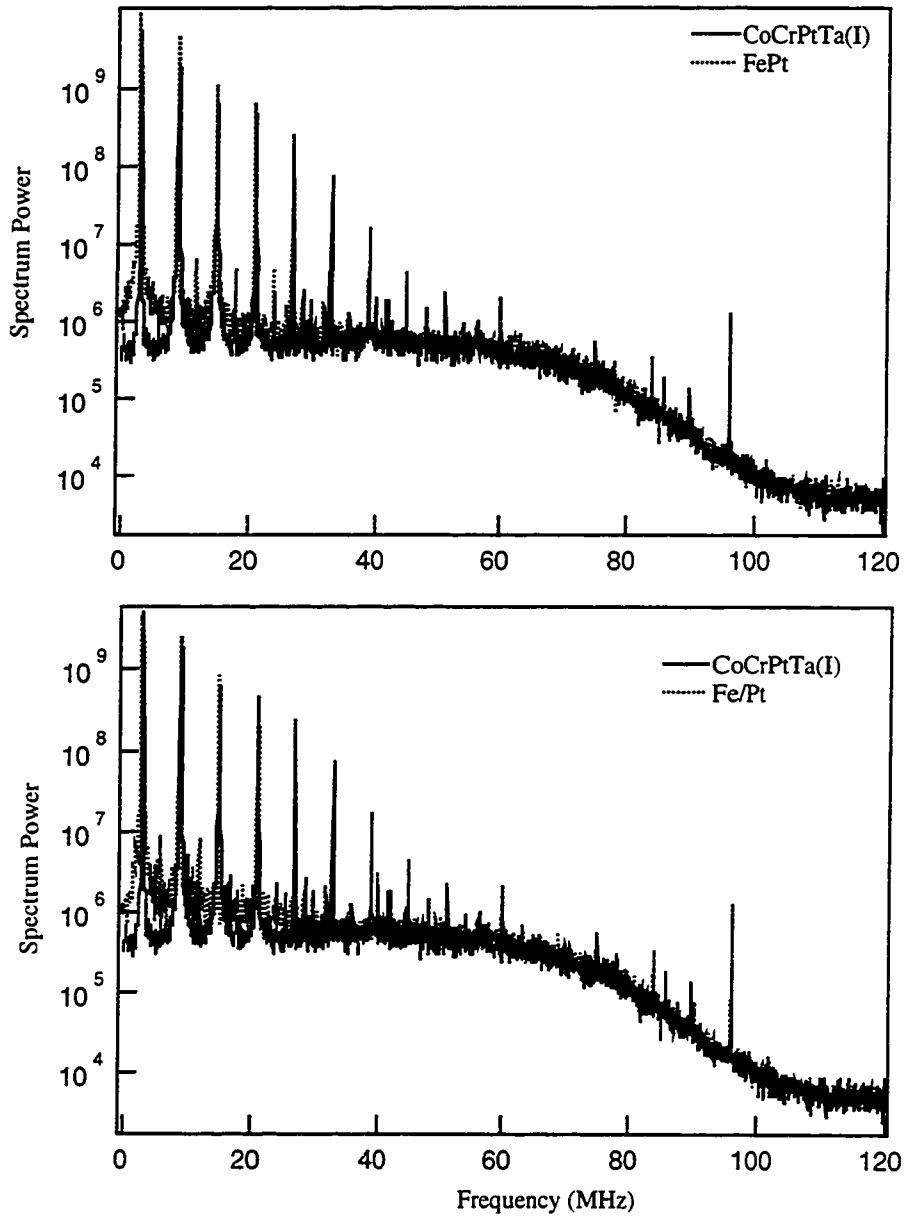
Fig. 4.6 Power Spectrum for FePt, Fe/Pt and CoCrPtTa(I) media

Fig. 4.7 shows the recording results of the MIG head on FePt, Fe/Pt and CoCrTaPt media. With the MIG head, we could write partially on high coercivity FePt and Fe/Pt media, but the resolution was limited, producing wider low frequency pulses. Amplitudes obtained from the ordered intermetallic were comparable to CoCrPtTa(I), but both media rolled off more quickly. The binary intermetallics have worse SNR than CoCrPtTa, similar to the results Coffey, et al. reported on ordered CoPt[4.4].

Fig. 4.7. Recording on FePt, Fe/Pt and CoCrPtTa (I) media with MIG head
(a) Roll-Off curves   (b) SNR vs. Linear Density

The FePtB disk, measured with the MR head, showed improved V_{p-p}, resolution and SNR than FePt media with comparison to the commercial CoCrPt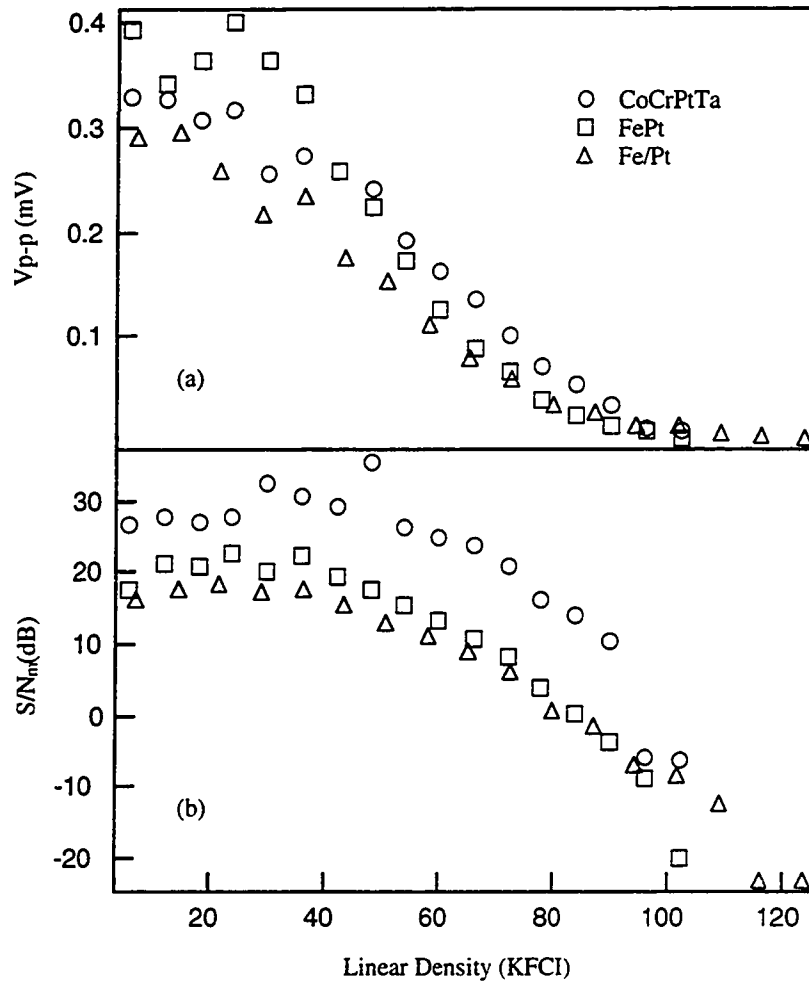Ta(II) medium (Fig. 4.8). In averaging the pulses, amplitude fluctuation is observed. The transition fluctuation amplitude is largely determined by the dispersion in the media characteristics, such as uniformity of grain size, orientation, exchange coupling, stress, etc. Since the uniformity of the FePtB has been illustrated by Fig 4.1(b), it is understandable that the FePtB has worse Vp-p than CoCrPtTa(II) medium. Usually these fluctuations are exacerbated by a poor record head field gradient. That is, if the head field gradient is poor, the transition length of neighboring bits and the fluctuation(noise) of the transition location will be large. [4.5]-[4.7] To provide good hard field gradient is a great advantage of near field recording. By using the same MR head and fly at near contact region, the medium noise level of FePtB and CoCrTaPt(II) media are quite similar as in Fig. 4.9.

FePtB media shows that the S/N_m ratio 5dB worse than the CoCrPtTa(II) medium in Fig 4.8(b), while the S/N_m ratio of the FePt and Fe/Pt media were 10 dB worse than the CoCrPtTa(I) media as in Fig. 4.7(b). Consequently, we could conclude that in comparison with the binary FePt composition, the FePtB medium has much lower noise, and this is presumably exchange decoupling due to segregation of boron during the anneal, since the Sherrer formula yields comparable grain sizes for FePt and FePtB made under the same conditions. Boron is insoluble at low concentration in either Fe or Pt[4.8], and grain boundary segregation of boron had been widely observed in NiAl and other alloy systems after annealing.[4.9],[4.10] Coffey, et al. reported similar noise reduction by the incorporation of ZrO_x into the CoPt medium matrix[4.4].
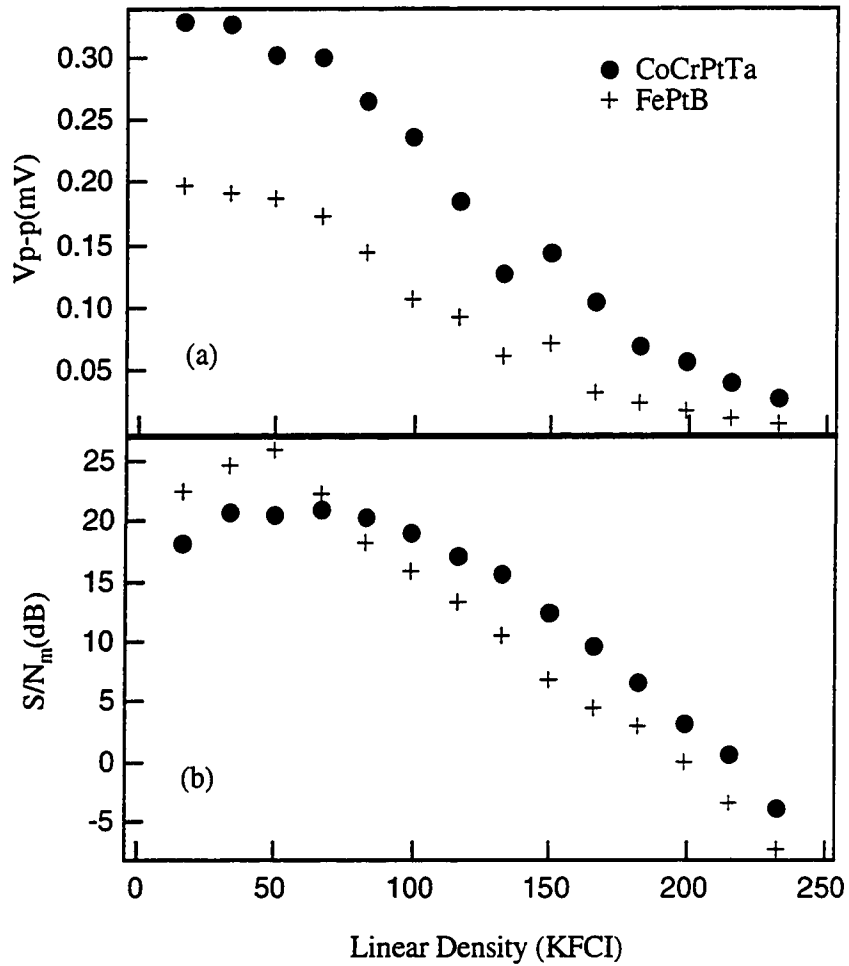
Fig. 4.8. Recording on FePtB and CoCrPtTa (II) media with MR head

(a) Roll-Off curves   (b) SNR vs. Linear Density

For recording media in general, grain size determines the level of the noise floor at low densities, while intergranular interaction contributes to the transition noise which causes the noise increase with density. The rate of the noise increase relates to the strength of the interaction. And the strength of magnetostatic interaction among grains can be correlated to the peak height in the δM measurement.

Fig 4.9 shows the noise power versus recording density for FePtB and CoCrTaPt(II) media, and there is no obvious superlinear noise region at high density. This clearly indicates that the both media have very little intergranular exchange interaction, agree with the δM measurements in Fig. 3.8. Similar results has been reported in BaM , CoPt media with negative dM feature and weak magnetostatic coupling.
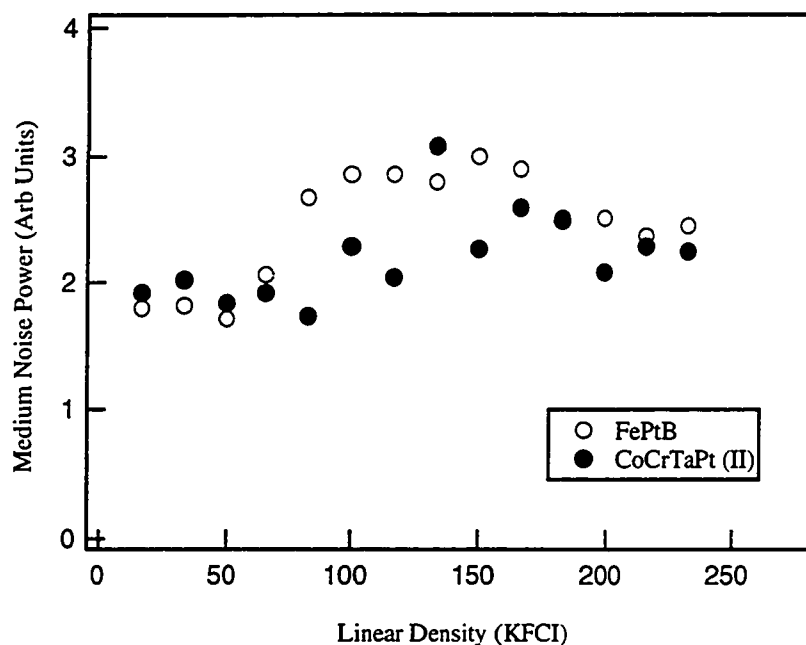
Fig. 4.9 Media Noise Power of FePtB and CoCrPtTa(II) media

4.4. Non-linear Transition Shift(NLTS)

Transition shift, also referred to as peak shift or bit shift, is defined as the normalized shift in detected position of readback bits with respect to the positions where they were written. When the pulse peaks shift from the center of the expected time intervals during detection, the chances of error increase. The bit shift are primarily

caused by three factors. (1) the interbit interference; (2) the addition of noises to the pulse waveforms by head, medium and electronics; (3) the writing process.

With the ever increasing storage density of magnetic recording products and the increase use of advanced channels, write process nonlinearities, including NLTS have become of central importance. One technique for reducing the impact of NLTS is write precompensation. For media development, it is of importance to evaluate the bit shift caused by interbit interference. Then a precompensation scheme could be designed and tested in the detection system. In this technique, a fixed amount of precompensation of data pattern dependent precompensation is used. NLTS can only be reduced but not entirely removed by using a linear equaling filter. The long range nature of the interactions, which give rise to NLTS, complicates the implementation of precompensation, and can limit effectiveness of this approach.

The interbit interference has both linear and non-linear components. The linear components results from superposition of isolated pulse waveforms which interfere to produce bitshift as they are spaced closer and closer together. Because it is linear, the linear bit shift may be equalized by linear networks in the read circuit. Medium non-linear bit shift arises from the interbit magnetostatic interactions that occur during the write process. Although the non-linear bit shift may be partially canceled by predistorting the write current waveform, it cannot be post-equalized by linear networks. Consequently, the measurement of the nonlinear transition shift is important to evaluate the performance at high recording density.

Several methods have been proposed to investigate the magnitude of the shift. The Time Domain Pseudorandom Sequence writes a specially designed pseudo-random sequence and measure its "linear impulse response". The shift is then measured by an

"echo" at a known position. [4.11][4.12] The Frequency Domain method is based on a special class of test patterns with the property that when bits are written at correct positions without shift, certain spectral components will be zero, when the transitions are shifted, the spectral components would appear and be used to calculate the nonlinear bit shift. [4.13][4.14]

Here we used the simplest measurement of dibit pattern method to calculate the bit shift. A dibit pattern, namely, two magnetization transition spaced apart by the bit cell length, was recorded. The distance between the two peaks of the readback pulses is the detected bit spacing. The bit shift is given by the difference between the detected and recorded bit spacing.
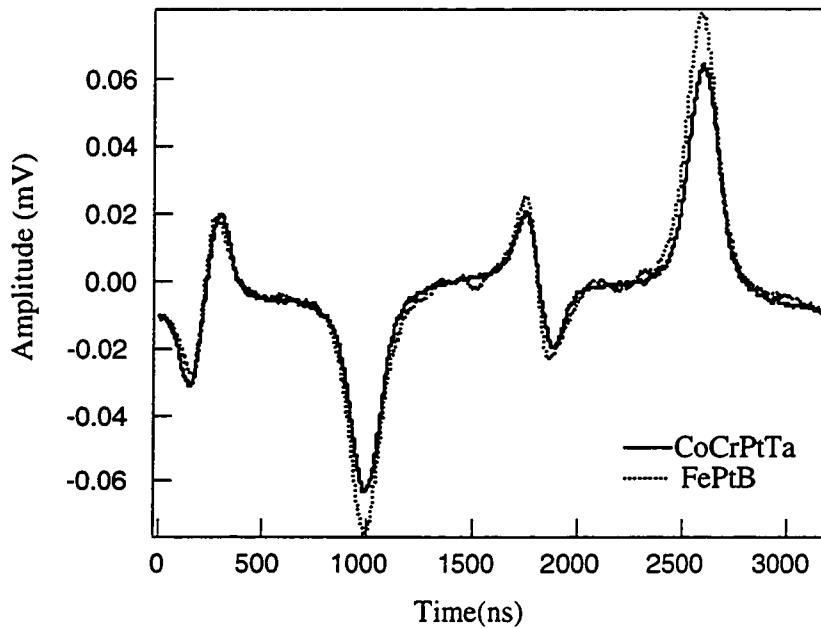

Fig. 4.10 Dibit pattern of FePtB and CoCrPtTa(II) media at 200KFCI

A 32-bit isolated bit and dibit pattern (NRZ "7FBF8040") was recorded to measure non-linear transition shift. For example, Fig. 4.10 shows a readback waveform for this pattern for the FePtB and CoCrPtTa(II) media at 200KFCI.

Bit shift was characterized by measuring nonlinear amplitude loss[4.2], e. g. the ratio of the measured dibit amplitude to that for a linearly superposed dibit. Fig. 4.9 shows the ratio of the measured dibit amplitude to that of the superposed dibit at various written bit spacing B. The inset to Fig. 4.11 shows the inferred nonlinear bit shift Δx calculated from the amplitude loss. From Fig. 4.11, we can see that the FePtB medium has somewhat better NLTS compared with conventional CoCrPtTa media at higher recording density.

Bertram[4.2] gives expressions based on magnetostatic interactions for the expected nonlinear bit shift. The bit shift is expected to scale inversely with $\Delta x/B \propto 1/B^4 H_c$. However, this functional form was found to only qualitatively agree with the measured bit shifts for both the FePtB and the CoCrPtTa.

Given the lower coercivity, smaller NLTS for the FePtB is unexpected. This may be due to the canted easy axis of the medium[4.15] or perhaps to the in-plane isotropy of the FePtB medium. A proposal made by Mallinson[4.16] implies that for a defined recording system, there should exist a medium easy-axis angle for which significant reduction of NLTS is apparent, there by remove the need for write precompensation.

The principle nonlinearity is thought to be due to the magnetostatic field, usually called the demagnetizing field, which exists in the recording medium. In the longitudinal recording mode, the demagnetizing field from the preceding transition, whilst opposing the magnetization of the next bit, assists in the writing of the next transition. Therefor the net transition is recorded further from the gap, where the head field is lower than would be the case if the demagnetization field were absent. In the perpendicular mode, the demagnetization field assists the magnetization. The
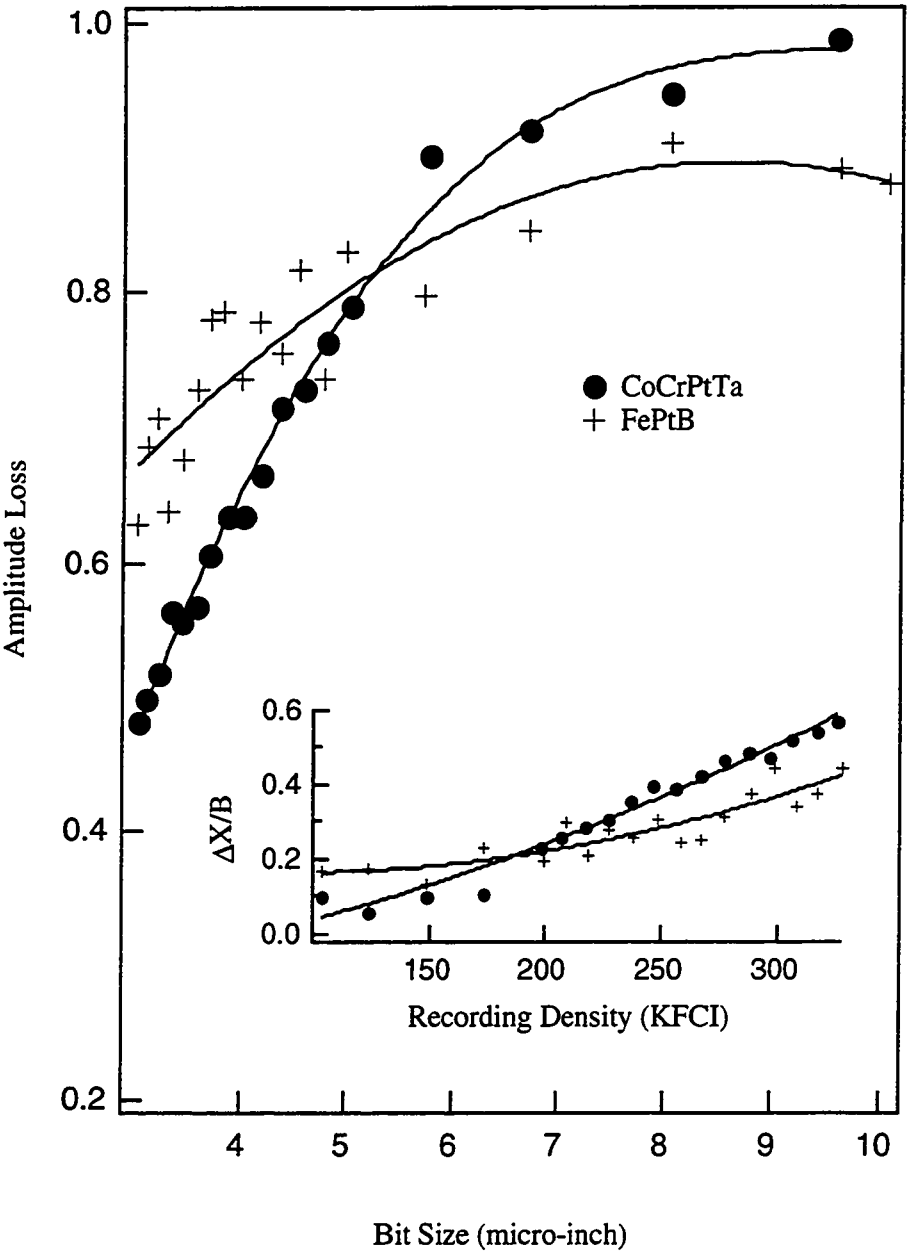
Fig. 4.11. NLTS of FePtB and CoCrPtTa (II) media

demagnetizing field now opposes the writing of the next transition, so that the next transition is recorded closer to the gap than would be the case without demagnetization field. Thus the sign and magnitude of the nonlinear intersymbol

interference depends on media orientation. Therefor there must exist an obliquely oriented recording media with optimized, even zero, nonlinear bit shift.

This media is highly oriented at an intermediate angle, neither perpendicular nor longitudinal. The precise angle leading to zero NLTS will depend on factors such as linear recording density, thickness of the media, and the proximity and magnitude of any magnetic images which are included in the writing head. This kind of obliquely oriented media has been studied in the metal evaporated tapes. The observation of the better NLTS in FePtB and their un-textured microstructure make it possible that FePtB could be benefiting from the canted easy axis.

Chapter 5. Suggestions on Future Work

5.1 Microstructure of FePtX thin films for recording

Clearly, the breadth of possible microstructures of thin film FePt and FePtX intermetallic compounds has not exhausted in this dissertation. Even within the context of ceramic substrates, it would be interesting to explore topics such as grain size dependence on different substrates, annealing temperature and different kinds of seed layers. Processing parameters such as sputtering temperature, gas pressure, ambient species, annealing condition etc. could be optimized to obtain the smallest grain size.

In conventional Co-alloy-based media, each bit might include hundreds of grains. There might be some fundamental difference in the FePtX(X=B, Ni) domain and grain size relationship from conventional metallic Co alloy media. With multilayer precursors, it may be possible to produce FePt media with domain size smaller than the grain size of the thin film, taking advantage of the stacking fault of the tetragonal unit cell of the FePt or the slight mismatch in orientation for each unit cell. The annealing time and temperature greatly influence the ordering mechanism, and lead to different magnetic properties and microstructure inside the thin film. Some further annealing could cause the regions of ordered structure to break away as separate phases, thus relieve the coherency strain and decrease the coercivity; and make it possible for the domain size to be smaller than the grain size[5.1].

At different annealing temperature, even though eventually the same ordering could be reached with constant temperature-time product, the nature of the ordering reaction differs. For instance, X-ray diffraction shows that at high annealing temperature, the

main cubic lines gradually broaden into bands and slowly change in position as the ordered structure develops. As the ordering advances, the tetragonal lines emerge from the band and eventually assume their final position[5.1].

For a "discontinuous" reaction[5.1] which happens at a relatively lower annealing temperature, the cubic lines remain sharp while the tetragonal lines slowly appear in their final positions and are also sharp. As the ordering progresses, the tetragonal lines increase in intensity at the expense of the cubic lines and no change in position is observed. [5.1]

We have sputtered FePt FePtB and FeNiPt thin films on polycrystalline ZrO_2 and single crystalline R-Plane Sapphire. Another possible high temperature substrate is single crystal Si with SiO_2 on top as a buffer layer, to prevent formation of silicate during annealing.

Since it is well known that growth of Pt on [0001] Al_2O_3 results in [1 11] oriented films, which can be used as seed for [1 11] alloy growth. [5.2],[5.3] Deposition onto Al_2O_3 at high temperature could be resulted in a strong [1 11] out-of-plan orientation, which is suitable for canted media [5.4]

Up till now, no FePt with (200) texture has been reported. In one of our experiments, we successfully grew thin films with large FePt(200) diffraction peaks on (024) single crystalline sapphire substrates. The coercivity and X-ray diffraction pattern are shown in Fig. 5.1 and Fig. 5.2.
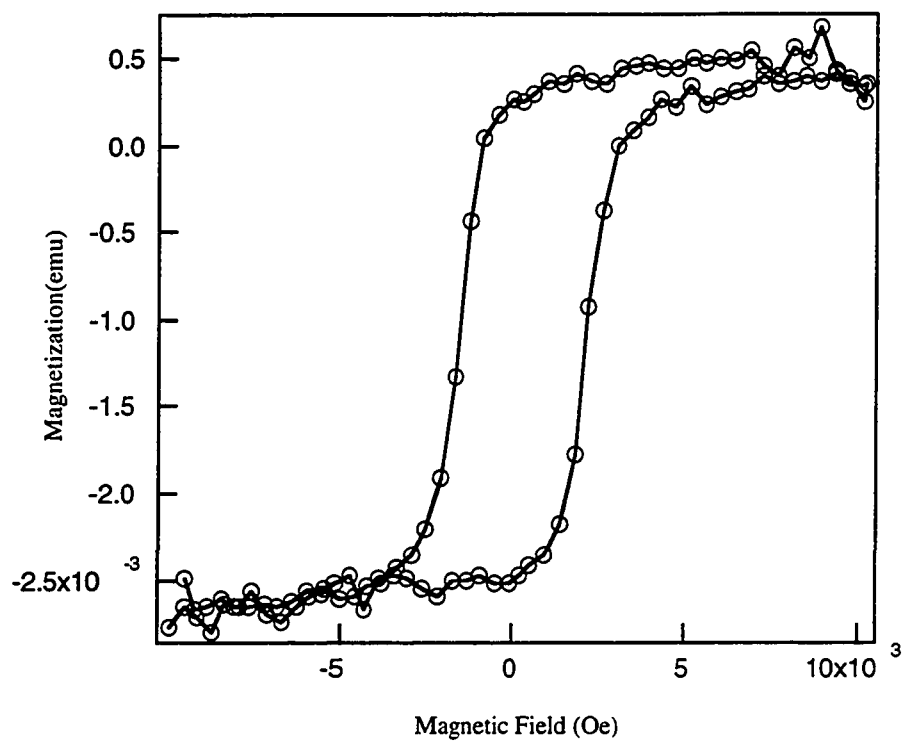
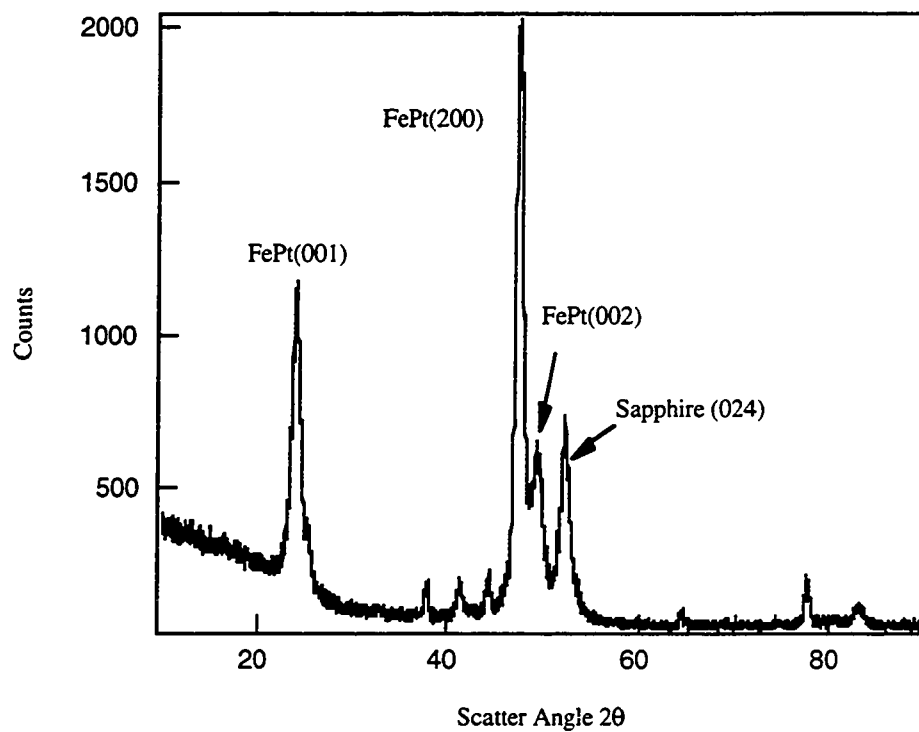Fig. 5.1 Hysteresis loop of (200) FePt

Fig. 5.2 X-Ray pattern for FePt with (002) epitaxy

Traditionally in Co based alloy system, third element additive is to boost the coercivity. While in the FePt system, we started from high coercivity, high anisotropy energy media which is not writable by currently available transducers. By doping a third element, we move their properties towards the region of feasible magnetic recording testing and evaluation. We have found that the properties such as exchange coupling and rotation coherency have improved with the decrease of coercivity by third element diluting. Such an approach will be problematical if coercivities in the range of 10kOe become necessary in the future. It would therefore be interesting to look for methods of reducing intergranular coupling that do not rely on dilution.

5.2 VSM Measurements

We have studied VSM Rotational Transverse Magnetometry to investigate anisotropy using a simple model of a uniaxial, coherently switching 2-D distribution of identical, non-interacting particles. It would be interesting to extend this model to the case of less homogeneous systems (particles of various anisotropy energy, with interactions), both to better characterize anisotropy and to investigate the transverse magnetization for values of $H/H_k < 0.5$.

References

1.1 Ed Grochowski, "The era of Magnetorisistive heads", IBM research home page, http://www.storage.ibm.com/hardsoft/diskdrdl/technolo/gmr/gmr.htm, 1997

1.2 Data Storage, Feb. 1998, pp. 12

1.3 S. H. Chararp, Pu-Ling Lu and Yanjun He, Thermal Stability of Record Information at High Density, IEEE Trans. on Magn. vol. 33, no. 1, pp. 978, 1997

1.4 Pu-Ling Lu, and S. H. Charap, High Density Magnetic Recording Media Dsign and Identification: Susceptibility to Thermal Decay, IEEE Tans. on Magn., vol. 31, No. 6, 1995

1.5 Pu-Ling Lu, and S. H. Charap, Thermal Stability at 10Gbit/in2 Magnetic Recording, IEEE Trans. on Magn., vol. 30, No. 6, 1994

1.6 D. N. Lambeth, E. M. T. Velu, G. H. Bellesis, L. L. Lee, And D. E. Laughlin, "Media for 10Gb/in^2 hard disk storage: Issues and Status", J. of Appl. Phys., 79(8), pp. 4496, 1996

1.7 J. Zhu, X. Ye and T. C. Arnoldussen, Effect of In-plane Easy Axis Orientation in Narrow Track Recording, IEEE Trans. on Magn., 29(1), pp.324, 1993

1.8 http://www.almaden.ibm.com/sst/disk/newmag.htm

1.9 J. Li, R. Sinclair, S. S. Rosenblum, J. Hayashi, As-deposited crystalline barium ferrite thin film media for logitudinal recording, J. Of Magnetism and Magnetic Materials, 153, pp. 246, 1996

1.10 X. Sui, M. Scherge, M. Kryder, J. E Snyder, V. G. Harris, N. C. Koon, Barium Ferrite thin-film recording media, J. of magnetism and Magnetic Matereials, 155, pp132, 1996

1.11 E. M. T. Velu and D. N. Lambeth, High Density Recording on SmCo/Cr Thin Film Media, IEEE Trans. on Magn., 28(5), pp. 3294, 1992

1.12 E. M. Velu and D. N. Lambeth, CoSm-based High-coercivity Thin Films for Longitudinal Recording, J. Appl. Phys., 68(5), 1991

1.13 J. A. Aboaf, T. R. McGuire, S. R. Her and E. Klokholm, Magnetic, Transport and Structural Properties of Iron-Platinum Thin Film, IEEE Trans. on Magn., 20(5), 1642, 1984

1.14 K. R. Coffey, M. A. Parker, and J. K. Howard, "High Anisotropy L1$_0$ Thin Films for Longitudinal Recording", *IEEE Trans. Magn.*, vol.31, pp. 2737, 1995.

1.15 E. S. Murdock, R. E. Simmons, R. Davidson, Roadmap for 10Gbit/in2 Media: Challenges, IEEE Trans. on Magn. vol. 28, no. 5, 1992

1.16 C. P. Luo, Z. S. Shan, D. J. Sellmayer, Magnetic Viscosity and Switching volumes of Annealed Fe/Pt Multilayer, J. of App. Phys. vol. 79, no. 8, pp. 4899, 1996

1.17 A. Z. Men'shikov, Y. A. Dorofeuev, V. A. Kazantesv and S. K. Sidorov, Magnetic Structure of Ordered Iron-Platinum Alloys, Phys. Met. Metall., 38, pp 47, 1974

1.18 T. B. Massalski, *"Binary Alloy Phase Diagrams"*, American Society for Metals, 1986

1.19 O. A. Ivanov, L. V. Solina, V. A. Demshina and L. M. Magat, Determination of the Anisotropy Constant and Saturation Magnetization, and Magnetic Properties of Powders of an Iron-Platinum Alloy, Phys. Met. Metall. 35, pp.81, 1973

1.20 R. A. McCurrie and P. Gaunt, The Magnetic Anisotropy of Ordered Equiatomic Platinum Cobalt, The Philosophical Magzine, A Journal of Theoretical Experimental And Applied Physics, 19(158), pp.339, 1969

1.21 P. D. Desai, D. T. Hawkins, M. Gleiser, K. Kelley, R. Hultgren, *"Selected Values of the Thermodynamic Properties of Binary alloy"*, American Society for Metals, Metals Park, Ohio, 1973

1.22 B. M. Lairson, M. R. Visokay, R. Sinclair, and B. M. Clemens, "Epitaxial PtFe(001) Thin Films on MgO(001) with Perpendicular Magnetic Anisotropy", *Appl. Phys. Lett.*, vol. 62, pp. 639, 1993

1.23 M. Watanabe and M. Homma, Perpendicular Magnetization of Epitaxial FePt(001) Thin Films with High Squareness and High Coercive Force", Jpn. J. Appl. Phys. 35, II(10A), L1264, 1996

1.24 A. Cebollada, D. Weller, J. Sticht, G. R. Harp, R. F. C. Farrow, R. F. Marks, R. Savoy, and J. C. Scott, "Enhanced Magneto-optical Kerr Effect in Spontaneously Ordered FePt Alloys: Quantitative Agreement between Theory and Experiment", *Phys. Rev.*, vol. B 50, pp. 3419, 1994

1.25 R. F .C. Farrow, D. Weller, R. F. Marks, M. F. Tonety, A. Cebollada, G. R. Happer, "Control of the Axis of Chemical Ordering and Magnetic Anisotropy in Epitaxial FePt Films", J. Appl. Phys., vol. 78, pp. 5967, 1996

1.26 R. F .C. Farrow, D. Weller, R. F. Marks, M. F. Tonety, S. Hom, G. R. Happer, A. Cebollada, "Growth Temperature Dependence of Long-range Alloy Order and Magnetic Properties of Epitaxial Fe_xPt_{1-x} (x≈0.5) Films", *Appl. Phys. Lett.*, vol. 69, pp. 1166, 1996

1.27 M. Watanabe, T. Nakayama, K. Watanabe, T. Hirayama, A. Tonomura, "Microstructure and Magnetic Properties of High-Coercive Fe-Pt Alloy Thin Film", *Materials Trans. JIM.*, vol. 37, pp. 489, 1996

1.28 D. M. Artymowicz, B. M. Lairson, B. M. Clemens, "Formation of Ordered Tetragonal PtCo from Epitaxial Pt/Co Multilayers", *J. Crystal Growth*, vol. 169, pp. 83, 1996

1.29 K. Barmak and R. A. Ristau, Grain Growth and Ordering Kinetics in CoPt Thin Films, J. appl. Phys., 79(8), 15, 1996

1.30 J. C. Woolley, B. Bates, "Ordering in CoPt-FePt Alloys", *J. of the Less-common Metals*, Vol. 1, pp. 382, 1959

1.31 T. Shimasu, E. G. Keim, T. Bolhuis and J. C. Lodder, "Activation Volume of FePt-TaN Nanocrystalline Thin Films with High Coercivity", *J. of Magn. Soc. of Japan*, vol. 21, no. S2, pp. 313, 1997

1.32 C. P. Luo, Z. S. Shan, D. J. Sellmyer, "Magnetic Viscosity and Switching Volumes of Annealed Fe/Pt Multilayers", *J. Appl. Phys.*, vol. 79, pp. 4900, 1996.

1.33 H. N. Bertram, *"Theory of Magnetic Recording"*, Cambridge University Press, New York, 274 (1994)

1.34 http://www.almaden.ibm.com/sst/hdi/density.htm

1.35 Kanu G. Ashar, "Magnetic Disk Drive Technology", IEEE press, New York, 1997

1.36 K. E. Johnson, E. Y. Wu and D.C. Palmer, J.G. Zhu, "Media Noise Improvement Through Head-Disk Spacing Reduction", IEEE Trans. on Magn., 28(5), pp.2713, 1992

1.37 T. Shimatsu, E. G. Keim, T. Bolhuis and J. C. Lodder, Activation Volume of FePt-TaN Nanocrystalline Thin films with High Coercivity, Journal of the Magnetix Society of Janpan, vol 21, No, S2, pp. 313, 1997

1.38 A. Taratorin, "Characterization of Magnetic Recording System, A Practical Approach", Guzi Technical Enterprises, 1996

2.1 K. O'Grady, Magnetic Characterization of Recording Media, IEEE, Trans on Magn., 26(5), pp. 1870, 1990

2.2 K. O'Grady, R.W. Chantrell, I. L. Sanders, Magnetic Characterization of Thin Film Recording Media, IEEE Trans. on Magn., vol. 29, no 1, pp. 286, 1993

2.3 E. P. Wohlfarth, Relations Between Different Modes of Acquisition of the Remanent Magnetization of Ferromagnetic Particles, J. of Appl. Phys., vol 29, pp. 595, 1958

2.4 P. E. Kelly, K. O'grady, P. I. Mayo, And R. W. Chantrell, Switching Mechanism in Cobalt-Phosphorus Thin Films, IEEE Tran. on Magn, 25(5), pp. 3881, 1989

2.5 A. Beardsley and J. G. Zhu, Significance of δM Measurements in Thin Film Media, IEEE Trans. on Magn. vol. 27, no. 6, pp. 5037, 1991

2.6 X. D. Che and H. N. Bettram, Phenomenology of dM curves and magnetic interactions, J MMM, 116, pp. 121, 1992

2.7 M. P. Morales and K. O'Grady, B. Zhang, W.R. Bennett and G. C. Rauch, Interactions and Reversal Processes in CoCrTa/CoCrTaPt Thin Films, IEEE Tran. on Magn., 32(5), pp.3593, 1996

2.8 A. R. Corradi, E. P. Wohlfarth, Influence of Densification on the Remanence, the Coercivities and the Interaction Field of Elongated γFe_2O_3 Powders, IEEE Trans. on Magn., Vol. 14, no. 5, pp. 861,1978,

2.9 B. D. Cullity, Introduction To Magnetic Materials, Addison-Wesley Publishing Co., 1972, pp.334

2.10 E.P. Wohlfarth, Ferromagnetic Materials, A handbook on the properties of magnetically ordered substance, Vol 3, North-Holland Publishing Company, 1982, pp50

2.11 E. C. Stoner and E. P. Wohlfarth, A Mechanism of Magnetic Hysteresis in Heterogeneous Alloys, Phil. Trans. of Roy. Soc. of London, vol. 240, A. 826, pp. 599, 1948

2.12 L. S. Jacobs and C. P. Bean, An Approach to Elongated Fine-particle Magnets, Phys. Rev., 100(4), pp. 1060, 1955

2.13 E. P. Wohlfarth, Hard Magnetic Materials, Advances in Physics, W18(30), 101, 1959

2.14 W. D. Doyle, Determination of the Anisotropy in Thin Permalloy Films, J. of Appl. Phys., vol. 33, no. 5, pp. 1769, 1962

2.15 H. Zijlstra, "Experimental Methods in Magnetism, 2. Measurement of Magnetic Quantities", North-Holland Publishing Company, Amsterdam, pp. 199, 1967

2.16 G. M. Kalvius, R. S. Tebble, Experimental Magnetism, vol I, John Wiley & Sons, 1979

2.17 I. S. Jacobs and F. E. Luborsky, Magnetic Anisotropy and Rotational Hysteresis in Elongated Fine-Particle Magnets, J. of Appl. Phys. vol. 28, no. 4, pp. 467, 1957

2.18 G. Bottoni, Rotational Hysteresis in Particle for Magnetic Recording with Different Switching Modes, J. of Magn. Magn. Mater., vol. 155, pp. 16, 1996

2.19 G. Bottoni, Rotational Hysteresis and Magnetic Anisotropy of Particles for Magnetic Recording, J. of Magn. Magn. Mater., nol. 140-144, pp. 2207, 1995

2.20 M. Takahashi, T. Shimatsu, M. Suekane, M. Miyamura, K. Yamaguchi, H. Yamasaki, Magnetization Reversal Mechanism Evaluated by Rotational Hysteresis Loss Analysis for the Thin Film Media, IEEE Trans. on Magn. vol 28, no. 5, pp. 3285, 1992

2.21 M. Takahashi, T. Shimatsu, M. Miyaura, K. Yamaguchi, and H. Yamasaki, Magnetic Evaluation of Intergranular Interactions in Thin-Film Media by Rotational Hysteresis Loss Analysis, J. of Magn. Magn. Mater., vol. 120, pp. 229, 1993

2.22 I. A. Beardsley, V. S. Sperious, Determination of Thin Film Media Model Parameters Using DPC Imaging and Torque Measurements, IEEE Trans. on Magn., vol. 26, no. 5, pp. 2718, 1990

2.23 P. J. Flanders, S. Shtrikman, Experimental Determination of the Anisotropy Distribution in Ferromagnetic Powders, J. of Appl. Phys., vol. 33, no. 1, pp. 216, 1962

2.24 E. P. Wohlfarth, The effect of particle interaction on the coercive force of ferromagnetic micropowders, Proc. Roy. Soc. (London), A232, 208, 1955

2.25 C. P. Bean and W. H. Meiklejohn, Rotational Hysteresis in Ferromagnetic Micropowders, Bull. Am. Phys. Soc.II, 1, pp.148, 1958

3.1 A. Tsoukatos, G. C. Hadjipanayis, Y. J. Zhang, M. Waite, C. P. Swann and I.. Shah, Thickness Effects on the Magnetic Hysteresis of Equiatomic CoPt Films, Mat. Res. Soc. Symp. Proc. Vol 232, 289, 1991

3.2 T. Suzuki, N. Honda and K. Ouchi, Preparation and Magnetic Properties of Sputter-Deposited FePt Thin Films with Perpendicular Anisotorpy, J. of Magn. Soc. of Japn, v0l 21(s2), 177, 1997

3.3 X. Sui, M. Scherge, M. Kryder, J. E Snyder, V. G. Harris, N. C. Koon, Barium Ferrite Thin-film Recording Media, J. of Magnetism and Magnetic Matereials, 155, pp 132, 1996

3.4 K. R. Coffey, M. A. Parker, and J. K. Howard, "High Anisotropy Ll_0 Thin Films for Longitudinal Recording", *IEEE Trans. Magn.*, vol.31, pp. 2737, 1995.

3.5 J. H. Westbrook, R. L. Fleischer, Intermetallic Compounds; Principles and Practice, vol. 1, pp.711, 1995

3.6 K. Barmak and R. A. Ristau, Grain Growth and Ordering Kinetics in CoPt Thin Films, J. Appl. Phys., 79(8), 15, 1996

3.7 J. C. Woolley and B. Bate, Ordering in CoPt-NiPt Alloys, J. of the less-common Metals, 2(1960)II-18.

3.8 L. H. Schwartz, J. B. Cohen, *"Diffraction from Materials"*, Springer-Verlag, New York, pp. 378, 1977

3.9 B. D. Cullity, *"Elements of X-Ray Diffraction"*, 2nd Edition, Addison-Wesley Publishing Company, Inc., 1972

3.10 B. Zhang, M. Lelovic and W. A. Soffa, Scrpt. Met. 25, 1577, 1991

3.11 B. Zhang and W. A. Soffa, Structure and Properties of Rapidly-Solidified Iron-Platinum and Iron-Palladium Alloys", IEEE Trans on Magn. 26, 1388, 1990

3.12 M. Watanabe, T. Nakayama, K. Watanabe, T. Hirayama, A. Tonomura, "Microstructure and Magnetic Properties of High-Coercive Fe-Pt Alloy Thin Film", *Materials Trans. JIM.*, vol. 37, pp. 489, 1996.

3.13 D. E. Speliotis, Correlation of Rotational Magnetic Properties and Noise in Thin film Magnetic Recording Media, IEEE Trans. on Magn., 24(6), pp.2979, 1988

3.14 T. Shimatsu, D. D. Djayaprawira, A. Endo, N. Iwata, M. Takahashi, T. Wakiyama, Intergranular Magnetic Coupling in CoNiCrPt and COCrTaPt thin-film media characterized by the Temperature dependence of the Rotational Hysteresis loss, J. Magn. Magn. Mater, 155(1996), pp242

3.15 X. Sui, M. Scherge, M. Kryder, J. E Snyder, V. G. Harris, N. C. Koon, Barium Ferrite thin-film recording media, J. of magnetism and Magnetic Matereials, 155, pp132, 1996

3.16 J. Li, S. S. Rosenbluem, H. Hayashi, R. Sinclair, Magnetic and structural characteristics of sputtered barium ferrite thin films, J. of Mangnetism and Magnetic Materials, 155, pp157, 1996

3.17 L. Callegar, E. Puppin, P. L. Cavallotti, G. Zangari, Electroplated, high Hc CoPt films: δM magneto-optical measurements, J. of Magnetism and Magnetic Materials, 155, pp.190, 1996

3.18 Y. Shiroishi, Y. Matsuda, K. Yoshida, H. Suzuki, T. Ohno, N. Tsumita, M. Ohura and M. Hayashi, Read and Write Characterization of Co-alloy/Cr Thin Films for Longitudianal Recording, IEEE Trans. on Magn. vol.24(6), pp.2730, 1988
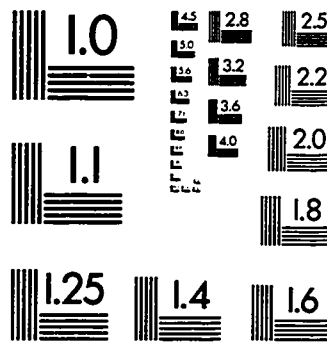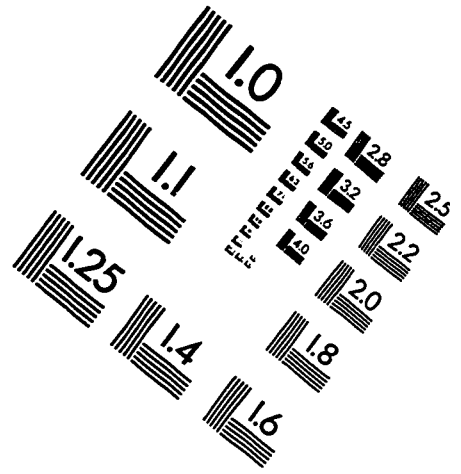
4.10 M. K. Miller, R. Jayaram and P. P. Camus, "Grain Boundary Composition in NiAl", *Scripta-Metallurgica-et-Materialia*, vol. 26, no. 4, pp.679, 1992

4.11 Palmer, P. Ziperovich, R. Wood, T. D. Howell, Identification of nonlinear write effects using psedorandom sequence, IEEE Trans. on Magn, 23(5), pp. 2125, 1990

4.12 X. Che and P. A. Ziperovich, A Time-Correlation Method of Calculating Nonlinearities Utilizing Pseudorandom Sequences, IEEE Trans. on Magn., 30(6), pp. 4239, 1994

4.13 Y. Tang and C. Tsang, A Technique for Measuring Nonlinear Bit Shift, IEEE Trans. on Magn., 27(6), 5316, 1991

4.14 X. Che, M. J. Peek and J. Fitzpatrick, A Generalized Frequency Domain Nonlinearity Measurement Method, IEEE Trans. on Magn. 30(6), 4236,1994)

4.15 S. R. Cumpson, S. E. Stupp, "Experimental and Theoretical Studies of Nonlinear Transition Shift in Metal Evaporated Tape", *IEEE Trans. Magn.*, vol. 33, pp. 2968, 1997

4.16 J. C. Mallinson, Proposal Concerning High-Density Digital Recording, IEEE Trans. on Magn., 25(4), 3168,1989

5.1 J. C. Woolley, B. Bates, "Ordering in CoPt-FePt Alloys", *J. of the Less-common Metals*, Vol. 1, pp. 382, 1959

5.2 B. M. Lairson and M. R. Visokay, R. Sinclair and B. M.Clemens, Appl. Phys. Lett. 61, 1390, 1992;

5.3 R. R. C. Farrow, G.R. Harp, R. F. Marks, T. A. Rabedeau, M. F. Toney, D. Weller and S. S. P. Parkin, J. Crystal. Growth, 47, 133, 1993

5.4 M. R. Visokay and R. Sinclair, Direct Formation of Ordered CoPt and FePt Compound Thin Films by Sputtering, Appl. Phys. Lett. 66(13), 1692, 1995

5.5 B.D. Cullity, Introduction To Magnetic Materials, Addison-Wesley Publishing Co., 1972, pp.458

IMAGE EVALUATION
TEST TARGET (QA-3)

150mm

6"